TIME SERIES ANALYSIS OF THE CHLOROPHYLL CONTENT IN THE MOZAMBIQUE CHANNEL USING GIS AND REMOTE SENSING

Fredrik Ingmar Boge

Master's Thesis in Geography- 2006

Department of Geography
University of Bergen

ACKNOWLEDGEMENTS

Now that the thesis is finally done there are many people to greet. First, I would like to thank my girlfriend Magdalena for supporting and understanding me during this long process. I would also like to thank my supervisor Anne Lucas for guiding me through the thesis and for all the valuable teaching. The GIS gang at the institute, Helge, Tore, Astrid and Karianne deserve their names here. The great members of the geography band “Svartediket” also need some attention. Other memorable things to mention from my geography studies are: the ping pong room at Merino, the coffee machine, Frank Zappa, and the sofa at the meeting room. The support from my family has been valuable to me. A big thanks to all the people who lend me a bed when I was commuting from Stavanger.

Fredrik Boge

27th of August, Bergen

Contents

List of figures

List of tables

1 INTRODUCTION

The availability of remotely sensed data has given researchers the possibility to investigate oceanographic regions in a manner that were previously impossible. In the last years, the measuring of the oceans from space greatly has improved the knowledge of the oceans by providing a synoptic and continuous view for monitoring the oceanographic environment. The oceans are a dynamic environment that is constantly changing character. Continuous monitoring is therefore necessary in order to capture the changes of the parameters of interest, a possibility offered by the use of satellite survey. Key data products include chlorophyll measurements, Sea Surface Temperature and Sea Surface Height. This thesis is using geographically referenced marine remotely sensed data to describe and quantify biological productivity in the Mozambique Channel, which is located in the southwestern Indian Ocean (Figure 1-1).

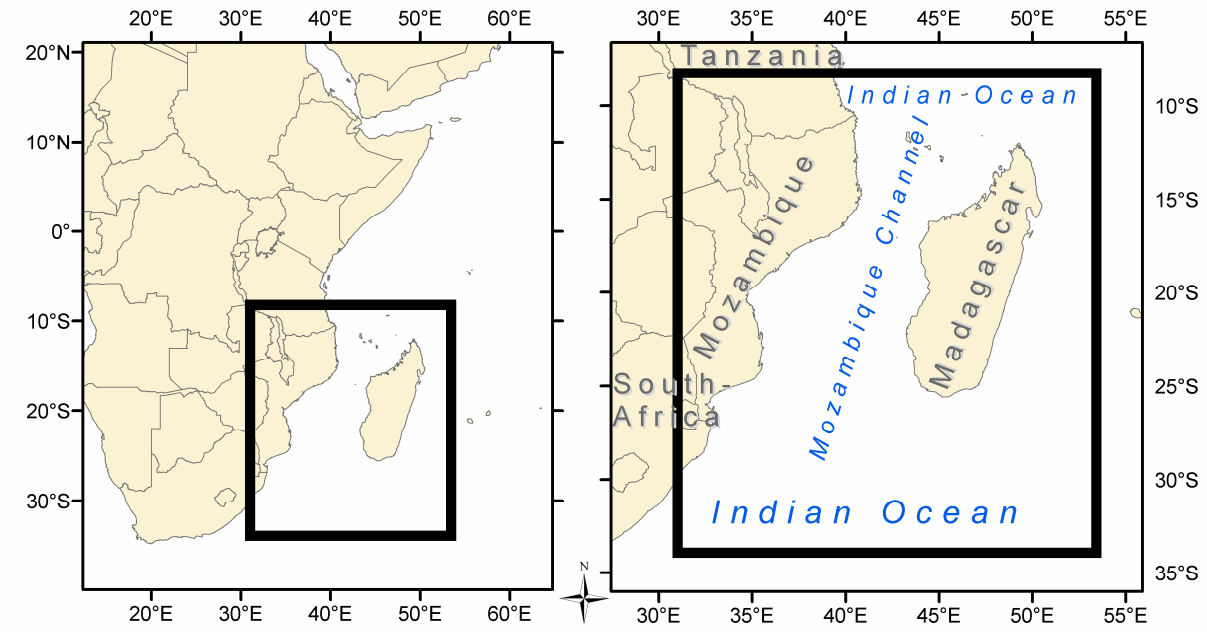

Figure 1-1. The study area. Limited by the black frame (about 31E-53.5E; 8.25S-34S). Data source: Digital Chart of the World (www.esri.com)

The emphasis of this study is the use of chlorophyll measurements from the MODIS Aqua sensor, the SeaWiFS sensor and GIS software for the investigation of spatial and temporal trends in the marine environment. A time series analysis is performed upon the data within a GIS environment in order to reveal seasonal changes in the chlorophyll content in the study area. GIS is an excellent tool for manipulation, analysis and visualization of geographically referenced data such as ocean color satellite imagery, which is stored in a raster format. After reviewing various GIS software, the IDRISI software was considered to be the most suitable

for analyzing the vast amounts of remotely sensed data needed in this thesis. This because IDRISI offered suitable time series analysis of remotely sensed data.

The study area also includes the Indian Monsoon Gyres Province in the northern part and the Indian South Subtropical Province to the south. As a whole, the open oceans in the study area generally contain very low concentrations of chlorophyll (between 0.05 and 0.3 mg/m³) throughout the seasons and, hence, low primary production. The high productivity areas are located in the coastal zone and on the continental shelf of East Africa and Madagascar. What becomes clear in this thesis is that the study area is experiencing large interannual and seasonal variations of chlorophyll in both the open oceans and coastal waters.

The northern part of the study area is affected by the Indian Ocean monsoon regime with dry austral winters and wet austral summers. This means that seasonal variations in the precipitation rate may influence the chlorophyll measurements due to variations in the river runoff and, hence, nutrient supply. The southern part of the study are experience regular austral winter blooms of phytoplankton growth. The flow regime in the study area is characterized by a southward flow in the Mozambique Channel and a relative rapid southward flow along the east coast of Madagascar. Together these flows combine into a net poleward transport waters from high latitudes to low latitudes through the study area.

Remote Sensing is a perfect method to continuously monitor the changes of marine features. One interesting point of this study is the possibility to conduct research on an oceanic region on a remote basis, both methodological, and during the work with the data. In a marine context field work is done by research vessels. The obvious advantage of remote sensing is the gain of perspective and, possible use of historical data and a continuous monitoring by regular revisits by the sensors. The SeaWiFS sensor, which is the present ocean color sensor that has the longest continuous time series, has collected data since August 1997 and still surveying the oceans of the earth. The temporal record can be accessed by researchers to both view and analyze the historical data. Often, remotely sensed data is the only way of getting scientific, continuous records in both space and time of oceanographic data. Historic records are available for downloading

1.1 Research objectives

The large amounts of satellite ocean color data used in this thesis need to significantly be reduced in order to reveal spatial and temporal patterns. The SeaWiFS and MODIS sensors are recording data over the study area on a daily basis providing snapshots of the current situation by measuring electromagnetic radiation upwelled from the sea. Examining daily snapshots over many years make it hard to compare the images and to track changes. The data needs to be broken down into interpretable information. In this thesis a description of the seasonal chlorophyll changes will be given in order to summarize the cyclic patterns. A time series analysis, Standardized Principle Component Analysis (SPCA) (Jensen, 2005; Eastman & Fulk, 1993) has been performed on multiple images. In the context of the thesis, two ocean color data sets are used: (1) averaged monthly chlorophyll content data from the SeaWiFS sensor with a spatial resolution of ~9km from September 1997 to September 2005, (2) averaged weekly chlorophyll content from the MODIS Aqua sensor with a spatial resolution of ~4km from 4th of July 2002 to 5th of September 2005. The reason why two different data sets with different temporal and spatial resolution are used is to explore the

All the images in both the data sets have been subscened to the extent of the study area. The SPCA analysis in these data will produce both spatial and temporal outputs suggesting where the chlorophyll varies over time in the study area and the relative magnitude of those variations. The outputs are called component images (explaining spatial variations) and component loadings (explaining temporal variations). The goal of such an analysis is not to describe the average conditions in the area over time, but merely a mapping of the variations from the average chlorophyll content over time. This procedure is useful in the analysis of time series data where the main target is to identify phenomena that vary over time.

The objectives for this thesis are:

1. Provide a synoptic quantification of the spatial pattern, timing and relative magnitude of the large scale seasonal and interannual chlorophyll cycle in the Mozambique Channel using the SPCA analysis and pairwise comparison.
2. Verify the results of the SPCA analysis with respect to the data itself by using time profiles from selected sites of the study area. The 9 km SeaWiFS data set is here used. This is done by creating time profiles from selected sites in the sites in the study area, which describes chlorophyll variations over time. The graphs are then compared with results from the SPCA analysis.

3. Explore the effect of using different spatial and temporal resolutions in the SPCA analysis.

The latter objective is motivated by the notion that choice of different temporal and spatial resolution will affect the results of an SPCA analysis. No clear guidelines on which spatial and temporal resolution is the most suitable for a SPCA analysis is found in the literature review.

As is known, the inherent uncertainty of the retrieved measurements of chlorophyll levels limits the ability to interpret actual concentrations and reduces the strength of time and space gradients. When the focus of an analysis is on the temporal and spatial variations of relative patterns, the data can provide a regional synoptic view of seasonal and interannual variability regardless of the uncertainty of the data. The main goal is not to compare the remotely-sensed data to in situ absolute values of chlorophyll concentration. Instead, variations of satellite measured chlorophyll concentration are used as an indicator of dynamics through time of phytoplankton biomass in the study region.

1.2 Structure of the thesis

The following chapter will consist of an area description regarding the present knowledge and findings of the Oceanographic regime in the study area. The third chapter is focused on the object of interest, namely phytoplankton. The fourth chapter will include the theory of ocean color remote sensing. The motivation behind including this chapter is to give a conscientious look over how the remotely sensed chlorophyll data that is used in this thesis are obtained. The fifth chapter focuses on the GIS method used in the Time Series Analysis of the satellite data. This includes a description on how the data is set up and prepared for the time series analysis. The sixth chapter includes the results of the SPCA analysis, the presentation of the seasonal averages and a discussion that looks upon the connections of the observed patterns to physical processes. The 7th chapter includes the results of the SPCA analysis of the alternative data sets.

2 DESCRIPTION OF THE STUDY AREA.

2.1 Current oceanographic knowledge

The aim of this chapter is to describe the oceanographic background and the current knowledge of the Mozambique Channel and surrounding areas, which is a part of the southwestern Indian Ocean. The study area is shown in Figure 2-1.

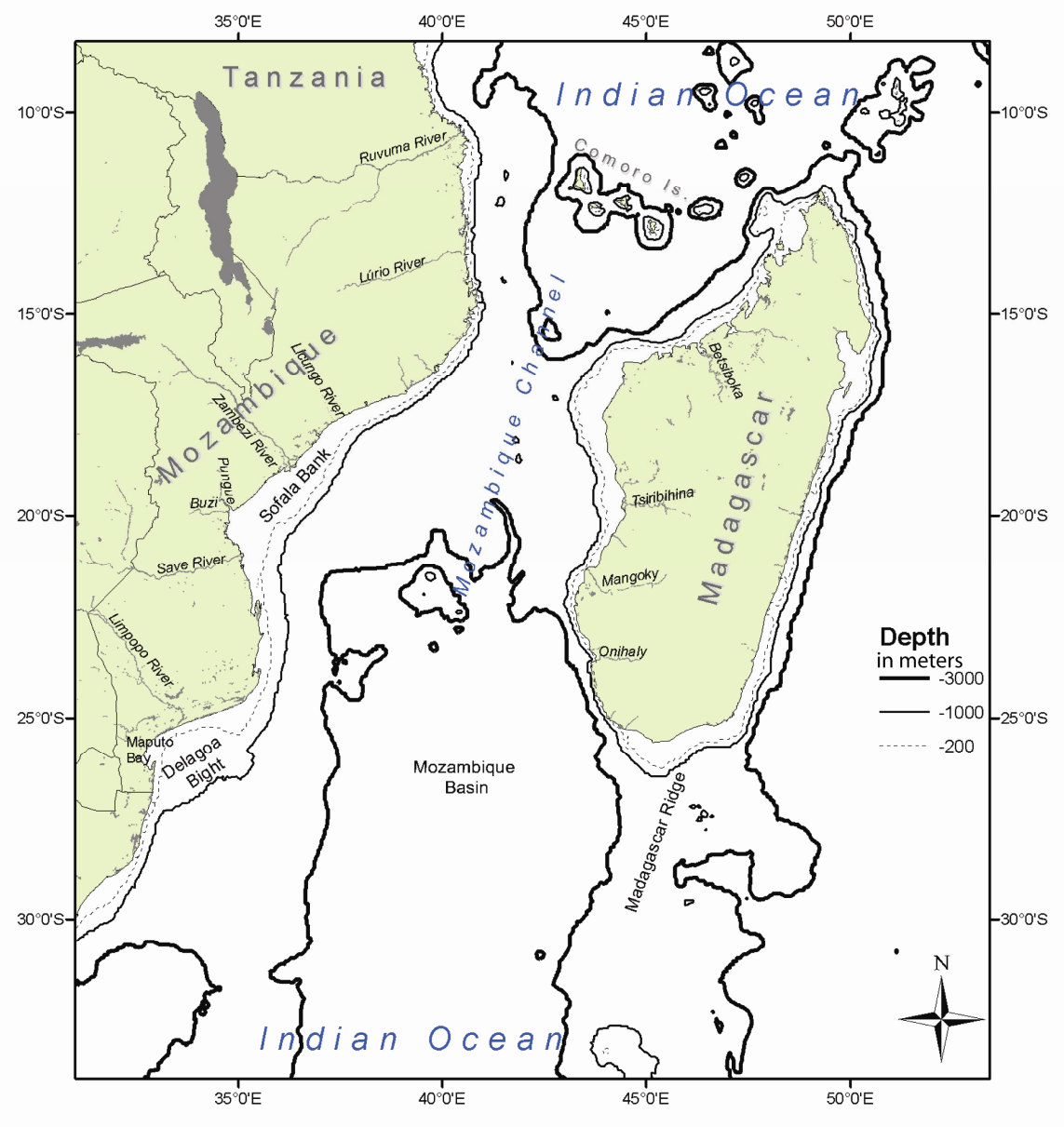

Figure 2-1. Map of the study area. Depth contours made from the CleanTOPO2 world relief data set (http://www.shadedrelief.com)

It is pointed out by Tomczak & Godfrey (1994) that the Indian Ocean as a whole, and also the Southwest Indian Ocean does not share a coastline with any of the past and present leading oceanographic nations. Compared with the Atlantic and the Pacific oceans is the Indian Ocean

not explored at the same level. Nevertheless, new research has brought old ideas into doubt with respect to important flow regimes in the Mozambique Channel. Data gathering methods employed by various scientists include both *in situ* observations and remote sensing. Combinations of these have improved the oceanographic knowledge of the Southwest Indian Ocean. Through the presentation of recent research it will be revealed that the study area is not yet fully understood and that temporal and spatial variation of oceanographic features are highly variant.

The sea of Mozambique is hydrodynamic distinct from other sections of East African marine environment because of the sheltering presence of Madagascar. The influence of the Mozambique Current is important as it carries Indian Tropical Surface Water (TSW) from the Southern Equatorial Current south through the Mozambique Channel. These factors create a relatively sheltered warm water environment along much of the Mozambique coast. The influence of the open ocean is felt only in the extreme north and the extreme south of the country. Ridderinkhof & de Ruijter (2003) summarize the present understanding of the large scale impacts of regional flow in the southwest Indian Ocean:

The large scale mass balance of the Indian Ocean is as a whole is influenced by the water flow through the Mozambique Channel because the flow from the tropics to the subtropics flows largely through the Mozambique Channel. This poleward flow balances the westward flow from the Pacific. The existence of a regional current flow in the Mozambique Channel is, from an oceanographic point of view, of great interest (Ridderinkhof & de Ruijter, 2003). The region of the southern Mozambique Channel is considered to be an important source region for the Agulhas Current (see Figure 2-2), the strongest western boundary current in the southern hemisphere (Quartly& Srokosz, 2004).

The flow through the Mozambique Channel together with the Southern East Madagascar Current, which flows southward along the east coast of Madagascar, is believed to be the two routes that the South Equatorial Current follows before feeding into the Agulhas current and, eventually, to the flow of warm and saline Indian Ocean water into the Atlantic where it compensates for the export of North Atlantic Deep Water. These flows, which feed into the Agulhas Current, are parts of the so called Greater Agulhas Current System (Machu *et al.*, 2005) and both exhibit very high levels of mesoscale variability. The classical question considering the flow regime in the Mozambique Channel is whether it is continuous or

discontinuous (DiMarco, 2002). This question will be addressed later on in this chapter. By a continuous flow it is meant that the watermasses is following a steady rout in a given direction throughout the seasons.

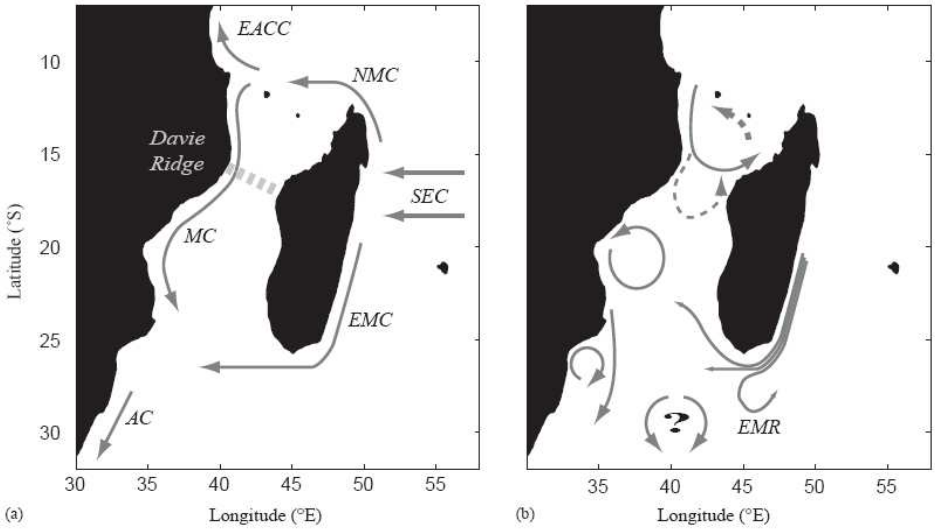

Figure 2-2. Circulation in the Mozambique Channel. a) shows Long-term mean flow from windforcing and mean water properties. b) shows different variability. SEC – South Equatorial Current, NMC – North Madagascar Current, EACC – East African Coastal Current, EMC – East Madagascar Current, MC – Mozambique Current, AC – Agulhas Current, EMR – East Madagascar Retroflection.

2.2 The flow in the Mozambique Channel

The South Equatorial Current is driven mainly by wind stress and flows westward across the Indian ocean before it reaches the coastal areas of eastern Madagascar around 20º S. The transport of this flow is ~50 Sv (1 Sv = 10^6 m/s²) (Schott & McCreary Jr., 2001). Here, the South Equatorial Current is divided into two parts. The southern flow is known as the East Madagascar Current and the volume transport is estimated to be ~20 Sv. The acceleration of this narrow current along the steep continental slope induces upwelling inshore, particular at the southern end of Madagascar where the shelf widens (DiMarco, 2002). When the East Madagascar Current passes the southern tip of Madagascar (Cape St. Marie), it flows westward towards the east coast of Africa and merges with the south flowing Mozambique Current before feeding into the Agulhas Current. The flow in the Mozambique channel is generally to the south, influenced by a persistent mesoscale anti cyclonic gyre field having three major eddies (possibly topographically induced) usually in the northern, central and southern part of the channel (Sætre & Jorge Da Silva, 1984).

The northern moving current, called the North Madagascar Current flows north along the east coast of Madagascar and turns west when it reaches the northern tip of Madagascar. The volume transport is estimated to be ~30 Sv (Schott & McCreary Jr., 2001). Schouten & de Ruijter (2005) documented an intrusion of low-chlorophyll waters spreading north of Madagascar in March 2001. This is suggested based upon an analysis of 4 years of MODIS data that this is a seasonal appearance. It is further concluded that this situation leads to eddie formation, which propagates though the Mozambique Channel. However, no conclusion is reached regarding the reasons of the intrusion. Upon reaching the coastal areas of eastern Africa, at ~11ºS, the Northeast Madagascar Current is divided into two parts. One part is moving northward and one part is moving southward into the Mozambique Channel. During the southwestern monsoon season from May to September, a part of the north moving flow (East African Coastal Current) continues north and enters the Somali Current. From November to February the northeast monsoon is present. Then, the East African Coastal Current is flowing northward to about 3º S before moving eastward to contribute to the Equatorial Countercurrent (DiMarco *et al.* 2002). de Ruijter *et al.* (2002) report that the southward moving flow by the Northeast Madagascar Current has approximately the same volume transport as the Northeast Madagascar current. Schouten *et al.* (2003) summarize the situation by stating that "it is unlikely that this strong southward flow is a permanent feature, but its strength shows that the time varying part of the circulation may have a strong impact on the large scale transport." Sætre & Jorge da Silva (1984) described the flow pattern in the Mozambique Channel by dividing it into a summer pattern (November to April) and a winter pattern (May to October). The flows are dominated by several eddies in the middle of the channel. A large anticyclonic eddie with a ~400 km diameter is documented in the summer in the middle of the southern part of the Mozambique channel. Several smaller eddies are found in the winter time. The study also indicates that there is large interannual variability in the flow pattern in the channel. One of the main outcomes of this study is the question that addresses the traditional understanding of a permanent western boundary current in the Mozambique Channel (Sætre & Jorge da Silva, 1984). It has been indicated that instead of a steady flow southward through the Mozambique Channel, which is the conventional explanation, there may exist a series of anti-cyclonic eddies in the channel. These are to a degree independent of Indian Ocean current patterns. The present view of the flow regime in Mozambique channel no longer considering the possibility of a steady flow through the Mozambique Channel (see doted line MC in Figure 2-3), but rather reaches the conclusion

that the southward flow is dominated by a train of southward flowing eddies (Quartly & Srokosz, 2004; Schouten & de Ruijter, 2005; Schouten *et al.* 2003 & DiMarco *et al.* 2002).

The flow structure in the Mozambique Channel has been estimated with the help of surface drifters and from hydrographic observations. The results are contradicting, most likely due to highly varying flow in the Mozambique Channel. Although their observations consisted of snapshots, DiMarco *et al.* (2002) suggested that eddies might be responsible for this. A research cruise conducted by de Ruijter *et al.* (2002) observed that the flow in the Mozambique Channel is dominated by a train of large anti cyclonic eddies with a diameter larger than 300 km. These eddies reach the bottom of the channel and propagate southward and they cause a net southward transport of about 15 Sv. The cruise was aimed at the determination of the sources of the Agulhas Current, both from the north (the Mozambique Channel) and the east (from east of Madagascar). The nature of the flow in the Mozambique Channel was investigated. The dominance of anticyclonic eddies was confirmed using a combination of in situ CTD and lowered ADCP current measurements, buoyant drifter tracks and satellite altimetry. The observed regular formation of Mozambique Channel eddies at the frequency of four per year was found to probably be due to a train of baroclinic Rossby waves that travels westward around 12ºS at a frequency of four per year (Schouten *et al.* 2001). The analysis indicated that Rossby waves carry variations which originate in the equatorial region across the subtropical gyre. Schouten *et al.* (2003) report that between 1995 and 2000, on average 4 eddies per year are observed from satellite altimetry to propagate southward through the Mozambique Channel into the upstream Agulhas region. Quartly and Srokosz (2004) reports 5 to 6 each year based on ocean color studies. Further south, these eddies have been found to potentially have influence on the timing and frequency of Agulhas ring shedding. Quartly & Srokosz (2004) points out that the train of southward moving eddies in the Mozambique Channel has a tendency to flow in the vicinity of the African coast. This again gives the appearance of a semi-permanent southward flowing Mozambique Current. Probably is this the reason for the idea of a continuous Mozambique Current. Topographically, the small Islands in the middle of the Mozambique Channel, Bassas de India and Île Europa, help restricting the path the eddies follow. A picture of the circulation in the Mozambique Channel region given by Schouten *et al.* (2003) is shown in Figure 2-3.

Ridderinkhof & de Ruijter (2003) used current meter moorings deployed along a transect at the narrowest section of the Mozambique Channel, at ~17ºS, with the intention to study the

current field and to estimate the volume transport. They estimated the mean total volume transport to be 14 Sv in the southward direction and found that there is great time variability in the volume transport. They found no seasonal variability, which corresponds with similar findings by Schouten *et al.* (2003). It was also discovered that the anticyclonic eddies are formed when transport through the narrowest part of the Mozambique Channel is at its strongest. Finally, it was concluded that there is no evidence for a boundary current along the African shelf or the Madagascar shelf and that the strongest currents were found in the middle of the Mozambique Channel.

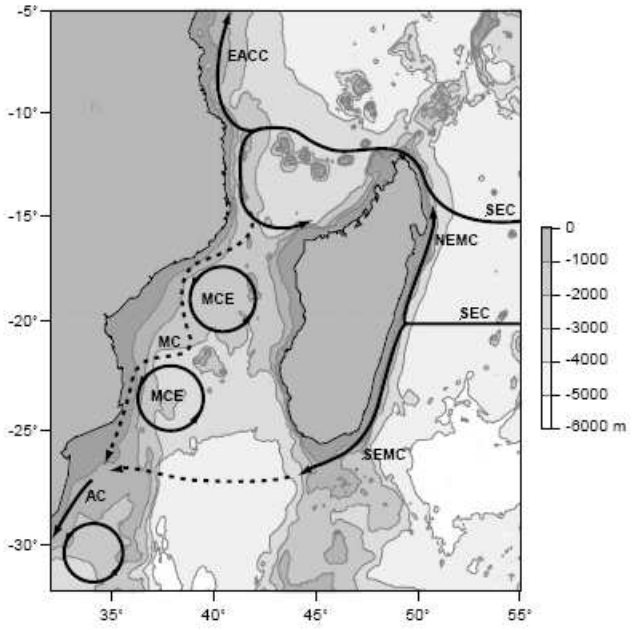

Figure 2-3. The main currents and flows around Madagascar and the Mozambique Channel. Features shown are the South Equatorial Current (SEC), the Northeast and Southeast Madagascar Currents (NEMC & SEMC) the East African Coastal Current (EACC), the Agulhas current (AC), Mozambique Channel Eddies (MCE) and the Mozambique Current. The latter has been drawn by a dotted line, as its existence and nature is unclear. The same holds for the connection between the SEMC and the AC, which is possibly formed near the southern tip of Madagascar. Text and figure taken from (Schouten *et al.* 2003).

2.3 Observations of the Eastern Madagascar Current and the East Madagascar Retroflection

As mentioned earlier in the text is the East Madagascar current comprised by a northern one and a southern one. This southern current consists of a narrow, intense western boundary current that follows the narrow continental shelf from 17º S until it reaches the southern edge of Madagascar. According to Tomczak & Godfrey (1994), the East Madagascar Current is apparently divided into three different possible paths (see Figure 2-2). One is continuing north along the west coast of Mozambique. One is heading west, feeding into the Agulhas current.

The north-south topography of the Madagascar Ridge, to the south of the island, may at times induce bifurcation of the East Madagascar current flow directly into the subtropical gyre by retroflection south of Madagascar. At other times the East Madagascar Current feeds directly into the Agulhas Current at the surface. When it occurs, the retroflection of the East Madagascar Current is accompanied by active meandering and eddy formation. But the overall large scale flow is to the west (de Ruijter *et al.*, 2004). From ocean color data Lutjeharms & Machu (2000) observed retroflections and anticyclonic movements of features in the south of Madagascar. de Ruijter *et al.* (2004) investigated the formation and movement of eddies over the southern Mozambique Channel with TOPEX/Poseidon altimetry data. The survey revealed that the formation and appearance of eddies in the period 1995-2000 seems to be related to the El Niño/Indian Ocean Dipole cycle. It was also noted that in periods of reduced eddie activity near Madagascar, there was no eddies that passed the narrowest part of the Mozambique Channel at 17ºS. It is suggested that the occurrence of "missing" eddies at the same time in the two regions may be due to a lagged response of Sea Surface Height anomalies in the equatorial parts of the Indian Ocean. Further, these anomalies are generated by anomalous easterlies during El Niño events, as noted by Schouten *et al.* (2002). Both the area south of Madagascar and the narrowest part of the Mozambique Channel are thought to be related to changes in the same large scale systems that involves the subtropical Indian Ocean. Another interesting finding by de Ruijter *et al.* (2004) is the observation of regular appearance of dipole-like vortex structures. These are interpreted as pairs of contra-rotating eddies and are located south and southeast of Madagascar. The behavior and movement were irregular but, in general, the propagation was to the southeast.

2.4 Conclusion

The later findings strongly suggest that the existence of the Mozambique Current as an "independent" western boundary current should be put in the abyss for good. The flow though the channel is guided by eddies which spawns at regular intervals. It is indicated that rather than having strong flow in the overall Indian Ocean circulation pattern, there may instead be a series of local anti-cyclonic current loops in the channel, largely independent of the larger Indian Ocean flow patterns, along with a deep cold water flow going north along the channel bottom which originates in deep Atlantic waters. It is also suggested that the flow and eddie formation is under direct influence of large scale climatic changes such as the ENSO cycle. It is just in the last few years the true nature of the flow regime in the Mozambique Channel has

started to be revealed. Still much work and research has to be done on various marine topics before a more complete understanding is reached.

The use of remotely sensed data in the survey of the study area has provided new oceanographic insights concerning the flow regime in the area by providing long term data of environmental parameters. The data types used include SST, Sea Surface Height and Ocean Color. Research performed on ocean color in the study area is presented in the end of chapter 4 (Remote Sensing of Ocean Color).

3 PHYTOPLANKTON AND ENVIRONMENTAL CONDITIONS

3.1 Introduction

One of the key products derived from remotely sensed ocean color data are measurements of chlorophyll-*a,* the most important pigment found in phytoplankton. Chlorophyll is used as an indication of phytoplankton abundance and is also used as a proxy for primary production in the oceans. Ocean color data is also valuable for tracking ocean features and describing currents as the free floating plankton follows currents and eddies. Since this thesis is using remotely sensed chlorophyll measurements as a data source for mapping variations in the phytoplankton concentrations over time, a presentation of the phytoplankton's nature and behavior will now be given. First, important phytoplankton types will be presented. The information is from Lalli & Parsons (1993). Second, the factors that control the phytoplankton growth and abundance are presented. Third, studies of satellite derived phytoplankton data from the Mozambique Channel are presented.

3.2 Different types of phytoplankton

Phytoplankton is the most numerous life form on our earth in both numbers and total weight and is a free floating photosynthetic algae with one cell, which is mostly concentrated in the productive photic zone in the ocean, and often has a patchy distribution. Phytoplankton forms the basis of the marine food web and is important for the global carbon cycle. There exist numerous types in various sizes. Concentration, distribution and composition can vary with time and space, but usually there is one type of phytoplankton which is dominant within a give area. The different species of phytoplankton can be restricted in locality. The benthic species of algae are limited in distribution to coastal, shallow areas because of the rapid attenuation of light with depth. Phytoplankton, on the other hand, can be found in all waters which are illuminated by sunlight.

3.2.1 Diatoms

Diatoms are a type of phytoplankton that is often the dominant type in temperate and high latitudes. They are found in all waters except in coastal waters. The cell size of the different diatoms varies greatly, ranging from around 2 µm to over 1000 µm and all types have an external skeleton. Diatoms usually reproduce by asexual division of cells and may lead to a rapid increase in population under favorable conditions. Sexual reproduction can also occur. The two common forms of diatoms are: the pennate form and the centric form, where the

latter is the most common with over 1500 types found. Diatoms can not move themselves. Since it is necessary to be close to be within the photic zone in order to catch light for the use in the photosynthesis, various mechanisms exist to prevent the diatoms sinking to the bottom. These include: small size, colony/chain formation, ionic regulation. Turbulence in the water also helps the diatoms being suspended in the waters.

3.2.2 Dinoflagellates

Dinoflagellates are the second most abundant phytoplankton in the sea. These plankton types also consist of one cell and generally do not form colonies, with the exception of a few species. Opposed to the diatoms, the dinoflagellates are can move in the water on their own. There are only a few species produces their energy solely by the means of photosynthesis (autotrophic). About 50 % of the dinoflagellates species feeds only upon other phytoplankton and zooplankton (heterotrophic). These species do not have chloroplasts and chlorophyll. Other species can feed both upon other plankton and use photosynthesis (mixotrophic). The dinoflagellates are found in all waters, and especially warm tropical and subtropical waters.

3.2.3 Others

Coccolithophorids are planktons with one cell which includes around 150 species. The size of the major part of the species are generally smaller than 20 µm. Coccolithophorids have a shell made up of numerous calcareous plates which are called coccolithes. Coccolithophorids are found in all waters, both coastal and oceanic. Most species occur in warm seas. The most abundant species is the *Emiliania huxleyi,* which can be found in all waters except in the Polar Regions. Cyanobacteria are blue-green algae, which are primarily found in tropical waters. Zubkov and Quaterly (2003) noted that these algae are present in the Mozambique Channel. A common genera is the *Oscillatoria,* which is relative abundant in tropical open oceans.

3.3 Primary Production

There are two important roles for phytoplankton in the global ecosystem: (1) Phytoplankton makes up the base for the marine food web. Small oceanic animals called zooplankton are grazing on the phytoplankton. In turn, larger species of fish and mammals consume the zooplankton. (2) Phytoplankton can fix inorganic carbon and convert solar to chemical energy and therefore contributes to the global carbon cycle. As the phytoplankton increase in number and mass, they convert the CO_2 in the upper water column to organic carbon. Their rate of

growth and of carbon fixation is called *primary production.* Measurements of ocean color from space depend on the small scale nature of photosynthesis. Most oceanic carbon is inorganic and the photosynthetic pigments within each phytoplankton cell make possible the reduction of carbon dioxide into organic carbon, so that solar energy is converted to chemical energy, with oxygen as a by product. The pigments consist of chlorophyll-*a*, accessory pigments chlorophyll *b* and *c* and the photosynthetic carotenoids. These pigments account for about 95% of the light absorbed by phytoplankton (Aiken *et al.,* 1995). These photosynthetic pigments absorb light energy in the wavelengths ranging from 400 nm to 700 nm, which is the photosynthetic available radiance (PAR).

The most important phytoplankton pigment is reckoned as chlorophyll-*a,* which is often used as an index for the phytoplankton biomass (the total weight of all organisms in a given area) (Morel, 1998). This because chlorophyll-*a* is present in all species of phytoplankton and can be measured both *in situ* and by remote sensing methods. In addition is chlorophyll-*a* the most important parameter which influence ocean color. Biomass is. Phytoplankton co-exists also with other small size organisms such as zooplankton, viruses etc. It turns out to be difficult to separate the optical properties for the various organisms in the oceans but measured optical signal from phytoplankton dominates over the others (Sathyendranath *et al.,* 2000). When dealing with phytoplankton in a remote sensing context it also involves other microscopic organisms because measured optical signal from phytoplankton dominates over other microscopic organisms (Sathyendranath *et al.,* 2000). Absorption and scattering coefficients can be estimated relative to chlorophyll-a. The absorption and scattering characteristics for phytoplankton varies with time, space and the phytoplankton's physiological condition (Kirk, 1994).Because the pigment packaging differs from species to species, the response to incident light can differ by species for the same chlorophyll concentration. Whereas chlorophyll is a measure of biomass, primary production is a measure of phytoplankton growth and the two are not necessarily related.

3.4 Phytoplankton growth

Knowledge of the primary production's magnitude is important for an understanding and management of the pelagic, benthic and neretic ecosystems, fisheries and aqua cultures, in edition of how increased nutrition supply influence primary production. Waste products from farming, industry and households can be transported into oceans via drainage and rivers. This water can be very nutritious and a consequence can be that phytoplankton is reproducing itself

strongly. This phenomenon is called a phytoplankton bloom. Good access to light, nutrients, and favorable water temperature are the key components which influence the phytoplankton production rate. The environmental factors can be either natural or human made. When the phytoplankton dies, the cells will be decomposed by bacteria. This process requires oxygen which can lead to anaxic conditions in the influence areas. Organisms which require oxygen will be heavily influenced by the situation and the result may for example be fish death and the biological productivity may shrink. Some types of phytoplankton produce toxic substances. If there is a high concentration this type of phytoplankton species a result can be fish death and other biological death; this phenomenon is often called harmful algae bloom (HAB).

The photosynthesis occurring is proportional with the light intensity up to some maximum value. If the light is even more intense, the amount of photosynthesis may decline (photoinhibition). The physical- chemical environment that controls the phytoplankton growth is not constant. The amount of radiation and temperature changes daily and seasonally and with latitude. In regions where there is a seasonal thermocline present periods of storms and intense winds will break down the thermocline and. Water from below and above the thermocline is mixed. Nutrients are then brought up to the euphotic zone . When the surface layer cools and the thermocline is weekend convection occurs and nutrients are brought up to the surface. Wind mixing, is generally latitude dependent and increases from the tropics to the poles. Nutrient availability and light availability is hence inversely related (Lalli & Parsons, 1993). Coastal areas have, in general a higher primary production than the open oceans. The most important factors are inputs from rivers and coastal upwelling which brings nutrients to the euphotic zone.

The amount of light strongly affects both the amount and rate of photosynthesis which is illustrated in Figure 3-1. The figure shows that there are seasonal variations in the phytoplankton content and that these are latitudinal dependent. Starting with (a) the mid-latitudes, there is a seasonal cycle where a shallow thermocline is formed in the summer, the spring bloom is lowering the nutrients and a bloom in the autumn sometimes occurs when the nutrients are recycled. In the high latitudes, a short summer leads to a strong phytoplankton bloom. The Nutrients are not lowered because there no thermocline and continuous vertical mixing bringing nutrients to the euphotic zone. In the tropics (c), the permanent thermocline

restrains vertical mixing which leads to a permanent impoverishing of the nutrients in the photic zone. Phytoplankton abundance is therefore limited through the seasons.

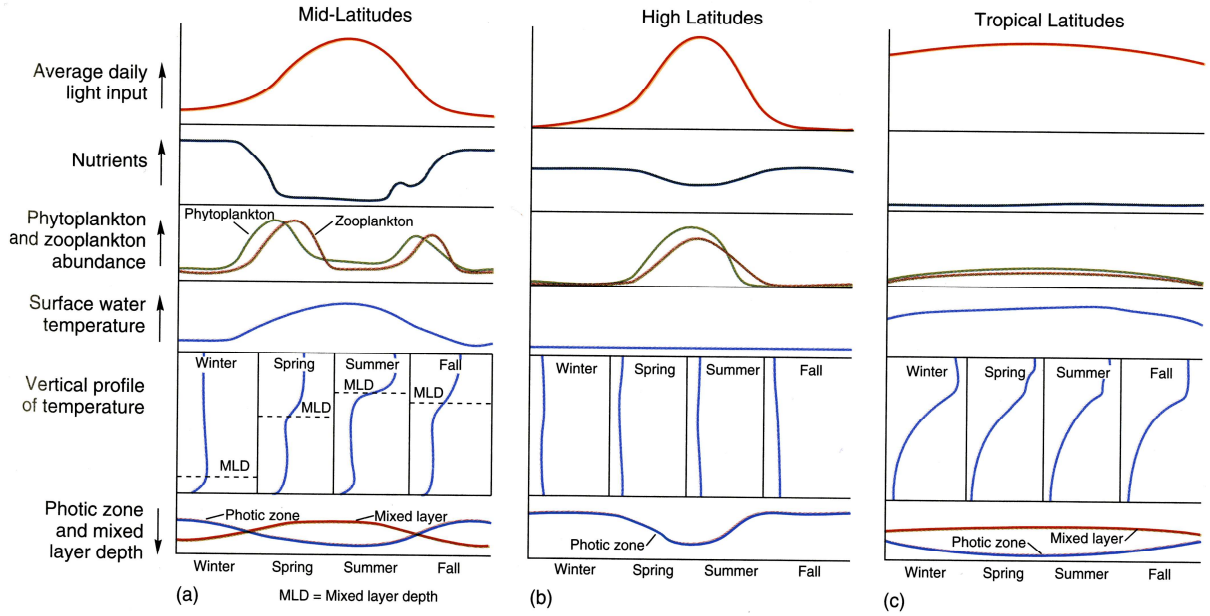

Figure 3-1. Seasonal variations in the nutrient concentration, phytoplankton biomass, water temperature and solar radiation intensity. Adapter from Segar (1998).

3.5 Biophysical Interactions

The biology in the oceans and, thus phytoplankton distribution and abundance is under influence of chemical and physical processes in the oceans. The spatial and temporal scales of these processes vary greatly. Biological distribution is often of a patchy nature which varies in time and space resulting from interactions between biological and physical factors (Srokosz, 2000). The dominant factors are changing with scale. The spatial resolution of the satellite sensor used is limiting the scales that it is possible to study (usually 1 km), but large scale processes (1000 km) and mesoscale processes (10-200 km) is possible to study.

3.5.1 Large scale

The link between the large scale physical structures and the biology, including phytoplankton distribution, was earlier determined *in situ* measurements from ship surveys. Now, the continuous use of remote sensing of ocean color has provided new insights regarding the spatial and temporal distribution of phytoplankton in the oceans of the earth. Latitudinal variation in the phytoplankton abundance and production is due to the fact that less radiation

is available to the photosynthesis from the equator to the poles. The inverse relationship is due to increased wind mixing which leads to nutrients being brought up to the euphotic zone. These two phenomena are temporally dependent. For example can phytoplankton blooms in the winter be due to increased wind activity (f. ex. winter storms) in this season.

3.5.2 Mesoscale

Mesoscale can be defined as phenomena in the spatial scale in the range of 10-200 km. Including in this is river plumes, gyres, rings, tidal and shelf-break fronts. Ocean fronts are regions where variables such as density, salinity and temperature experience a strong gradient over relative short distance. The spatial scale of fronts varies greatly and is determined by topography and ocean climate (Lalli & Parsons, 1993). Fronts are important because higher biological activity is associated with them (Mann & Lazier, 1996). Frontal processes, such as upward velocities, can bring nutrients up to the euphotic zone, which results in increased phytoplankton production. On the other hand, can downward velocities bring the phytoplankton outside of the photic zone, thus limiting the photosynthesis.

3.5.2.1 River plume fronts

Rivers carrying freshwater to the sea is often brining along high loads of nutrients, which provides favorable conditions for phytoplankton growth off the river mouth. The less saline and lighter water, which is entering the ocean waters, has an elevated surface and is brought forward by gravity and is lying on the top of the denser and more saline ocean waters. The fronts are usually distinctly marked by lines of foam and by a clear variation in color. (Mann & Lazier, 1996). The river flow may also lead to nutrients being brought up to the sea surface. If the spatial scale is unrestricted by coastal topography and stirring by winds are weak, the freshwater discharge tends to flow parallel to the coast due to the Coriolis effect. An example of this is shown in Figure 3-2. The runoff from the Zambezi River in Mozambique is clearly flowing to the left upon entering the Mozambique Channel as indicated by the low salinity. In a study by Grange *et al.* (2000) clear correlation between the amount or runoff and the amount of phytoplankton concentration was found in the Kariega and Great Fish estuaries on the South African east coast. Siddorn *et al.* (2000) used SeaWiFS data to map the Zambezi river plume.

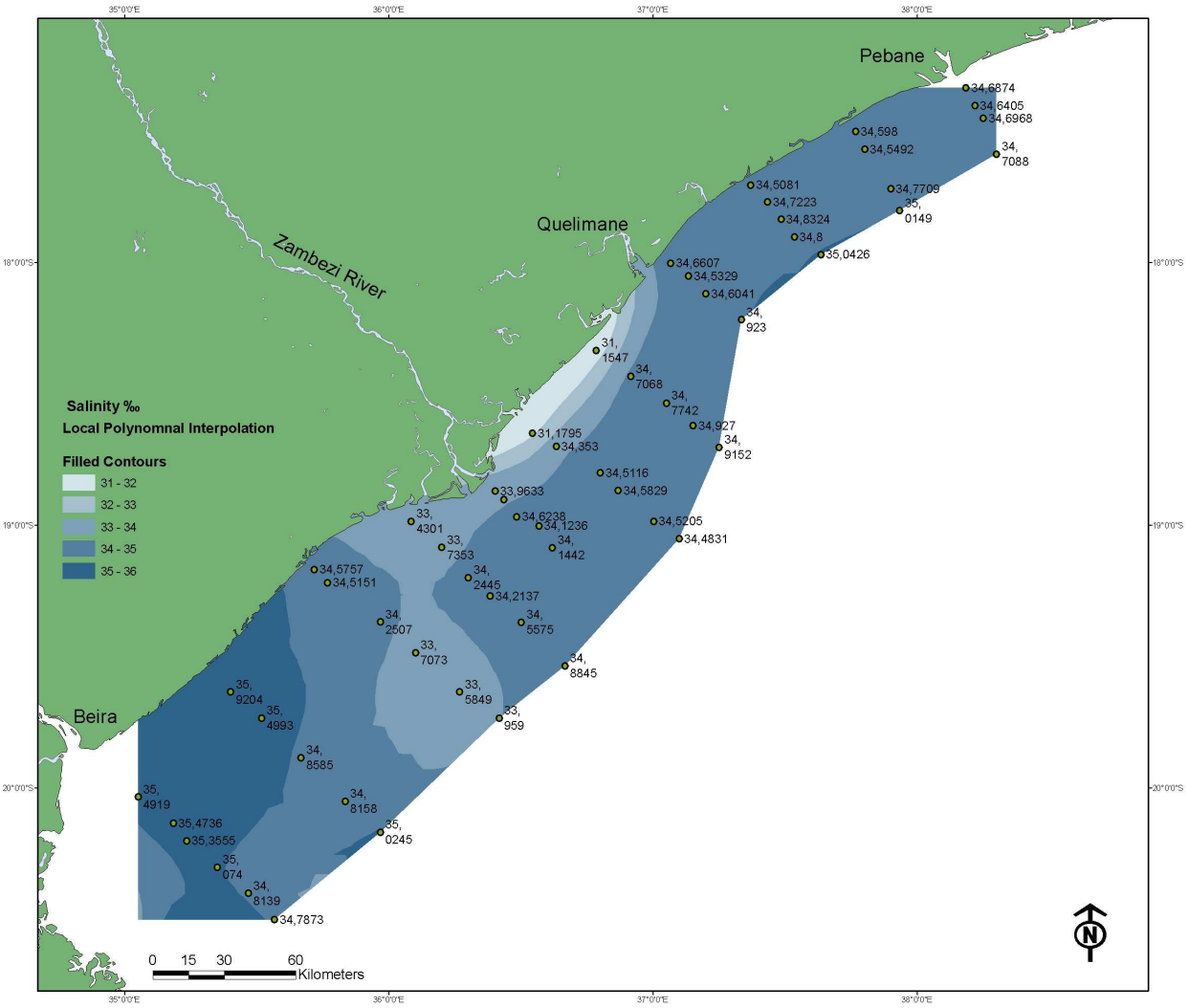

Figure 3-2. Sea surface salinity from the Sofala Bank, Mozambique. CTD data from February 2004. An interpolation has been performed for easier visualization. Data collected and provided by the Fisheries Institute in Maputo, Mozambique.

3.5.2.2 Upwelling Fronts

Coastal upwelling is driven mainly by winds causing surface waters to diverge from the coast and to be replaced by the upwelling of cold, nutrient rich waters from below. The new nutrients in the euphotic zone may lead to increased primary production. The interface between the upwelled colder waters and the offshore waters constitutes an upwelling front (Longhurst, 1998).

3.5.2.3 Shelf-Break Fronts

Along the edges of the continental shelves one may find shelf-break fronts. This type of front is created when (1) the bathymetry is rapidly shallowing a cross a continental shelf, (2) the speed of currents change when the waters feels the bottom, and (3) by tidal movement (Lalli & Parsons, 1993). Nutrients that are brought to the euphotic zone by turbulence as the current

velocity increases over a shelf can be used by phytoplankton. The shelf break can therefore experience high primary productivity.

3.5.2.4 Tidal fronts

Tidal flow on the continental shelf performs frictional stress in the seabed. The stress leads to turbulent energy which again leads to vertical mixing. Variation in the amount of tidal stirring of divide the shelf seas into well mixed and stratified zones separated by high gradient fronts (Simpson, 1981 in Mann & Lazier, 1996).

3.5.2.5 Eddies and gyres

Eddies and gyres are circular currents in the ocean, where the latter is associated with bathymetric features and large scale motions, and the former is a lower amplitude current variation of a smaller scale (usually between 10 and 100 km) (Mann & Lazier, 1996). Anticyclonic eddies and gyres experience a clockwise rotation in the northern hemisphere and an anti clockwise direction in the southern hemisphere. Due to the Coriolis Effect is the net transport to the core of the ring. The convergence of the water masses leads to an elevated surface and a deepening of the thermocline. Anticyclonic eddies and gyres are characterized by low production since no new nutrients are brought up to the euphotic zone.
Cyclonic eddies and gyres are circulating in a clockwise direction in the southern hemisphere and in an anticlockwise direction in northern hemisphere. The Coriolis Effect result in divergence which carries water away from the circulation core. Colder water from below is brought up along with the nutrients resulting in more primary production.

3.6 Summary

The amount of solar radiation and nutrient availability are the two major factors that control the phytoplankton abundance in the sea. Each phytoplankton species has its own particular reaction to the different physical factors. Nutrient availability is determined by physical forces which influence the vertical mixing. Conditions for phytoplankton growth are met when nutrients are available and the presence of solar radiation is sufficient. Then the phytoplankton population is readily observed from space by remote sensors. In this chapter, a short description of various phytoplankton species has been give in addition to a description of the environmental behavior. A special feature of the phytoplankton communities is their patchy distribution with sharp boundaries between. This means that research cruises easily can miss an area with an abundant phytoplankton distribution. Again, remote sensing is very

useful for detecting areas of enhanced phytoplankton production that is not sampled by ship survey.

4 REMOTE SENSING OF OCEAN COLOR

4.1.1 Definition of Remote Sensing

Remote sensing can be defined as the science and art of obtaining information about an object, area or phenomenon through the analysis of data acquired by a device that is not in contact with the object, area or phenomenon under investigation. The first keyword, analysis of data, indicates that it not only includes data gathering, but also the analysis of this data and the interpretation of further use of the results. The second, not in contact, contrasts it with *in situ* measurements in which the measuring devices are either immersed in or touch the object of observation. According to the definition given, seeing is remote sensing, an indeed it is. But usually the term is used for a sub – field, remote sensing from space, i.e. getting measurements from spaceborn devices such as satellites.

Remote sensing of ocean color is an analysis of variations in magnitude and spectral quality of upward radiance from the sea with the purpose of quantifying information of substances in the ocean and their concentration (Sathyendranath *et al.,* 2000). Ocean color is determined by scattering and absorption of visible light in the ocean and gives information about the concentration of phytoplankton and suspended materials in the upper layer of the ocean. The color producing agents (CPAs) are pure water, phytoplankton, and organic and inorganic substances which are suspended in the water. The water color can be considered as a convolution of light interactions with CPAs and water molecules, and as such is not infrequently exploited as a quality characterizing the current ecological/sanitary/resources status of the aquatic environment (Pozdnyakov & Grassl, 2003). This information can be used to investigate biological productivity in the oceans; give information about marine optical properties; give information about interaction between wind, currents and marine biology; and provide knowledge on how human activities influence the marine ecosystem. Passive remote sensing systems for measurement of ocean color uses sensors that can measure radiometric flux in various wavelengths in the visible and near infrared (NIR) part of the electromagnetic spectrum. The sensors are usually placed on a satellite or a plane and operate in daylight.

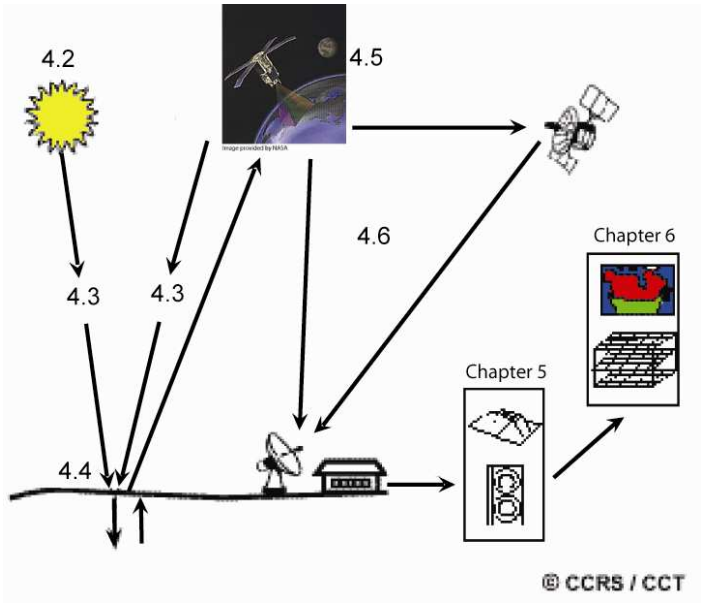

Figure 4-1. The remote sensing process. Chapter sections are shown on the image. Modified from "Fundamentals of Remote Sensing" (http://www.ccrs.nrcan.gc.ca/resource/tutor/fundam/pdf/fundamentals_e.pdf)

The structure of this chapter will follow Figure 4-1. First, properties of electromagnetic radiation, the element which is measured by remote sensors is considered (4.2). As the electromagnetic radiation reaches the atmosphere and is subject to scattering and absorption (4.3). When reaching the earth's surface, the radiation is further modified by scattering and absorption (4.4). The scattered or emitted radiation is recorded by a remote sensing device after passing the atmosphere (4.5). The recorded energy is transmitted to a receiving station for processing (4.6) The next step is to analyze the images in order to extract useful information about the features of interest (this is the methods and is described in chapter 5) The last element in the remote sensing processes is to apply the information interpreted into new information, increased insights and problem solving for the target or area of interest (described in chapter 6).

4.2 Electromagnetic radiation

In order to produce an image using data obtained by a remote sensor, it is necessary to measure electromagnetic (EM) radiation reflected or emitted from a scene. The nature of the electromagnetic radiation is therefore necessary to know. Every object with a temperature above absolute zero (-273°C) can absorb, emit or reflect RM. When recording the emitted or reflected energy and applying knowledge to the behavior as it traveling trough the atmosphere and interacts with features of the earth, the character of the feature of interest can be revealed. The measurements of ocean color are based on EM radiation of 400-700 nm wavelength. EM

radiation has a dual nature which can be described as both particles and waves. The wavelength of the electromagnetic radiation is a critical feature in remote sensing because the energy reflected or emitted from the earth's surface is recorded in narrow bands at certain wavelengths. The amount of energy that is detected within each band is containing information about the features of interest. Wavelength and frequency by a wave of EM radiation is related by the formula:

$$c = \lambda v$$

where λ =wavelength (m)

v = frequency (cycles per second,Hz)

c = speed of light (3×10^8 m/s)

This means that the shorter the wavelength, the higher is the frequency, and visa versa.
If we consider electromagnetic energy as being composed by photons we have the formula

$$Q = fh$$

where Q = energy of a quantum (joules J)

h = Planck's constant 6.626 x 10 -34 J sec

f = frequency

By substituting c=f λ for f, then Q = hc / λ. The equation tells that longer wavelengths have lower energy levels and shorter wavelengths have higher energy levels. Any object at a temperature higher than absolute will emit some radiant energy; therefore earth also emits radiation. The amount of radiation an object emits depends primarily on It is temperature. The equation for total exitance from a surface at given temperature is given by Stefan – Boltzmann's law:

$$M = \sigma T^4$$

where M = total radiant exitance from the surface of a material, watts m²

σ = Stefan-Boltzmann constant, 5.6697 x 10 -8 W m-2 K-4

T = absolute temperature K of the emitting material

Dominant wavelength radiation from an object is related to temperature by the following equation (Wien's displacement law):

$$\lambda = \frac{A}{T}$$

where λ = λ of maximum spectral radiance exitance μm

A = constant, 2898 μmK

T = temperature, K

The wavelength at which an object is emitting maximum energy is inversely proportional with temperature. The properties of the EM radiation are important to know since passive systems depend on solar radiation and their characteristics will have an impact on the outcome.

4.3 Transmission through the atmosphere

The atmosphere may absorb, reflect or scatter the rays to an extant such that only a small portion of the radiance measured by a satellite can be traced back to the water-leaving radiance, which is the only radiant feature that carries useful information about ocean color. The absorption is also affected by atmospheric aerosols, which include the water droplets and salt nuclei in the marine boundary layer, and the particulate matter generated over land by biomass burning, human made pollution and volcanic eruptions (Martin, 2004). The presence of fixed concentrations of atmospheric gases such as oxygen, carbon dioxide, plus the variable concentrations of water vapor absorb EM radiation at certain wavelengths which means that only a few windows exist in the visible, infrared and microwave for earth observations as shown in Figure 4-2. The visible part of the EM spectrum is an example of an atmospheric window suitable for remote sensing.

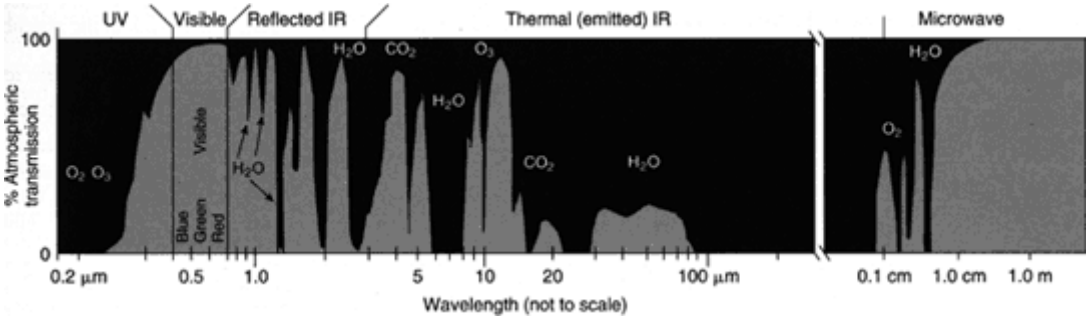

Figure 4-2. Diagram of atmospheric windows—wavelengths at which electromagnetic radiation will penetrate the Earth's atmosphere. Chemical notation (CO_2, O_3) indicates the gas responsible for blocking sunlight at a particular wavelength. Source: (http://earthobservatory.nasa.gov/Library/RemoteSensing/remote_04.html).

4.3.1 Scattering

Scattering is an important consideration in remote sensing investigations. It can severely reduce the information content of remotely sensed data to the point that loses contrast and it becomes difficult to differentiate one object from another. Scattering affects the directions of the light field after an interaction with a substance or a medium and can be wavelength dependent, which means that within a light- substance interaction some wavelengths will be redirected and some continue unaffected by the interaction. Scattering differs from reflection in that the direction associated with scattering is unpredictable. There are essentially three types of atmospheric scattering: Mie-, Rayleigh- and Nonselective scattering. The size of the wavelength of the incident EM radiation and the relative diameter of the feature the EM radiation is interacting determines the type of scattering. The different types of scattering processes can be divided into *elastic* and *inelastic* scattering. Elastic scattering is when the energy level of the EM radiation is not changed after the scattering has occurred (e.g. the frequency and wavelength of the EM radiation is constant). Inelastic scattering involves a change in the energy level of the EM radiation after the scattering has occurred (e.g. the frequency and wavelength of the EM radiation have been changed).

Rayleigh scattering (molecular scattering) occurs when the effective diameter of the matter (usually air molecules such as oxygen and nitrogen in the atmosphere) are many times smaller (usually <0.1) than the wavelength of the incident electromagnetic radiation. This type of scattering is mostly influencing the shorter wavelengths like UV radiation and in the blue part of the electromagnetic spectrum and is taking place in the upper part of the atmosphere. Rayleigh scattering can be considered to be elastic scattering since the photon energies of the scattered photons is not changed.

Mie scattering (nonmolecular or aerosol particle scattering) takes place in the lower 4.5 km of the atmosphere, where there may essentially spherical particles present with diameters approximately equal to the size of the wavelength of the incident energy (Jensen, 2005). For visible light, the main scattering agents are dust and other particles ranging from a few tenths of a micrometer to several micrometers in diameter. The amount of scatter is greater than Rayleigh scatter, and the wavelengths scattered are longer.

Nonselective scattering occurs because of radiance interaction with particles with a greater diameter than the radiance wavelength. This holds for light in both the visible and near infrared part of the electromagnetic spectrum. Nonselective scattering takes place in the lowest part of the atmosphere where there are particles >20 times the wavelength of the incident electromagnetic radiation. All wavelengths are scattered, in equal amounts in all directions

Raman scattering occurs when radiation changes its energy level (e.g. frequency and wavelength) as it is scattered. Usually this kind of scattering involves exciting some vibrational mode of the molecules, giving a lower scattered photon energy, or scattering off an excited vibrational state of a molecule which adds its vibrational energy to the incident photon (Cracknell & Hayes, 1993).

4.3.2 Absorption

Absorption is the process where the radiant energy is absorbed and converted into other forms of energy. The absorption of radiant energy may happen either in the atmosphere or in the earth's surface. When EM energy interacts with a feature and the incident energy is transformed into heat motion and is subsequently reradiated at a longer wavelength, absorption occurs. It also occurs when incident energy of the same frequency as the resonant frequency of an atom or molecule is absorbed (Jensen, 2004). In a medium like air, absorption and scattering are frequently combined into an extinction coefficient.

The different constituents of the atmosphere that have an influence on the radiance can be divided into well-mixed, constant constituents and variable constituents (Martin, 2004). The constant constituents include oxygen, nitrogen, and trace gases. Since the troposphere is well mixed, their relative concentration is constant regardless of geographic location. The different features in the atmosphere that have optical influence on EM radiation are presented here:

- Atmospheric aerosols are small liquid or solid particles suspended in the atmosphere and are divided into marine-, land- and volcanic generated aerosols. The volcanic aerosols are emitted into the atmosphere by volcanoes and consist of droplets of sulfuric acid and other suspended materials. These aerosols can cause trouble for the algorithms used for calculating SST and ocean color because of the scattering and absorption from the constituents. The effect can last for years.

- Clouds are made up from small liquid and ice particles with sizes that range from under a micrometer to a few millimeters. Compared with the surface of the oceans, thick clouds are very reflective in the visible/infrared. The liquid water and ice crystals contained in clouds can scatter and absorb radiation. This means that where there are thick clouds present, accurate measurements are difficult to obtain.
- Atmospheric Water in the atmosphere is major contribution to the atmospheric absorption, despite its small contribution to the atmospheric mass.
- Ozone is an principal component of the stratosphere and forms from the dissociation of oxygen molecules by solar radiation. In a remote sensing context, the ozone attenuates visible radiation with a seasonal and latitudinal dependence and must be considered when retrieving ocean color signals.

4.4 Light interaction with the oceans

4.4.1 Considerations

The presence of phytoplankton (microscopic algae) in the upper layer of the ocean changes the ocean color as seen from above. The reason for this is the selective absorption of blue light by phytoplankton pigments (primarily chlorophyll-a) for use in the photosynthesis process. Changes in ocean color can be observed by spectro-radiometers that measure the water leaving radiance in several intervals in the visible part of the electromagnetic spectrum. This technique is limited by several factors: (1) Information about phytoplankton can only be measured in the upper layer of the ocean because light does not penetrate far in water due to absorption of radiation by water molecules. (2) The largest part of radiation measured by an ocean color sensor has its origin in the atmosphere from aerosol- and molecular scattering. Removal of atmospheric radiation contribution is crucial for ensuring data of good quality. (3) Just one component in the marine ecosystem, that is phytoplankton, can be observed from space. Retrieval of ocean color is a complex task. Unlike observations in the infrared, where the radiation is emitted from the top 10-100 nm of the sea surface, ocean color radiances in the blue-green can be upwelled from depths as great as 50 m. Also, because in the visible, aerosol and molecular scattering dominate atmospheric attenuation, the water-leaving radiances only compromise about 10% of the total received radiance (Gordon, 1997). This means that determination of the water-leaving radiances requires precise determination of all other radiances in order to isolate it. Both freshwater and seawater is a mixture of suspended material which is optically significant and highly variable in type and concentration. Optical

properties of seawater and freshwater show large temporal and spatial variation because of the different constituents that are present in the waters (Mobely, 1994).

At all wavelengths received by an ocean color sensor, the properties of these depend on the small scale interaction of the radiation with the air/water interface. The ocean is absorbing in the infrared to such an extent that absorption and emission are limited to the upper most 1-100 μm of the ocean; and the upper most 1-3 mm in the microwave (Martin, 2004). When not considering the atmosphere, the ocean color sensor will receive signals in these bands that is only dependent on the scattering and reflection at the ocean surface. The measured radiance in the visible part of the EM spectrum is in addition dependent on the backscatter of solar radiation in the water column. Thus, there are three different ways the surface itself influences the light that leaves the ocean surface in the direction of the sensor (Robinson, 2004). (1) The surface directly reflects light and skylight. This is angularly dependent. (2) There may be present colored particles at the surface which reflects the radiation. (3) The air-water interface refracts the light coming from below the sea surface.

4.4.2 Pathways to the sensor

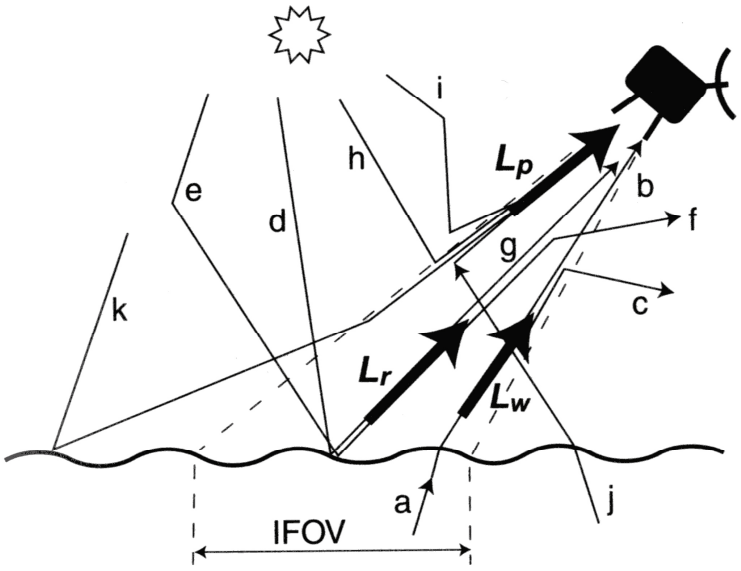

Figure 4-3. Possible paths of Electromagnetic radiation between the sea and the sensor. Adapted from Robinson (2004). IFOV – Instantaneous Field Of View: the area on the surface that is viewed by the remote sensor from a given altitude at any given time

Figure 4-3 illustrates the various pathways can take before it is measured by an ocean color sensor. The different radiation highways consist of:

(a) Electromagnetic radiation which is leaving the sea surface within the IFOV of the sensor

(b) The part of the water leaving radiance L_w which is measured by the sensor

(c) Radiation from the water leaving radiance L_w which is scattered out of the IFOV of the sensor. The radiation can also be absorbed and not detected by the sensor

(d) Electromagnetic radiation from the sun which is reflected by the sea surface into the IFOV of the sensor. This phenomenon is called sun glitter.

(e) Electromagnetic radiation which is scattered in the atmosphere by particles and molecules before it is reflected by the sea surface into the IFOV of the sensor. This phenomenon is the sky glitter

The sun glitter (d) and the sky glitter (e) both make up the radiance just above the sea surface L_r, which is the combination of all radiances due to sea surface reflection

(f) This is the portion of L_r which is scattered out of the IFOV view by molecules and aerosols in the atmosphere

(g) Electromagnetic radiation from L_r which is measured by the sensor

(h) Electromagnetic radiation from the sun which enters the IFOV in the atmosphere and is scattered towards the sensor

(i) Electromagnetic radiation which is previously scattered in the atmosphere before it reaches the IFOV of the sensor. The radiation is then scattered towards the sensor

(j) Electromagnetic radiation which has been upwelled from an area outside the IFOV. The radiation is later scattered by the atmosphere into the IFOV and measured by the sensor. This part of the measured radiance is not a part of the water leaving radiance L_w, which is per definition the brightness of the sea *within* the IFOV of the sensor (Robinson, 2004).

(k) Electromagnetic radiation which is reflected by the sea surface outside the IFOV and subsequently scattered by the atmosphere into the IFOV and measured by the sensor

The remote sensing sensor measures the signal of upwelling irradiance, which is the solar radiation reflected from the water surface and backscattered from the water column and the atmosphere, at some height from the ocean surface. The basic equation of radiative transfer

for ocean color of water bodies assumes separability of the radiance contributions from atmospheric and oceanic components (Gordon & Wang, 1992):

$$L_t(\lambda) = L_r(\lambda) + L_a(\lambda) + L_{ra}(\lambda) + T(\lambda)L_g(\lambda) + T(\lambda)L_w(\lambda)$$

where

- L_t is the total radiance measure by a sensor
- L_r is the radiance resulting from multiple scattering by air molecules in the absence of aerosols
- L_a is the radiance resulting from multiple scattering by aerosols in the absence of air
- L_{ra} is the period of multiple interaction between molecules and aerosols
- L_g is the radiance at the sea surface that arises from sunlight and skylight reflecting from this surface including reflection from whitecaps
- L_w is the water leaving radiance
- T is the total transmittance that takes into account the propagation L_w and L_g from the sea surface though the atmosphere to the remote sensing instrument

4.4.3 The water-leaving radiance

The water-leaving radiance, L_w, is the part of the total measured radiance by a ocean color sensor that is containing information about constituents that is coloring the oceans. While Figure 4-3 shows the total amount of radiation measured by a sensor is Figure 4-4 showing constituents and factors that is influencing L_w .Electromagnetic energy that enters a water column is optically influenced by: (1) absorption and scattering by pure water and (2) scattering and reflection by suspended material. These interactions determine the color of ocean waters, which is the water-leaving radiance. The scattering of photons is a function of wavelength of the photon, and the size and shape of the features that the radiance interacts with. Three groups of substances are reckoned as being significant for the absorption properties in sea water in addition to sea water itself, namely: phytoplankton, colored dissolved organic matter and inorganic suspended material

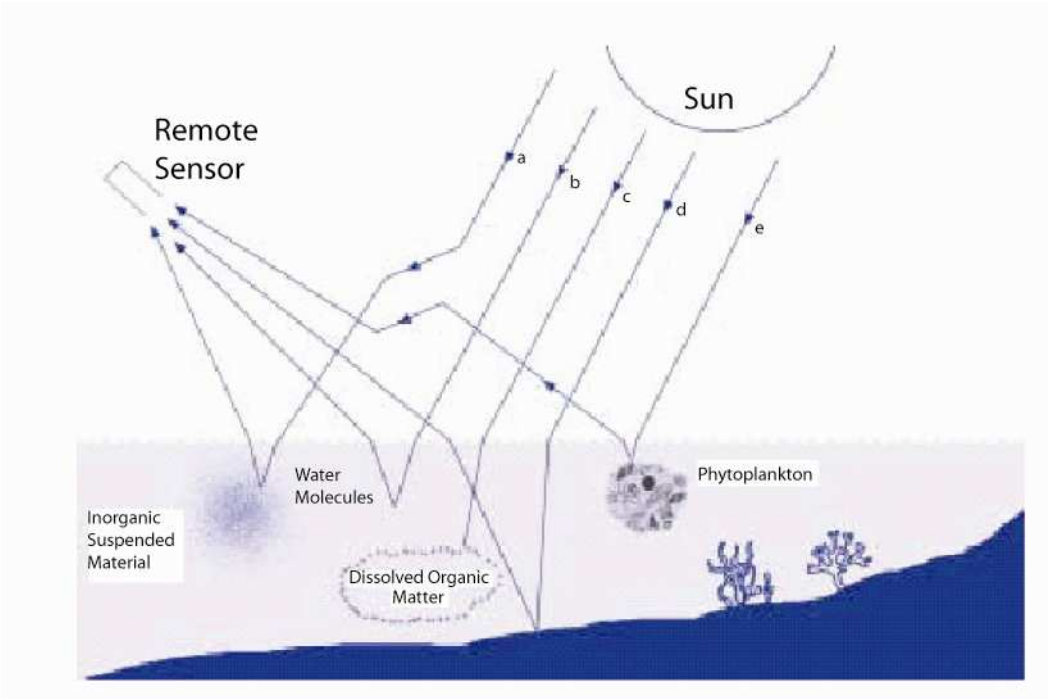

Figure 4-4. Factors that influence the water-leaving radiance: (a) Radiance scattered by inorganic suspended material. (b) Radiance scattered by water molecules. (c) absorption by colored dissolved organic matter. (d) Bottom reflection. (e) Radiance scattered by phytoplankton. Modified from Sathyendranath *et al.*, (2000).

4.4.4 Absorption and scattering of constituents in sea water

Downwelling solar irradiance, penetrating through the air-water interference into the water and from the subsurface layer into deeper layers, is absorbed or scattered/back-scattered on its way by water itself as well as by optically active substances (OAS) in the sea water. Absorption and scattering processes attenuate the irradiance and change its spectral composition. Interpreting the measurement result of underwater irradiance and optical remote sensing there is a need for information on the optical properties of the water constituents. The total absorption and backscattering coefficients can be expressed as the sums of the corresponding coefficients of these substances (Arst, 2003).

Scattering of light in the ocean waters is partly dependent on the size of the particulate that interacts with the EM energy. Viruses has diameters of 10-100nm and because of their small size they can act as Rayleigh scatterers. Bacteria generally have a diameter of 0.1-1 μm and can absorb significantly in the blue part of the EM spectrum. Phytoplankton has a diameter that ranges from 2-200 μm. Because they tend to have a diameter that is larger than the wavelengths in visible, they tend to be Mie scatterers. From Mobely (1994), we find that even

if there is only a small amount constituents of some sort generates a strong forward scatter and thereby increases the scattering coefficient.

Colored dissolved organic matter (CDOM) is a group of organic suspended substances which consists of humic and fulvic acids. They may have a local origin from degradation of phytoplankton and other organisms, or they may have an external origin. Rivers are an example of the latter, where they accumulate CDOM during the journey to the oceans. In areas which is not influenced by river runoff CDOM is related to the concentration of primary production, then as a by-product of degradation by algae cells (Carder *et al.,* 1989).

Marine colored dissolved organic matter (CDOM) absorbs light in an exponentially decreasing manner as a function of wavelength. Pheopigments, detrius, and bacteria similarly absorb more strongly at 412 nm than they do at 443 nm. Phytoplankton, on the other hand, absorb more strongly at 443 nm than at 412 nm. Thus, by measuring the relative amounts of radiance leaving the sea surface at both these wavelengths, it is possible to estimate the relative amounts of phytoplankton and the other absorbing substances (Carder *et al.*, 1999). CDOM has earlier been thought of as a terrestrial product or as a product with a terrestrial origin, but CDOM is also made when grazing, photolysis (a chemical reaction that breaks down compounds to due to light) and various other mechanisms degrades plant matter at and downstream from phytoplankton blooms (Carder *et al.*, 1999).

Bottom effect

Reflected radiance from the sea bottom in shallow areas with clear waters may influence the water-leaving radiance. The maximum depth where a sensor receives a signal will vary with wavelength and turbidity. Scattering by water molecules will limit the distance of penetration in the water. Absorption by suspended organic material and phytoplankton will in addition limit the radiation as a function of depth. The amount of influence is connected to depth, clarity and types of substances present in the water.

4.4.5 Different types of water, Case 1 & Case 2.

According to the optical classification by Morel & Prieur (1977) can waters be classified as either Case 1 or Case 2. Case 1 waters are those water masses where phytoplankton and associated materials is the dominant factor which influences ocean color and the optical properties of water. Case 2 waters are those ocean areas where other substances than

phytoplankton, such as CDOM and inorganic suspended material, varies optically independent of phytoplankton and where these plays important roles for determining ocean color. Case 2 waters are typically found in coastal areas and inland lakes while Case 1 waters are typically found in the open oceans.

This type of classification does not imply the possibility that other substances than phytoplankton have impact on the optical characteristics of Case 1 waters. The contribution of other substances is fairly small and can be modeled as a function of the phytoplankton concentration (Yoder, 1999). An implication of the classification is that the optical properties of Case 1 water can be modeled as a function of chlorophyll-a concentration (Sathyendranath *et al.,* 2000). This because one assumes that other optically active substances than phytoplankton co-varies with phytoplankton in Case 1 waters and that chlorophyll-a is reckoned as an indicator of phytoplankton concentration. Thus, if the chlorophyll-a variable is the only color index that is taken into account (because of the assumed co-variation with other substances), this will lead to that the optical properties at any given wavelength can be foreseen if we know the value of an optical property, for example chlorophyll-a absorption, in the green part of the electromagnetic spectrum.

In case 2 waters there are no longer just one dominant optical variable. In addition of phytoplankton there is suspended inorganic material and CDOM as the most important factors. The concentration of the various optical parameters can vary independent of each other and have different optical characteristics One can no longer assume that there is a more or less direct link between optical properties and chlorophyll-a concentration as in Case waters. CDOM is only affecting the absorption coefficient while suspended materials can heavily influence the scattering coefficient, with less affect for the absorption (Morel *et al.,* 1998). Measured changes of reflected radiation which correspond with change in the concentration are often very small.

4.5 Ocean Color Satellites

The focus in this part will be the characteristics of some past and present ocean color sensors. The forerunner of all ocean-color satellite sensors, the CZCS (1978-1986), has led to a series of increasingly-sophisticated instruments: MOS, OCTS, POLDER, and SeaWiFS launched in 1996-1997, and MODIS, MISR, OCM, GLI, OCI, OSMI, MERIS, and POLDER-2 launched in 1998-2000. The sophistication, and expected improvements, have mainly consisted in

better radiometric performances (in terms of dynamical range and signal-to noise ratio), and in increased number of spectral channels (from 5 for CZCS up to 36 for MODIS and GLI). Many additional channels are actually devoted to terrestrial vegetation and atmospheric features, since these new instruments are designed to fulfill multipurpose missions. Other kinds of sophistication were also introduced to allow multi-angle viewing capability (POLDER, MISR), and, in addition, to determine the state of polarization of the reflected radiation (POLDER 1 and 2). Such increased complexities in the sensor's design were a response to the demands of the scientific community, and were essentially based on new research objectives or exploratory projects. This goal implies the development of new experimental algorithms, and the definition of new products for the user community (Morel *et al.*, 1998). There will next be a short introduction of some selected ocean color sensors. The characteristics for all the ocean color sensors can be seen in Table 1. The CZCS, SeaWiFS and MODIS sensors are described in detail. The CZCS sensor was chosen because it was the first ocean color sensor that was launched and provided the pratical proof of method of ocean color remote sensing, while the SeaWiFS and MODIS sensors are described because data from those sensors are used in this thesis.

Table 1: Characteristics of past and present Ocean Color sensors

Sensor	**CZCS**	**OCTS**	**POLDER**	**MOS**	**SeaWIFS**	**OCI**
Agency	NASA	NASDA	CNES	DLR	NASA/OSC	Taiwan
Platform	Nimbus-7	ADEOS-1	ADEOS-1	IRS-P3	OrbView-2	ROCSAT
Start of operation	October 1978	August 1996	August 1996	March 1996	September 1997	January 1999
End of operation	June 1986	June 1997	June1997	-	-	
Inclination (˚)	99.3	98.6	98.6	98.7	98.2	32
Equator crossing	12.00	10:41	10:41	10:30	12:00	09:00/15:00
Altitude (km)	955	804.6	804.6	817	705	600
Nadir resolution (km)	0.825	0.7	6.0 x 7.0	0.5	1.1	0.8
Swath (km)	1566	1400	2400	200	2800	704
Tilt (˚)	±20	±20	Variable	None	±20	None
Calibration method	Lamp	Solar, lamp	None	Solar, lamp	Solar, lunar	

Sensor	**OCM**	**MODIS Terra**	**MODIS Aqua**	**OSMI**	**MERIS**	**GLI**	**POLDER-2**
Agency	ISRO	NASA	NASA	KARI	ESA	NASDA	CNES
Platform	IRS-P4	Terra	Aqua	Kompsat	Envisat	ADEOS-2	ADEOS-2
Start of operation	May 1999	January 2000	May 2002	December 1999	March 2002	December 2002	December 2002
End of operation	-	-	-	-	-	-	-
Inclination (˚)	98.3	98.2	98.2	98.1	98.5	98.6	98.6
Equator crossing	12:00	10:30	13:30	10:50	10:00	10:30	10:30
Altitude (km)	720	705	705	685	800	803	803
Nadir resolution (km)	0.36	1.0/0.5/0.25	1.0/0.5/0.25	0.85	1.2/0.3	1.0/0.25	6.0 x 7.0
Swath (km)	1420	2330	800	1150	1600	2400	
Tilt (˚)	±20	None	None	None	None	±20	Variable
Calibration method	Solar, lamp	Solar, lunar, lamp	Solar, lunar, lamp	Solar	Solar	Solar, lamp	none

4.5.1 Coastal zone color scanner (CZCS)

The observation of ocean color from space began in 1978 with launch of the Coastal Zone Color Scanner (CZCS) which was placed on the NIMBUS-7 satellite. The CZCS mission ended in June 1986, with some degradation problems in the later years. The mission goal was proof of concept and not that much as an operating satellite. Until 1996, all our practical experience of satellite ocean-colour techniques came from a single, experimental, satellite sensor: the Coastal Zone Colour Scanner (CZCS). Then, a new era began with the launch of the SeaWiFS sensor.

4.5.2 SeaWiFS

The *SeaStar* satellite (Orbview-2) developed by ORBIMAGE, Inc., in conjunction with NASA, carried the SeaWiFS into orbit using a Pegasus rocket on August 1, 1997. The final orbit was 705 km above the earth with an equatorial crossing time at 12 p.m. SeaWiFS builds on the knowledge gained about ocean remote sensing using the CZCS. The SeaWiFS sensor consists of an optical scanner with a 58.3º total field of view. Incoming radiation is collected by a telescope and reflected onto the rotating half-angle mirror. The radiation is then relayed to dichroic beamsplitters that separate the radiation into eight wavelength intervals. SeaWiFS has a spatial resolution of 1.13×1.13 km (at nadir) over a swath of 2800km, and a revisiting period of 1-2 days (depending on the latitude).

SeaWiFS records energy in eight spectral bands with narrow wavelength ranges tailored for the detection and monitoring of specific ocean phenomena, including ocean primary production and phytoplankton processes, ocean influences on climate processes, and the cycles of carbon, sulfur, and the cycles of carbon, sulfur, and nitrogen. In particular, SeaWiFS has specially designed bands centered at 412 nm (to identify CDOM through their blue wavelength absorption), at 490 nm (to increase sensitivity to chlorophyll concentration), and in the 765 and 865 NIR (to assist removal of atmospheric attenuation) (Robinson, 2004).

4.5.3 Moderate-resolution imaging spectrometer (MODIS) Aqua/Terra

The MODIS sensors are placed on NASA's EOS *Terra* (a.m. equatorial crossing time) and *Aqua* (p.m. equatorial crossing time) satellites. The sensor yields simultaneous observations of high-atmospheric, oceanic (SST and chlorophyll), and land surface features (Barnes *et al.*, 1998). MODIS is placed in a 705-km sun-synchronous orbit. The temporal resolution is 1-2 days and has a field of view of ±55º off-nadir, which provides a swath width of 2330 km. MODIS is a whiskbroom scanning imaging radiometer consisting of a cross-tracking scan mirror, collecting optics, and a set of linear detector arrays with spectral interference filters located in four planes. The sensor collects data in 36 spectral bands: 20 bands from 0.4 to 3 μm and 16 bands from 3 to 15 μm. MODIS provides a spatial resolution from 250×250 m (bands 1 and 2) to 500×500 m (bands 3 though 7) and 1×1 km (bands 8 through 36) (Esaias *et al.,* 1998).

4.6 Processing and parameters

4.6.1 Algorithms for the calculation of the chlorophyll content

To date, most of the quantitative applications of ocean color remote sensing have focused on the determinations of abundance and distribution of phytoplankton chlorophyll in the oceans. The determinations are essentially based on changes of ocean color from blue to green as the chlorophyll concentration changes. There are two major subdivisions of the algorithms used for calculating concentrations of chlorophyll-a based on radiance measured by ocean color satellites, namely: empirical and semi-analytical algorithms.

4.6.2 Empirical algorithms

Empirical algorithms are essentially based on applying a simple regression between the field determinations of pigment concentration and the spectral ratios of ocean reflectance or normalized water-leaving radiance. The input parameter in empirical algorithms is the water-

leaving radiance of various wavelengths and the output parameter is the chlorophyll concentration (Martin, 2004). The empirical algorithms are designed to work in Case 1 waters. In Case 2 waters, the agents vary independently of phytoplankton and each other. The consequence of the complexity is that single-variable optical models based on chlorophyll are generally inadequate; they break down in Case 2 waters. There is a general problem with performing satisfactory calculations of chlorophyll-a in Case 2 waters.

The following information is taken from Martin (2004). The value of using empirical algorithms is that they provide long term records from the CZCS, and later from SeaWiFS and MODIS observations. The SeaWiFS Bio-optical Algorithm Mini-Workshop began in 1997 the collection of *in situ* radiances and the corresponding chlorophyll values on a global basis. The SeaWiFS algorithm that proved the best fit on the data set was the maximum band ratio Ocean Chlorophyll-4 (OC4) empirical algorithm. This algorithm is the currently used algorithm used in the calculation of chlorophyll values which is available in the SeaWiFS standard products. The algorithm used whichever R_{rs} ratio (443/555, 490/555, 510/555) is the largest. OC4 is calculated from the following fourth order polynominal:

$$R_{MAX} = Maximum \text{ of } \left[\mathrm{R}_{\mathrm{rs}} - ratio(443/555, 490/555, 510/555)\right]$$

$$R_L = \log_{10}(R_{MAX})$$

$$\log_{10}(Chlorophyll \text{ concentration}) = 0.366 - 3.067R_L + 1.930R_L^2 + 0.649R_L^3 + 1.532R_L^4$$

It is known that this algorithm overestimates chlorophyll levels in Case 2 waters (Darecki & Stramski, 2004). The OC4 algorithm is shoved to produce chlorophyll measurements that lies within ±35% compared with the *in situ* data from the SeaBAM data set.

The MODIS empirical algorithm, called OC3 is based on the same principles as the OC4 algorithm and is based on the use of three bands instead of four. This because MODIS is short of the 510 –nm band that is used in the OC4 algorithm. The OC3 algorithm is written in the following way:

$$R_L = \log_{10}(\max\left[R_{rs} - ratio(443/551, 488/551\right])$$

$$\log_{10}(ChlorophyllConcentration) = 0.283 - 2.753R_L + 0.659R_L^2 + 0.649R_L^3 - 1.403R_L^4$$

The SeaBAM data set was used to create the algorithm. The OC3 algorithm is known to overestimate the chlorophyll concentration where the concentration are small, in addition to overestimation in Case 2 waters (Darecki & Stramski, 2004). The standard MODIS and SeaWiFS products are seen in Table 2 and 3.

Table 2. Current MODIS standard products. Source: Ocean Color Web

Geophysical Parameter Name	Description	Units
nLw_412	Normalized water-leaving radiance at 412 nm	mW·cm-2·µm-2·sr-2
nLw 443	Normalized water-leaving radiance at 443 nm	mW·cm-2·µm-2·sr-2
nLw_488	Normalized water-leaving radiance at 488 nm	mW·cm-2·µm-2·sr-2
nLw_531	Normalized water-leaving radiance at 531 nm	mW·cm-2·µm-2·sr-2
nLw_551	Normalized water-leaving radiance at 551 nm	mW·cm-2·µm-2·sr-2
nLw_667	Normalized water-leaving radiance at 667 nm	mW·cm-2·µm-2·sr-2
Tau_869	Aerosol optical thickness at 869 nm	dimensionless
Eps_78	Epsilon of aerosol correction at 748 and 869 nm	dimensionless
Chlor_a	OC3 Chlorophyll a concentration	mg·m-3
K490	Diffuse attenuation coefficient at 490nm	m-1
Angstrom_531	Angstrom coefficient, 531-869 nm	dimensionless
SST	Daytime Sea Surface Temperature	degrees Celsius

Table 3. Current SeaWiFS standard products.

Geophysical Parameter Name	Description	Units
nLw_412	Normalized water-leaving radiance at 412 nm	mW·cm-2·µm-1·sr-1
nLw 443	Normalized water-leaving radiance at 443 nm	mW·cm-2·µm-1·sr-1
nLw_490	Normalized water-leaving radiance at 490 nm	mW·cm-2·µm-1·sr-1
nLw_510	Normalized water-leaving radiance at 510 nm	mW·cm-2·µm-1·sr-1
nLw_555	Normalized water-leaving radiance at 555 nm	mW·cm-2·µm-1·sr-1
nLw_670	Normalized water-leaving radiance at 670 nm	mW·cm-2·µm-1·sr-1
Tau_865	Aerosol optical thickness at 865 nm	dimensionless
Eps_78	Epsilon of aerosol correction at 765 and 865 nm	dimensionless
Chlor_a	OC4 Chlorophyll a concentration	mg·m-3
K490	Diffuse attenuation coefficient at 490nm	m-1
Angstrom_510	Angstrom coefficient, 510-865 nm	dimensionless

4.6.3 Semianalytic algorithms

Semianalytical algorithms have been developed with the goal of performing well in Case 2 water without compromising in Case 1 waters. The algorithm combine theoretical models of the relation of remote sensing reflectance to the backscatter/absorption ratio with empirical

models of the dependence of absorption and backscatter on the optical active substance in the waters, where the empirical relations change with season, geography and sea surface temperature (Carder *et al.*, 1999; Martin, 2004).

The remote sensing reflectance model used to develop the algorithms for the MODIS sensor has a few parameters that can not be fixed and applied to the entire globe (Carder *et al.* 1999). They are site and season specific. This is due to the inherent variability of many bio-optical constituents. In a case study by Darecki & Stramski (2004) from the Baltic sea, it is shown that all the MODIS pigment algorithms checked (chlor_a_3, chlor_a_2, chlor_MODIS and MODIS CZCS_pigm) as well as the SeaWiFS OC4v4 algorithm was not performing well in the study area. There was a systematic and large overestimation in chlorophyll retrievals. Case 2 waters in the Baltic are often dominated by CDOM. Large discharge from rivers, limited exchange with waters of the North Sea and a relatively shallow sea floor significantly influences the optical properties in the Baltic. The best performance was of the SeaWiFS OC4v4 algorithm, which is currently used for global SeaWiFS processing. Among the MODIS algorithms the chl_a_2 was performing best. The development of the chlor_a_2 and the OC4v4 are based on the same dataset (SeaBAM), with the difference that chlor_a_2 uses three MODIS bands and OC4v4 uses four SeaWiFS bands (they are both purely empirical). The SeaBEAM dataset is much larger than the data set used for producing the other MODIS algorithms. A problem with the use of the current algorithms mentioned, is that most of the empirical data used in the development of the MODIS and SeaWiFS algorithms were collected in ocean waters with relatively little CDOM concentration, compared with typical Case 2 waters (Darecki & Stramski, 2004), like large parts of the Baltic study area. This study shows that for coastal/turbid waters, like the Baltic ocean, the standard SeaWiFS/MODIS algorithms may not give satisfactory results. If the algorithms are to be used for Case 2 waters caution have to be made about how reliable the calculations are compared with the *in situ* measurements.

4.6.4 The use of Level 3 data

One of the goals of launching a number of ocean color sensors placed on different platforms is to build up a long-term, multi-sensor, multi-year, ocean-color archive. The derived ocean color measurements can be used for to resolve inter-annual to decadal changes in ocean phytoplankton biomass in response to global environmental changes. There are different obstacles that obscure this goal. These includes different the characteristics of the sensors

(number of bands, band width and centres, variations in the signal to noise characteristics, differences in viewing geometry), differences in calibration methods and differences in algorithms used for producing geophysical quantities.

The Level 3 products have proven to be useful for research, applications. Level 3 products are the only way to synthesize the enormous numbers of observations made from satellites and it may prove more useful than Level 2 products. It allows general features, as well as the mean temporal evolutions, to be described and quantified. The use of Level 3 data reduces the amount of data significantly. In practice, Level-3 products are the only ones that can be readily stored and manipulated by users examining regional and global scale applications. Corresponding volumes of Level-2 data would be hard to manage and time consuming to use. A limiting factor of Level-3 data is the fact that when focusing on very small scale phenomenon and short time events the spatial resolution may not capture the significant events. These situations may be better examined with Level 2 data.

Calculation of temporal and spatial averages for remotely sensed ocean data in is a standard procedure for overcoming the cloud cover problem, and is also used for data reduction. A calculation of averages is ideal for, to some extent, “fill in” the data gaps that exist due to clouds. If an area is heavily influenced by clouds, a daily snapshot doesn’t reveal much information. It is also possible that the area which a study focuses on is missing completely. Averaging images over time enhances the completeness of the data and, therefore, makes interpretation easier. On the other hand, you may loose information, especially if the features of interest have a shorter temporal persistency than the temporal bins in the study area. If for example a phytoplankton bloom is existing for one week, then will a monthly or seasonal average blur the pattern of the bloom.

4.6.5 Level-3 Grid characteristics for SeaWiFS and MODIS Aqua and Terra

The gridding scheme consists of rectangular bins, arranged in zonal rows. The basic bin size is 4.62 km. The mapped products (equal angle grid) are provided at three different spatial resolutions: 4.88 km, 39 km and 1 degree, and at daily, weekly (8-day), monthly, seasonal and yearly temporal resolution.

4.6.6 Accumulating and averaging individual pixels into bins

Binning algorithms used for the different ocean color missions varies in many ways. They use different spatial and temporal bin sizes, calculate statistics of binned data in different ways, and use different schemes for weighting the data in each bin. NASA is currently using the arithmetic average to create Level-3 SeaWiFS and MODIS products, while NASDA, the Japanese space agency, uses the geometric mean for OCTS and GLI products. If there is a single high variable on the mean this may have an influence on the averaged bin.

4.7 Ocean color in the Southwestern Indian Ocean

The greater Agulhas system, which is includes the Mozambique Channel, is dominated by high mesoscale turbulence. The distribution of phytoplankton in the area is reflected by this activity (Machu *et al.* 2005). North of 35º S the growth of phytoplankton is limited by nutrient supply through the year. Deeper stratification, enhanced cross-frontal transport and higher detritus remineralization explain the higher concentrations of phytoplankton found in austral winter. To the east of southern Africa, the subtropical gyre of the South Indian Ocean is characterized by very low concentrations of chlorophyll a (~0.1 mg/m³). Machu & Garcon (2001) averaged SeaWiFS chlorophyll-a concentrations for each season within the box 25º E-45º E; 25º S-35º S for two years (October-1997-September 1999). The results showed that there is a clear seasonal behavior within the area. A maximum is found in the winter (0.33-0.39 mg/m³), with a corresponding minimum in the summer (0.16-0.18 mg/m³). The findings are supported by Read *et al.*(2000), which conclude that the general low concentration is due to low and limiting concentrations of nutrients. Reasons for this situation may be hydrographic influences, light limitation, nitrate and silicate limitation and grazing control.

Quartly & Srokosz (2004) studied eddie activity in the southern part of the Mozambique Channel using ocean color data. They point out that the use of ocean color chlorophyll-a calculation is not guided by the interpretation of the absolute values, but by the use of phytoplankton and chlorophyll-a as tracers for describing and mapping boundaries between different water masses. Interpretation of the chlorophyll-a bins, which span from September 1997 to January 2003, reveals interesting information and confirms earlier findings. When evaluating the chlorophyll images it was noticed that the East Madagascar Current contains relative low chlorophyll levels. The origin of the East Madagascar Current is the South Equatorial Current which consists of warm low saline water masses with insignificant nutrient levels. A train of eddies, consisting of relative low chlorophyll-a levels, propagates in a

southward direction along the coast of Africa. This is also noted by de Ruijter *et al.* (2003) & Schouten *et al.* (2003). In their study, Quartly & Srokosz (2004) estimated an eddie velocity of 7 km day^{-1}. It is noticed that the propagation of the features is not a steady one. At the shelf east of the Limpopo River (in the southern Mozambique) it has earlier been observed frequently occurring lee eddies. But they are not considered to be permanent. The authors note that the shelf is wide at that area. Combined with river runoff from the Limpopo River and coastal upwelling, this shelf area contains relative high chlorophyll concentrations. This frequently observed eddie may be enhanced by the propagation of southward moving anticyclonic eddies

South of Madagascar eddies are mapped frequently during the time period of the data set. These are not permanent features but occur periodically. Quartly & Srokosz (2004) notes that the eddies observed are either formed as a lee eddie in the shelter of Madagascar, or they are fully developed eddies which are drifting into the region. They become visible when they draw high productivity coastal waters around themselves and become marked with relatively higher chlorophyll- content than the surrounding water masses. The existence of some of the observed eddies was confirmed using TOPEX/Poseidon sea surface height anomaly data. It is reported that eddies are moving in a westward or west-southwestward direction with an average speed of 7.5 km day^{-1}, with greater speeds when eddies are present in the middle of the Mozambique Channel. Hovmüller diagrams were produced from the chlorophyll data with transects along the observed propagation routes. The diagrams show that there is large interannual variability in the chlorophyll content along the transects. These variations are interpreted to be westward moving eddies.

Ho *et al.* (2004) investigated upwelling areas south of Madagascar with SeaWiFS ocean color data. It is noticed that when the East Madagascar Current is diverging from the coast of Madagascar, upwelling is induced along the southern coast of Madagascar. Ho *et al.* (2004) point out that earlier remote sensing studies of the region largely have used SST as mapping resource. Further, it is pointed out that the SST difference between the upwelled cold water and the surrounding water masses is not always large enough to be separable. Ocean color sensors can detect the upwelled water in a better way because of the higher nutrient content. Thus, the phytoplankton has favorable conditions and the concentration can be detected by remote sensors. An EOF analysis is used for mapping the spatiotemporal variations of phytoplankton in the region. The first mode indicates that high variations are found along the

coast of Madagascar. There are also high concentrations existing along the coast of Madagascar. These areas represent the upwelling areas. High amplitudes are found in austral winter and summer. They can be related to current induced upwelling, not to local winds. The East Madagascar Current defines the eastern and southern boundary of the areas with high chlorophyll content and hinders the waters to move eastward and southwestward. The current helps the high chlorophyll water in a southwestward direction.

4.8 Conclusion

In this chapter there has been a short introduction of the theory behind ocean color remote sensing and the production of satellite images. In addition is a review of research using ocean color data on the study area presented. In the last few years there has been a major development in both the technology and the availability of satellite imagery. Much of the data that is made available has already been extensively pre-processed into Level 3 data. Level 3 data has the advantage being user friendly. Little on-site user driven processing of the data is needed. Still, knowledge of the processing steps taken is needed in order to make efficient use of the data and to bypass pitfalls

My choice of using SeaWiFS and MODIS Level 3 data is defended by:

- the sensors are providing long time series and are still operating,
- the Level 3 data is temporally averaged, which reduces the cloud cover and leads to more completer images (the images used in a SPCA must be complete in order to perform the analysis),
- (3) the data MODIS and SeaWiFS data are free of charge,
- (4) the Level 3 data from both the sensors have been processed in and projected in the same manner which make comparison and time series analysis between images of the same area possible,
- (5) the issue of storing capacity. High resolution Level 1 and Level 2 data requires a huge storing capacity, especially when dealing with long time series. This was also contributing to the choice of Level 3 data in this thesis

It is important to acknowledge the Level 3 data is only a representation of reality. A specific pixel covering containing a given chlorophyll value is only the average of what has been measured from daily overpasses. Say, for example, that a Level 3 monthly (31 days) average

image for a given time period is complete with no holes due. It is possible that some areas have been cloud covered for 30 days and that only measurement from one day is contributing to the average. It can also be likely that, for example, there have been great variations in the chlorophyll content within the mentioned areas. The Level 3 data will then give a false impression of that month. On the other hand is the use of the mentioned Level 3 image the only way getting a complete image. The ultimate question is whether the Level 3 data is fit for use for a given task, or not. This again depends on what the task is and especially the temporal and spatial scale and the temporal persistency of the phenomena of interest.

5 MATERIALS AND METHODS

5.1 Introduction

The chapter is divided into three parts. First, there will be a short introduction of the data sets that were used in the thesis. Second, there will be a description of the GIS processing that was performed on the data sets. Third, there will be a description of the time series analysis technique, called Standardized Principle Component Analysis (SPCA), which is used to extract temporal and spatial variations from the ocean color data sets.

The choice of analysis is based on the need for quantification of changes in space and time for the ocean color data. The 4D nature of ocean color marine data makes it necessary to use a time series analysis technique that can analyze changes and variations of a variable in both time and space. Performing time series analysis on multiple image data sets is dependent upon procedures that make sure that the comparison and analysis of the data is valid. Since all remotely sensed images are influenced by geometric distortion is it necessary that all use of multi-temporal images in an analysis is involving accurate geometric co-registration to register images to each other or to a common coordinate system (Aplin, 2006). In addition are remotely sensed images subject to atmospheric, illumination and radiometric distortions. Differences in instrument calibration, viewing angles from the sensor and atmospheric conditions, make it necessary to perform corrections in order to perform sound comparisons between the images. All of the images must be in the same standard in order to be comparable Level 3 data in the analysis of chlorophyll variations in the Mozambique Channel is based on the before mentioned criteria regarding the use of multi-temporal satellite data.

5.2 The data

Ocean color data (chlorophyll measurements) from both the SeaWiFS and the MODIS Aqua sensors covering the study area is used in this thesis. The motivation behind using two data sets covering the same area is to explore the differences between the two In addition to identify spatiotemporal variations of chlorophyll content in the study area, there is also an intention of comparing the effect of different spatial and temporal resolutions in a time series analysis. The different parameters are described below. SeaWiFS has provided data since 1997 and has a longer time series than MODIS Aqua, which has only been operational since 2002.

5.2.1 The MODIS data

Seasonal, monthly and 8-day averaged MODIS Aqua Level 3 chlorophyll-a data with global area coverage were downloaded from the NASA Ocean Colorweb (http://oceancolor.gsfc.nasa.gov). Data from July 2002 to September 2005 was accessed. The original data was stored in Hierarchical Data Format (HDF), which is a library and multi-object file format for the transfer of graphical and numerical data between machines. Each image consists of 8640 columns and 4320 rows and covers the whole world. The spatial extension of each bin is nominally 0.04166667 decimal degrees in the latitudinal and longitudinal directions at the equator; this corresponds approximately to a 4 km resolution. The MODIS chlorophyll-a content have been calculated with the OC3M algorithm (http://oceancolor.gsfc.nasa.gov).

5.2.2 The SeaWiFS data

Seasonal and monthly averaged SeaWiFS Level 3 chlorophyll-a data with global area coverage were also downloaded from the NASA Ocean Colorweb (http://oceancolor.gsfc.nasa.gov). Data from September 1997 to September 2005 was accessed. Each image consists of 4320 columns and 4320 rows. The spatial extension of each bin is nominally 0.0833333 decimal degrees in the latitudinal and longitudinal direction; which approximately corresponds to a 9 km resolution. The chlorophyll products were produced with the standard NASA algorithm OCv4 (O'Reilly *et al.*, 2000).

5.2.3 Processing algorithms

Algorithms used for calculating the geophysical values for chlorophyll-a from measured radiance from space are still under development and continues to improve. Sometimes it is also necessary to redefine or create new products in order to meet the needs for the ocean color community. Details about the current and past reprocessing can be found at (http://oceancolor.gsfc.nasa.gov/REPROCESSING/). The downloaded data for this study used the following reprocessing:

- MODIS Aqua reprocessing 1.1 from August 4, 2005.
- SeaWiFS reprocessing 5.1 from July 5, 2005.

5.3 The GIS processing, comments and assumptions

Originally, the data from both the data sets was given in byte binary values from 0-255, with 255 serving as the land- and cloudmask. All the Level 3 data was originally projected in an Equidistant Cylindrical projection where all meridians are standard equally-spaced vertical

lines and all parallels are horizontal, equally spaced and has equally long lines. In IDRISI the data were resampled into a Equidistant Cylindrical projection where all meridians are standard equally-spaced vertical lines and all parallels are horizontal, equally-spaced and have equally long lines. An algorithm needed to be used on the data sets in order to calculate the geophysical values. The algorithm was given in the enclosed Metadata in the form:

$$\text{Geophysical value} = 10\text{^}(0.015 * PixelValue) - 2$$

5.3.1 Cloud removal

Clouds obscures the information collected from satellites. Cloud infected pixels, need to be removed, such that only reliable information remains in an image and further analysis can be performed. The study area is often subject to frequent and persistent cloud cover. Since a Time Series Analysis in IDRIS Kilimanjaro requires a complete data set with no holes (Eastman & Fulk, 1993; Jensen, 2005), it is clear that the data gaps must be filled such that each image contains continuous data. The data used for filling the holes in the images have to be representative. The methods used must be as close to reality as possible in order to be usable. In general, there are two different methods of filling in these gaps, namely interpolation and backfilling:

Interpolation can be a useful method of calculating unknown values in space if the data are spatially autocorrolated. However, the patchy nature of phytoplankton does not necessarily imply that measured values outside a cloud covered area have significance for the latter area even if it is in the vicinity. Consider an elevated level of phytoplankton concentration that may exist within a cloud covered area and the measured chlorophyll-a concentration outside the cloud covered area is lower than within the clouded area. It is not possible to estimate chlorophyll-a values correctly with the Interpolation method within the cloud influenced area. After scrutinizing the downloaded images, the conclusion was that the Interpolation method was not considered to be appropriate for the filling in of missing information due to large cloud covered areas in some of the images. The method is especially subject to errors when the missing values are present in coastal waters where, in general, the chlorophyll-a levels are greater than in the open oceans. The interpolation is then based on open ocean measurements that are lower than the coastal measurements and, thus, it is not possible to perform an estimation that is representative for the real world geophysical values. The interpolation

method works best if the sample data that is the basis for the interpolation is evenly distributed in space.

Backfilling of data into the areas of missing values can contribute greatly to a data set's completeness if the fill in data is significant for individual time dates. Spatially filtered data can be backfilled onto the original image where only the newly calculated values from the filtering process is put back onto the original image. This method can be said to have high significance for the areas of missing values because the filtered backfill data is calculated directly from the image that is being backfilled. There is off course possible to use other sources of data when backfilling missing data. For example one can use *model data* or *temporal averaged data*.

For their study of the eddie activity in the southern part of the Mozambique Channel, Quartly & Srokosz (2004) used 6 day bins SeaWiFS chlorophyll-a data. Figure 5-1 shows that there are periods of the year where clouds obscure the data, especially the periods between the middle of November until the end of January.

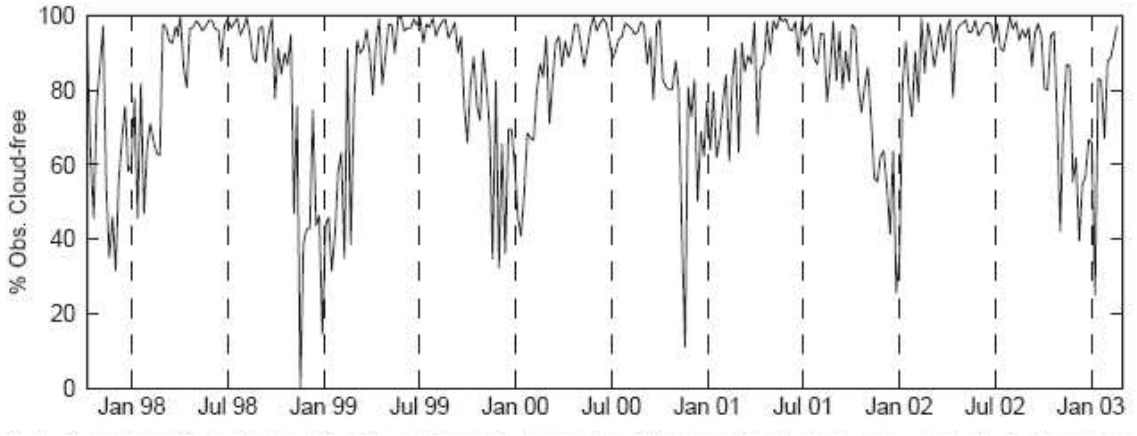

Figure 5-1. Cloud cover for the Southern Mozambique Channel. Adapted from Quartly & Srokosz (2004)

The regular cloud cover pattern shows a strong seasonal behavior. A visual inspection of the MODIS Aqua weekly data and SeaWiFS monthly data used in my study revealed a similar pattern. As mentioned before, the gaps due to clouds must be filled in before performing a Time Series Analysis (TSA). The approach to this problem is based on the use of backfilling of temporally averaged data.

5.3.1.1 Method for SeaWiFS cloud removal

For SeaWiFS data the TSA is based on monthly averaged data. The reason for this is that the TSA in IDRISI is restricted to 256 images. Weekly averages are then unsuitable because the number of weeks between September 1997 to September 2005 exceeds the TSA threshold. The holes in the Monthly data were backfilled in the following way: I wanted to make a data set, which was complete, to use as a backfill for the missing values. An assumption was made that the chlorophyll-a levels in the study area was having a seasonal behavior. The idea is to let the Monthly climatologies be the foundation for the backfill. To be sure that the Monthly climatologies were complete (there were some data gaps), seasonal climatologies were backfilled for the missing values in the monthly climatologies. The resulting images was then used to backfill the monthly images. The result was a complete time series of monthly data with no missing data due to cloud cover.

5.3.1.2 Method for MODIS cloud removal

For the MODIS weekly data the backfill process was a little bit different. At this point I also wanted to produce a data set which was complete and representative for filling in the missing values in the weekly data. Monthly data was used as a base. Monthly climatologies were used for filling in the gaps in the monthly data. Seasonal data was also filled in to be that the data set was complete. In the end the complete data set was used for filling in the corresponding weekly data, resulting in a complete weekly data set. Both the SeaWiFS and MODIS Aqua data sets where now ready for use in a Time Series Analysis.

5.3.2 Further processing

The IDRISI TSA function can only handle multiple images in a byte binary format. This means that the time series chlorophyll-a images with geophysical values can not be used. Only integer numbers from 0-255 are usable in the TSA. One solution is to truncate the data, by removing the decimals. But in this way the details of the data would be lost. The redundant data needed to be forced into a byte binary format. For this purpose, a reclassification needed to be performed. Another problem was that IDRISI can not classify data based on upper and lower boundaries with decimals. This means that it is impossible to put all the values between 1 and 1.5 directly into one class. Only integers are accepted as class boundaries. The solution was to multiply all the images with 1000. The number was chosen in order to keep enough usable information before byte binary classification is performed. After experimenting with various classification intervals and testing those in the TSA function, an interval of 0.05 was chosen, which corresponds to intervals of 50 in the rescaled images. This means that all the

values between 0 and 0.05 were put into category 1; all the values between 0.05 and 0.1 were put into category 2 and so on. Category 0 was saved for the landmask. Category 255 included all the pixels with values >12.55. With this method you lose direct information regarding the classified values. The pixel values of the classified images are only indirectly related to the originally measured chlorophyll-a content and can be regarded as qualitative data. Low numbers correspond to low chlorophyll content while high numbers correspond to high numbers. It is difficult to justify this kind of operation because the geophysical values are completely transformed. But on the other hand is interpretation of the results from a TSA of a qualitative kind, not a quantitative. Therefore, the classified byte binary input values from the TSA ready data sets are related to the real geophysical values. The absolute values are not as important as temporal gradients of phytoplankton biomass. One might say that the new byte binary maps can be described as scaled representations of chlorophyll content. A time series analysis was then performed on the MODIS weekly data set and the SeaWiFS monthly data set. A description of the technique can be found in Jensen (2005). To summarize the data flow a generalized description of the work is given in the figure below. A more detailed flow chart can be found in appendix A.

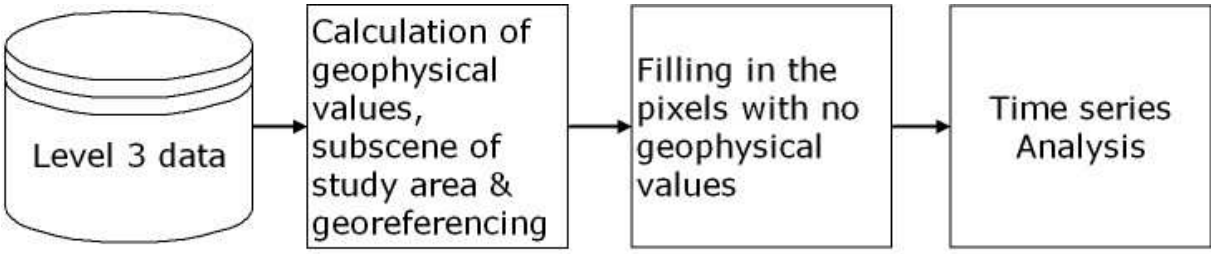

Figure 5-2. General flow of the data process

5.3.3 Ocean features versus temporal and spatial resolution

Lutjeharms *et al*. (1981) and de Ruijter *et al.* (2002) is observing that the rotation period of 4-10 days. The 8 day MODIS data then should have a sufficient temporal resolution for getting a clear signal. The monthly averaged data is more problematic, it is likely that moving eddies is not captured in the images, but is blurred by the average. Figure 5-3 show the connection between the temporal persistency and scale for some ocean features. As is seen, can it be problematic for the SeaWiFS 9 km monthly data to capture patches of phytoplankton and even frontal systems. However, the long term trend is still believed to be mapped. It is likely that the MODIS 4km 8day data records more of the specific features.

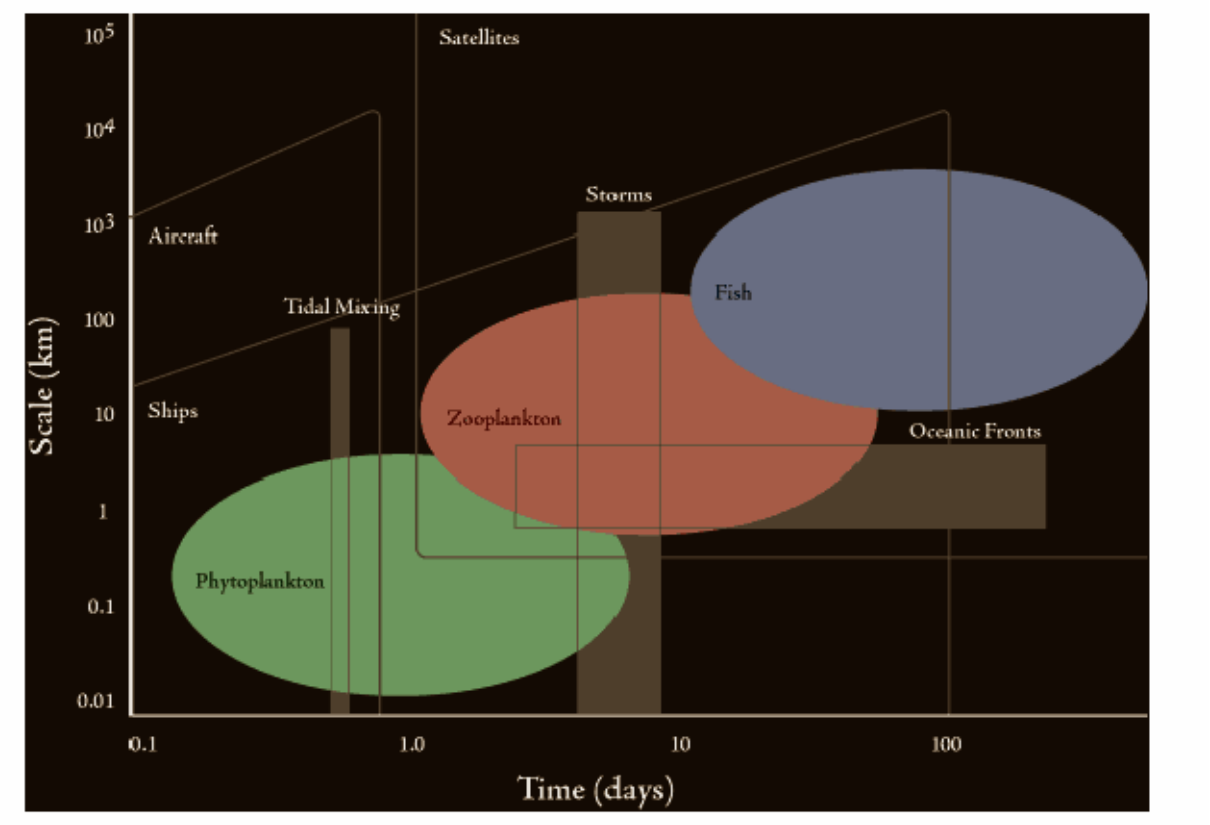

Figure 5-3: Diagrams shows the spatial and temporal persistency for some oceanographic phenomenon in relation to various measurement platforms (Source: http://daac.gsfc.nasa.gov/CAMPAIGN_DOCS/OCDST/classic_scenes/01_classics_tasmania.html)

5.4 Time Series Analysis

The SPCA analysis has been used in earlier studies for describing variability of ocean color data (Yoder *et. al., 2002;* Ho *et al.,* 2004). The time series analysis, as implemented in the IDRISI software, has also been used by Lucas & Budgell (2004) for the investigation of long term variability of SST in the North Sea.

Dominant time/space patterns of chlorophyll variability over the study area during the period of interest are quantitatively summarized using a standardized principle component analysis (SPCA). In Oceanography, this time series technique is known as Empirical Orthogonal Function (EOF) (Emry & Thomson, 1997). In this study, the term SPCA is used.

The general objectives of a SPCA are: (1) data reduction and (2) interpretation of large data sets. When dealing with large data sets with numerous data layers, it is almost impossible to keep track of the variations from layer to layer just by visible interpretation. This is true for both the MODIS and SeaWiFS data sets. When dealing with 3 years of weekly data from the

MODIS sensor and 8 years of monthly data from the SeaWiFS sensor it is difficult to describe the variations, propagations and distributions over time for the chlorophyll content. A purely visual descriptive approach of each image is not sufficient or practical to reveal information from the data sets. It can be valuable to describe the spatial variations at specific times, but this is not the focus in this thesis. Focusing on specific snapshots of an area does not tell anything of how a system is varying as a whole; it only gives information of what the situation is at a particular time. From this point of view it must be argued that a SPCA is a more appropriate approach for revealing patterns over time and space. This is because this statistical technique is analyzing both space and time components, which make the SPCA useful.

The time series technique transforms the original remotely sensed data set into a smaller and easier to interpret set of uncorrelated variables that are representing the most of the information in the data set (Jensen, 2005). Spatial and temporal signatures from the data sets are isolated. SPCA has the advantage of providing a compact description of the spatial and temporal variability of time series data in terms of orthogonal functions (Emery & Thomson, 1997). This procedure can be very useful in the analysis of time series data sets where the interest is in the identification of phenomena or signals that propagate over time. The implementation of SPCA is based on the computation of eigenvalues from correlation matrices. SPCA is taking care of that each image is equally weighted when new component images are calculated. SPCA is considered to be the best approach for long-sequence, time-series analyses (Eastman and Fulk, 1993).

Principal component analysis decorrelates multivariate data by translating and/or rotating the axes of the original feature space, so that each data point receives a value in the new component space. The first component, or new axis, is defined by the direction of greatest variance in all of the input data and corresponds to the mean. The second component is orthogonal to it and accounts for the maximum remaining variation not accounted for by the first component. Each following axis is defined in the same way. Because the way they are selected, each successive component contains less of the total data set variance. Later components will usually contain information that is essentially noise with respect to the phenomenon that is analyzed and, thus, can then be put aside. Noise elements are likely to be isolated in their own components, and may easily be separated from the desired signal. On the other hand, there is always a possibility that the later components containing a low proportion

of total data set variance might represent informational variance. In general, the computation of 8 component images is sufficient in most cases (IDRISI Manual), but this may depend on the nature of the data set.

The TSA function in IDRISI Kilimanjaro (http://clarklabs.org), which is a SPCA analysis function implemented in the software, produces outputs in the form of component images and component loadings which corresponds to spatial and temporal outputs. The loadings are a measure of the degree of correlation between each original monthly input image and the new component patterns. SPCA allows us to segregate the various patterns of variability embedded in time series data set into different components. The IDRISI Kilimanjaro Time Series Analysis is limited to 256 images. The results are both temporal and spatial in nature, and are made up by an ordered set of uncorrelated component images and loadings. Temporal loadings and spatial components should be interpreted together in order to reveal spatial and temporal variations. While the statistical SPCA modes do not necessarily correspond to direct physical forcing mechanisms, portioning the spatial and temporal variance of a data set into modes reveals spatial functions having time-varying amplitudes that can be interpreted in relation to physical processes (Yoder *et. al.*, 2002). It must be pointed out that the outputs of a SPCA are not containing data of a geophysical nature. The formal description of the SPCA can be found in the Appendix.

5.4.1 Comments

Now that the time series technique is presented it is a need to discuss the use of the linear rescaling of the geophysical values that was applied to the SeaWiFS and MODIS data sets. As mention was the rescaling done in order to implement the data sets in the GIS. The original chlorophyll data that were downloaded had been rescaled with a log transformation. I rescaled the data back to geophysical values. The question is what effect the scaling is having on the analysis and which type of data that is most suitable for performing the SPCA. The restrictions of the GIS software made a linear rescaling of the geophysical data necessary. The advantage is that the linear nature of the data sets is kept and that the output values are a good representation of the data sets even if some accuracy is lost. The work on making the data suitable for SPCA analysis in IDRISI was time consuming, but necessary, when the goal was an implementation and analysis of the geophysical values. The next chapter will reveal that significant parts of the study area can be classified as low productivity waters with low chlorophyll values throughout the seasons. The seasonal variability is also relative low. The

high productivity areas are restricted to the coastal zone and the seasonal variations are of a much higher magnitude than in the open oceans. In a linear data set is the open ocean low chlorophyll variability through time is having much less variations compared with a log scaled data set. This means that there are relative more emphasize on the lower chlorophyll values in the log scaling than in the linear scaling The difference is illustrated in Figure 5-4

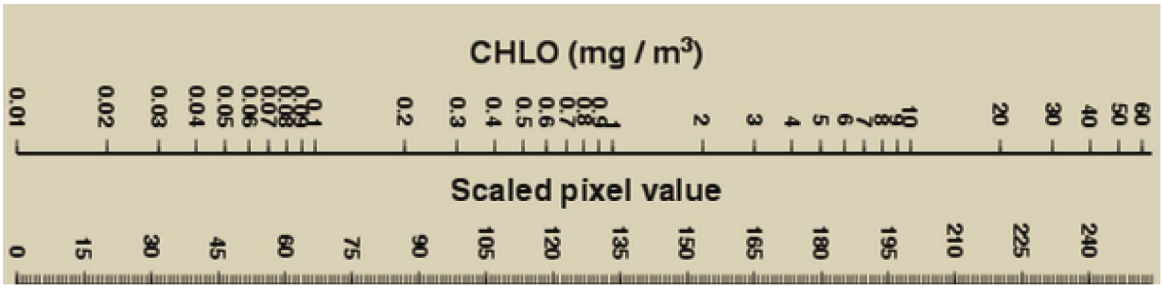

Figure 5-4. Scalings. Source: Ocean Color Web (http://oceancolor.gsfc.nasa.gov/)

A SPCA analysis performed on a log transformed data set would be likely to show some different patterns compared with the results from linear data because of the equal weighting each value have in the analysis. Small scale variation lower part of the chlorophyll values will, in a log transformation, contribute more to the overall variations than a linear scaled data set. Chapter 7 will include a SPCA of the SeaWiFS 9km data set with of the effects of using the log scale versus the linear scale in an SPCA analysis.

5.5 Conclusion

This chapter has described the data flow to produce the time series analysis which is performed on three different data sets from the study area. The time series function in IDRISI is itself a simple implementation. Classification of the original read data values into byte binary values was a way of bypassing the problem with IDRISI's inability to handle data with decimals. In practice, this classification is probably not influencing the data sets usefulness in a SPCA. The classified data set is only containing lesser information than the original real data. Because of the statistics used in the TSA are the outputs of components and loadings not containing geophysical data even if the original data was utilized in the analysis and would therefore not keep the original data format even if the original data where used. The classified data sets are containing data which can be regarded as scaled with respect to the original data.

What is the influence of the byte binary classification on the data sets? It is likely that the linear classification of the data is hiding some of the low chlorophyll in the images due to class boundaries. Variation within each class is not accounted for. The influence is probably most noticeable in areas with low chlorophyll values and little variation between the seasons. These areas include the open oceans in the study area. Nevertheless, the classification is well suitable method for converting the data into byte binary format without using rounding or truncation. The last to methods are unsuitable for the byte binary conversion of chlorophyll data.

The use of the IDRISI software for processing the data was limited by, as mentioned in the previous section, by several problems that had to be bypassed. Still, I wanted to keep the workflow as a whole within the IDRISI software. It was not realistic to export the large amount of data to other softwares, like Matlab or MF Works, because of huge time consume of exporting and importing a large number of files. If I chose another software, like Matlab, to perform the analysis, the problems that I have encountered may not have met. It is likely, however that other problems may have been faced. All GIS programs have their strengths and weaknesses. The strength of the IDRISI software is the analytical capabilities of raster data, like remote sensing images, especially in the analysis of time series data. Another advantage is that IDRISI is not commercial software and the price is therefore reasonable compared with other commercial GIS softwares, and that the IDRISI is relative user friendly. Especially the modelling option was extensively used for processing of the data used in this thesis.

6 RESULTS AND DISCUSSION

Before discussing the results of the SPCA analysis, the seasonal chlorophyll-a climatologies for the study area and the yearly average as obtained by the SeaWiFS sensor is presented. This is to give a general overview of the general seasonal variations as interpreted from the climatological maps. A simple change analysis between the seasonal climatologies is also performed. Second, the results of the SPCA of the SeaWiFS 9 km data set are presented.. Finally, time profiles from 15 selected sites are used for verification of the SPCA analysis. Some of the sites are located in the vicinity of river mouths where river runoff data is available. Variations in the seasonal river runoff may induce variations in the phytoplankton stock because of the various amounts of nutrients brought out in the oceans by the rivers. The river runoff data, the chlorophyll time profiles and SPCA analysis results are compared.

6.1 Yearly mean and the seasonal climatologies

6.1.1 Yearly mean

An overall chlorophyll mean is calculated from the SeaWiFS 9 km monthly images from September 1997 to September 2005 and is shown in Figure 6-1. The most appropriate way to visualize the chlorophyll data would be to use a log color stretch on the pixel values. However, none of the GIS programs available to me were able to perform such a stretch. I experimented with linear stretches, but these were not showing satisfactory results. The solution was to classify the data. There is always a risk that a classification can be misleading and that it may miss important patterns, but the classification ranges chose was appropriate in this case.

There is a clear distinction between open oceans and coastal regions, where the latter contains enhanced chlorophyll levels compared with the former. In general, the region is dominated with low levels of productivity in the open oceans. The sea east of Madagascar, between 15º S and 25º S, is dominated by surface water with chlorophyll levels of >0.1 mg/m³. These low levels can be contributed to the South Equatorial Current flowing westward to Madagascar. This current is a hot, saline current with very little nutrients and, hence, is limiting the phytoplankton growth. In the southeastern corner (50º E-53º E; 27º S-32º S) there is also, in average, chlorophyll levels of >0.1 mg/m³. In the area as a whole, except coastal areas, the average chlorophyll levels lie between 0.1 and 0.2 mg/m³. In the coastal waters south of

Madagascar there is clearly a high productivity area with a tail shape in the southwestern direction. The effect of eddies dragging chlorophyll rich coastal surface waters offshore in a west, southwestern direction and coastal upwelling due to the South Madagascar Current can explain the high chlorophyll levels in this area.

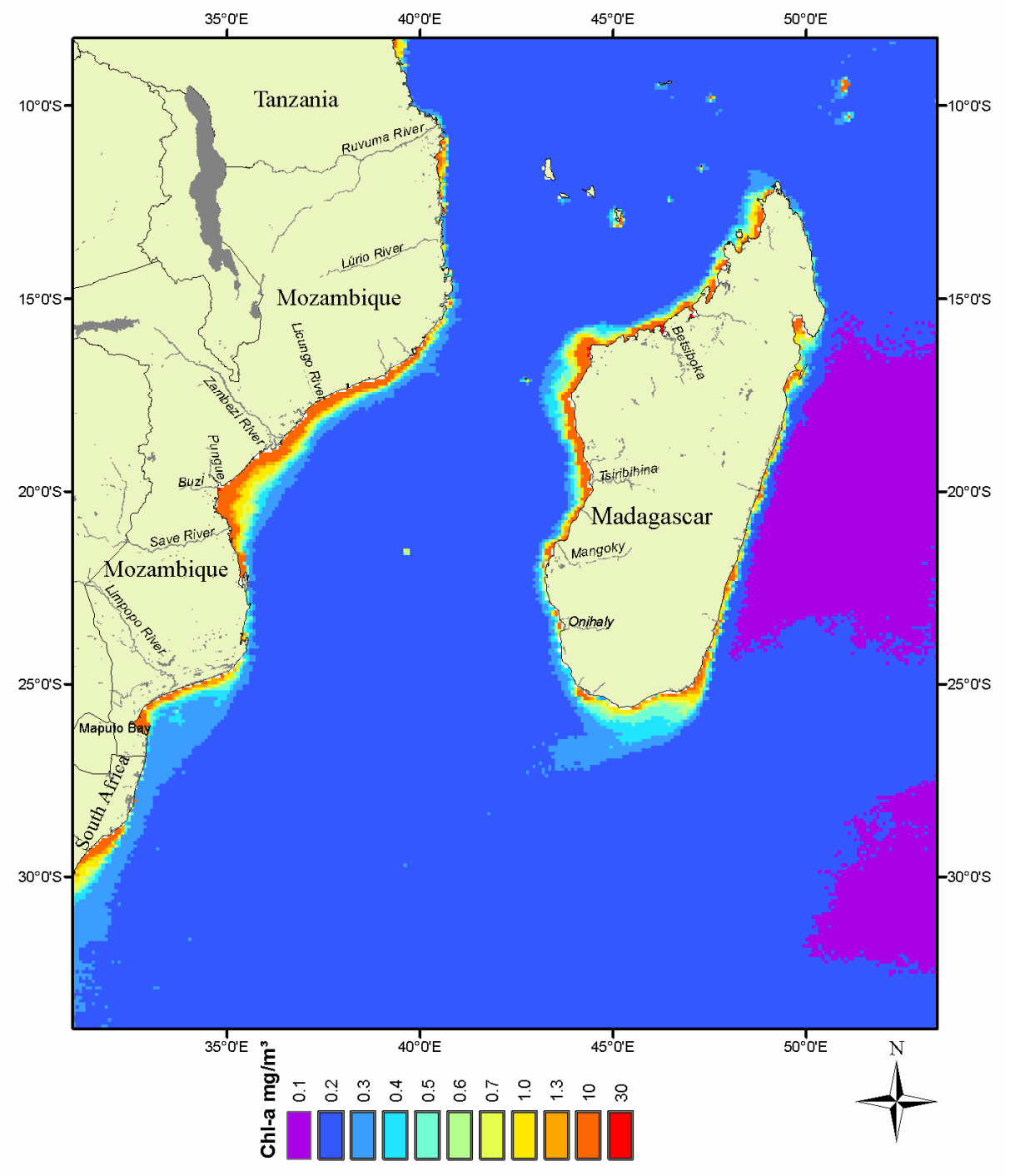

Figure 6-1. Classified image showing the overall chlorophyll concentration average based on SeaWiFS data from September 1997- September 2005 with 9 km resolution. Important rivers are also shown.

Along the east African coast from 15º S to 22º S, which includes the Sofala Bank of Mozambique, there are also measured higher average chlorophyll levels than in the open oceans, most likely due to the large rivers (Zambezi, Pungue, Buzi and Licungo) that discharge freshwater and nutrients. The chlorophyll content is gradually decreasing from over 1.3 mg/m³ in coastal areas to between 0.1 and 0.2 mg/m³ in the open oceans. Along the coast (22º S-24º S) further south, the chlorophyll content is more similar to the open ocean water. The continental shelf is narrowing along this coastline. Continuing southward along the coast from 24º S to 26º S (Delagoa Bight), the chlorophyll levels are again enhanced. The continental shelf is here widening. The chlorophyll content are lowered again from 26º S to 28º S, where the continental shelf is more narrow From 28º S to 30º S higher levels are seen. The eastern part of the African coast that is within the study area is divided into zones or areas with high and low chlorophyll concentrations respectively. Much of the same patterns as along the east African coast can be found around the coast of Madagascar, with alternating concentration from higher to lower chlorophyll concentration. In the coastal areas of western Madagascar (22º S-24º S) there is also, on average, low concentration of chlorophyll. Further north from the north tip of Madagascar at12º S to 22º S at the west coast, one can see elevated levels of chlorophyll. At the narrowest part of the Mozambique Channel, around 16º S, there is an area where the chlorophyll concentration is high also at some distance from the coast of Madagascar. In the northeastern Madagascar coastline (12º S to 16º S) relative low average chlorophyll levels are measured. If we look further south (16º S-25º S) along the east coast of Madagascar, elevated measurements of chlorophyll are found. On average, the chlorophyll values in the coastal zone do not surpass 10 mg/m³.

6.1.2 Seasonal Climatologies

We now turn to the seasonal climatologies as averaged from the SeaWiFS sensor. The data have first been classified for easier interpretation. The climatologies are showing the mean chlorophyll-a content in the study area for each season. The austral seasons are named in the maps and are defined in the following way. The seasons are defined according to definitions given in the NASA Ocean Color Web (http://oceancolor.gsfc.nasa.gov/).

- Spring = September, October, November
- Summer = December, January, February
- Autumn = Mars, April, Mai
- Winter = June, July, August

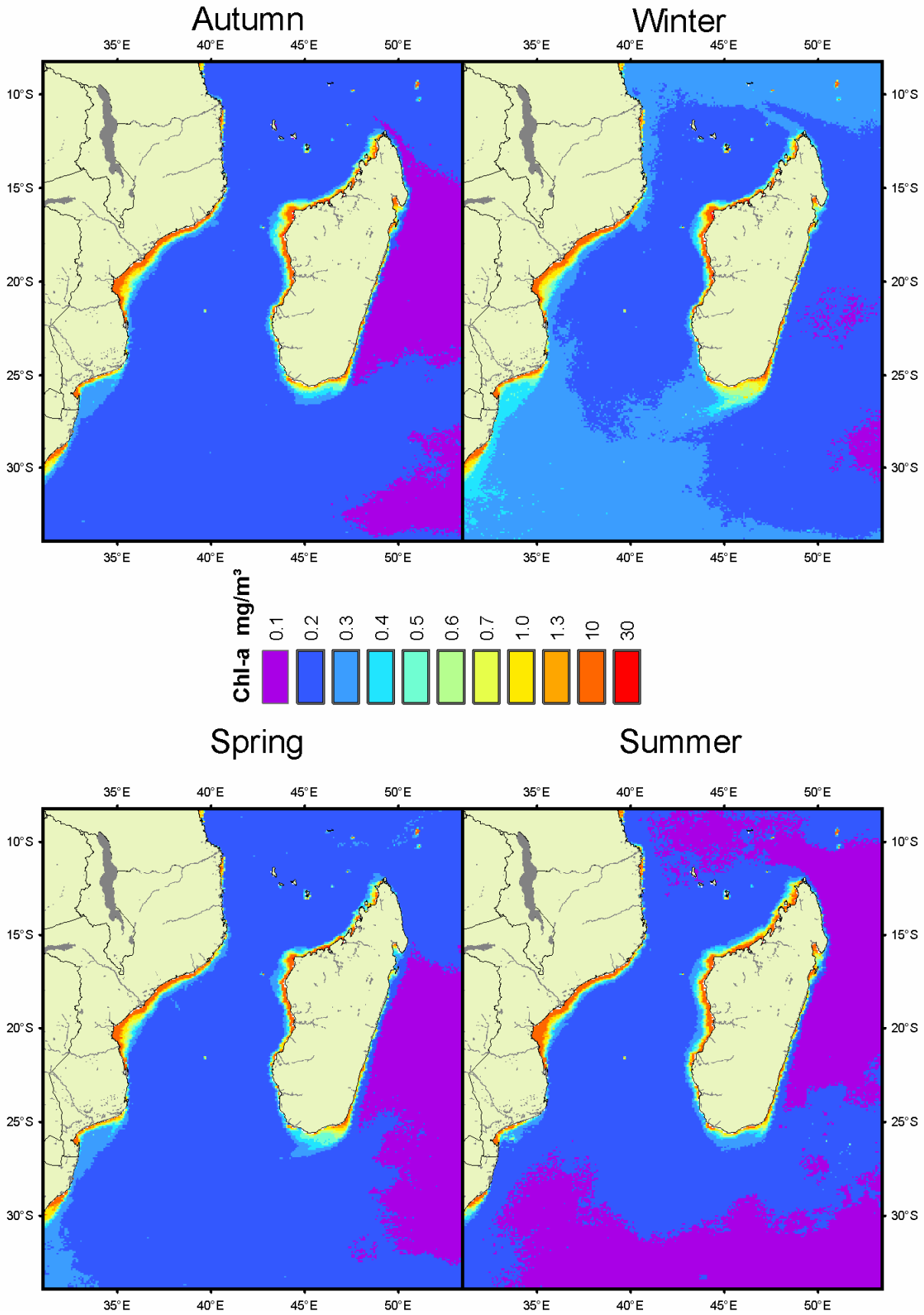

Figure 6-2. Classified seasonal Chlorophyll-a concentration from the SeaWiFS sensor. Resolution 9 km.

Clear seasonal variation in the chlorophyll content in some areas in the study area (Figure 6-2). These data only reveals information about the average conditions within a three month period and does not reveal year to year anomalies and variation. In the box (25º S-35º S; 30º E-45º E), from the south of Madagascar to the east coast of Africa to the southern limit of the study area, there is a clear winter bloom of phytoplankton with elevated chlorophyll concentrations compared with the other seasons. The chlorophyll-a concentration in the bloom ranges from 0.2-0.3 mg/m³ with slightly more (0.3-0.4 mg/m³) in the southwestern corner of the study area.

During spring and autumn is the southwestern part of the study area within the box (25º S-35º S; 30º E-45º E) dominated by surface waters with chlorophyll levels of 0.1-0.2 mg/m³. In the summer months is the box area containing even lower chlorophyll levels (0-0.1 mg/m³) south of 30º S and east of 33º E. The variations are clearly seasonal with a winter maximum and a summer minimum. A similar seasonal pattern can also be observed in the waters east and north of Madagascar. Relative higher chlorophyll concentrations are found in the winter period than the rest of seasons. The winter concentration lies between 0.1-0.2 mg/m³, except some patches at 20º S-23º S which has a lower concentration than 0.1 mg/m³. During the rest of the year is the open ocean east of Madagascar dominated by chlorophyll concentrations of lower than 0.1 mg/m³. If we look at the waters north, east and west of the northern tip of Madagascar, a tongue of lower chlorophyll content than the surrounding waters is seen extending in the a northwesterly direction in the Autumn, Winter and the Summer period in the classified maps. This low chlorophyll feature can be contributed to the warm, saline and low nutrient Northeast Madagascar Current which origins from the South Equatorial Current, as seen in Figure 2-3. In the summer period is the low (0-0.1 mg/m³) chlorophyll areas east of Madagascar extending westward from the northern tip of Madagascar to 42º E, of the coast of eastern Africa. Also in this northern part of the study area there is a seasonal pattern with a winter maximum and summer minimum. Interpretations of the seasonal climatologies by comparing only the visible differences between the season is a difficult task because it may be problematic to just see the differences and similarities based on differences in colors.

6.1.3 Seasonal changes between the climatologies

The next step is to get a clearer visualization of the magnitude of the seasonal change from season to season. This is done by subtracting each of the four climatologies from the

following climatology in time and is a straightforward change detection technique. The results are shown in Figure 6-3

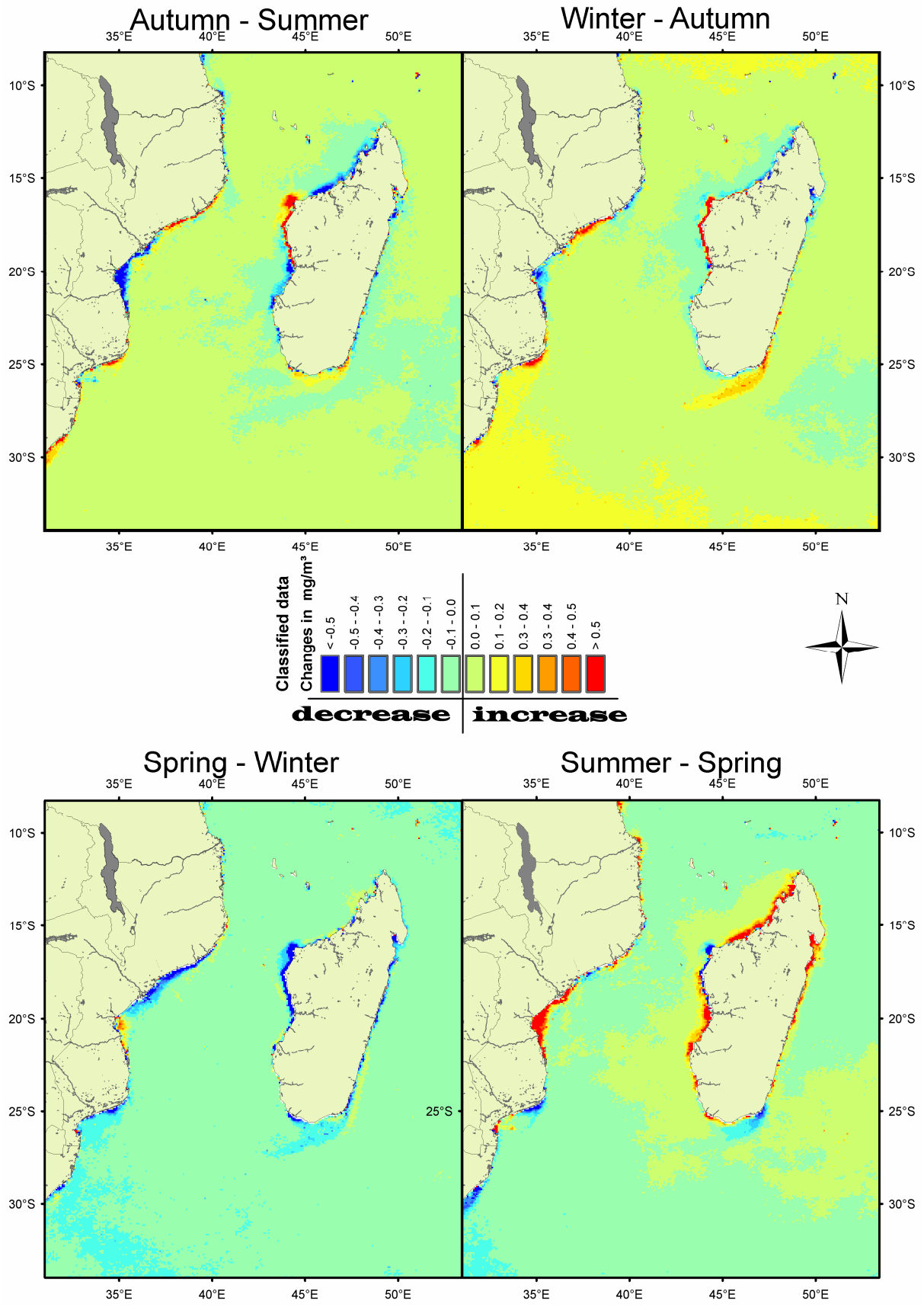

Figure 6-3. Classified average seasonal change in the Mozambique Channel.

Only the change is now observable. The four maps are highlighting patterns that are difficult to grasp by just looking at the four climatologies. The classes are colored according to the degree of positive or negative change between a season and the next following season in time. Although the classes (12) greatly exceed the maximum 7 classes usually used in categorical maps, the maps are giving a fairly comprehensive overview of the changes in chlorophyll content for the averaged seasons. It must be clear that some of the values were higher and lower than the categories indicates.

The categories were chose because an investigation of the results revealed that the major part of the study area exhibited variations in these ranges. The first impression of the seasonal change images is that the greatest account of change is seen in the coastal areas. Comparing Figure 6-2 with the maps in Figure 6-3, the spatial areas of coastal change is now easier to see. The presentation is focused on the main spatial changes of the average chlorophyll content from season to season. The data reduction induces some important restrictions upon the interpretation of the seasonal change images. First, since the seasonal climatologies are averaged over time, the maps are not showing any real state of the seasonal content, but merely a representation of the long term trend. Second, individual seasonal change from year to year is not mapped. Anomaly years or seasons will also influence on the result. In addition may the definition of seasons confuse the seasonal signal.

6.1.3.1 Coastal areas of eastern Africa

(1) The upper left image is composed by subtracting the summer climatology from the winter climatology. The positive values are those areas where the chlorophyll content is higher in the autumn months than in the summer months. The negative values are those areas where chlorophyll content in the summer months. The first impression is that the greatest variations between the autumn and the summer are in coastal areas. Small, but significant, variations are seen in the open oceans. Inspection of the east coast of Africa from south to north reveals some interesting findings. At 30º S along the east coast of Africa are there an area which have clear positive values. An inspection reveals that the positive values lie approximately between 0.5 and 1. From 28º S to 26º S there is significantly less negative change (0.1- 0.2). At the Sofala Bank coastline from 22ºS to 18ºS there is clear negative values greater than 0.5. From 18ºS to 16ºS there is positive change values of over 0.5. It seems like the location of negative change values along the coast is located in the vicinity of the large rivers.

(2)At the upper right map (Winter – Autumn) in Figure 6-3 the change pattern along the coast is the same as in the Autumn-Summer. It is a clear indication that there is a general trend from the autumn months to the winter months.

(3) The Spring – Winter map in the bottom left corner shows a different situation. At 29º S at the coast of Africa there is an area which contains negative values, and corresponds to the same area of change mentioned in the other maps. This area is, however, of smaller spatial extent than the others. Further north at 26º S at the bay of Maputo there is positive change present, although this area also is of a smaller spatial extent than in the Autumn – Summer and Winter – Autumn maps. From 22º S to 20º S it is found positive values in the coastal areas, and negative values along the coast from 20º S to 16º S. Further north, only insignificant change values are found. The changes in the Spring – Winter image are of the opposite kind than those seen in the Winter- Autumn image. The main difference is that the spatial extent of the change areas and amount of change is smaller. The change pattern along the African coast along in the Spring-Winter map is much the same as in the Autumn – Summer map, with differences in change in degree and spatial extent of the change areas. The coastal area near the Zambezi river mouth at 36º E 19º S are containing positive values in the Autumn- Summer image but negative values in the Spring – Winter map.

(4) Moving on to the lower right Summer – Spring map there are much of the same pattern as found in the Autumn – Summer map for the coastal Africa. A significant exception is the coastal area from 22º S to 18º S. Here, the near shore areas are highly positive, ranging from 1 to 1.5 in positive change. From 18º S to 17º S we find patchy areas of negative change, ranging from 0.3 to 0. 8. Further north, a more diffuse pattern is found. The change pattern is somewhat mixed, with both positive and negative change pixels that alternates. At the river mouths at 40º30´E 10ºS20´S, 40º30´E 13º30´S, 39º40´E 16º30´S and 39º7´E 16º50´S positive change values ranging from 0.5 to 1 are found.

6.1.3.2 Open Oceans

First, the area south of 25º S is considered, with the exception of the area south of Madagascar. In general the amount of change is much less than in the coastal areas for all the maps. This is expected since Figure 6-2 is showing general low chlorophyll content in all four seasons for the open oceans. The Autumn-Summer map is showing more or less continuous

positive values from 0.1 to 0.2 is dominating for the southern and southwestern part of the study area. The Winter – Autumn map reveals clear positive change values in the south/southwestern part of the study area, which corresponds to the winter bloom seen in Figure 6-2 and Figure 6-3. The amount of change lies between 0.1 and 0.2 (yellow color). Further north the changes are positive, but very small (between 0 and 0.1). A closer inspection reveals that within this class, the classification is hiding a longitudinal gradient. As seen in Figure 6-4, the change values are increasing with increasing latitude.

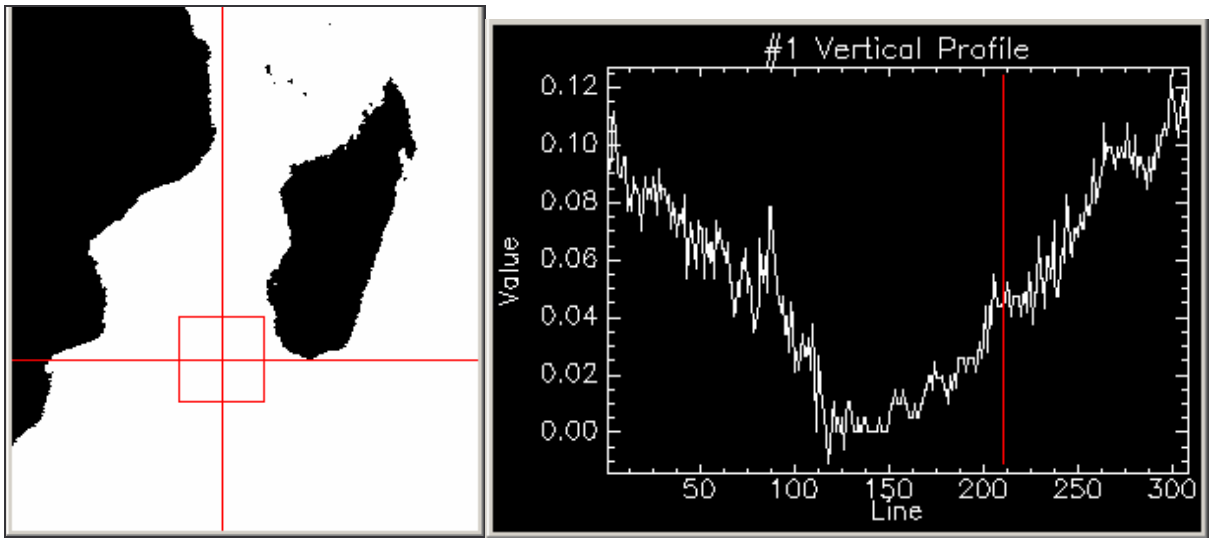

Figure 6-4. Figure in middle shows the placement of a vertical transect in the Mozambique Channel at 41ºE. Figure to the left is showing the change values on the y-axis and the number of pixels from north to south on the y-axis. The horizontal line is placed on 25ºS and is seen in the vertical profile.

It must be noted that the absolute change values are very small, but still shows a distinct pattern. Moving to the Spring-Winter map, the change values are small, negative and lie between 0 and 0.1. In the southwestern corner of the map, south of ~29º S and west of ~37º E, the areas is dominated by negative change values that lie between 0.1 and 0.2. The same pattern is found in the Summer-Spring map. Small negative change (0 to 0.1) is found throughout the area, except southeast and southwest of the southern tip of Madagascar. Here, the change values are slightly positive which lies between 0.1 and 0.2.

The waters east of Madagascar are experiencing little change throughout all the four seasonal change maps when disregarding the coastal areas. This is expected since the chlorophyll content in general is very low during all the seasons as seen in Figure 6-2. The Autumn – Summer map shows negative change values in the in the vicinity of the coast in the range of 0 to 1. The open ocean north of 22ºS the change values are positive and also lie between 0 and 1.

The Winter- Autumn map shows a pattern where the area from ~15º S to ~23º S contains positive change values between 0 and 0.1, and the patchy area between ~23º S and ~30º S has negative change values in the range of 0 to 0.1. In the Spring-Winter map the area as a whole is categorized by change negative change values from 0 to 0.1. The Summer – Spring map also contain the negative change values (0 – 0.1) for the whole area except between ~22º S and ~30º S, were the change is positive.

6.1.3.3 Northern part

Next, the northern part of the study area, which is approximately bound by the rectangle 40º E 8º S and 53º E 12º S, is scrutinized. The area northeast of the northern tip of Madagascar (~49º E 12º S) in the Autumn-Summer map is characterized by negative change values between 0.1 and 0.2. This area stretches eastward to the coastal areas of Africa. To the south, all the way through the Mozambique Channel, except coastal areas, the pixels contain negative change values between 0 and 0.1. At ~51º 6´E 10º 16´S and 51º E 9º 30´S, both positive and negative change values are found in two limited areas. The Winter–Autumn map contains positive change values for the northern area (40º E 8º S and 53º E 12º S). Patchy areas with positive change values between 0.1 and 0.2 are found between ~8º S and ~10º S. South of 10ºS and in between the patchy areas the change values lies in the range of 0 and 0.1. Spring – Winter map shows homogeneous negative change values through out the area. The change values lies between 0 and 0.1. At ~50º E 8º S and ~53º E 8º S the change values are negative and with values between 0.1 and 0.2. The Summer - Spring map is showing the same pattern as the Spring –Winter map. The negative change values falls also here into the range of 0 to 0.1.

6.1.3.4 The Mozambique Channel

Here, the area is defined as the open ocean that is sheltered by the presence of Madagascar and lies between ~12º S and ~26º S .The Autumn – Summer map show that there are small changes all through the channel. The change values are negative and lie between 0 and 0.1. Of the coast of Madagascar, between the northern tip at ~12ºS and around ~16ºS the change values are positive and lie between 0 and 0.1. From ~18º S to ~23º S the change values also experience positive values between 0 and 0.1. The Winter – Autumn map shows a uniform change pattern all through the channel with positive values between 0 and 0.1. The exception is west of Madagascar from ~12º S to ~22º S, were small negative change values between 0 and 0.1 are found. The Spring – Winter map shows a homogene change pattern all through

the channel with negative change values between 0 and 0.1. The Summer – Spring map shows that the western part of the Mozambique channel is dominated by positive change values in the range of 0 to 0.1. The eastern part of the Mozambique Channel experience small negative change values that lie between 0 and 0.1.

6.1.3.5 Coastal waters of Madagascar

The coastal waters dominated by relative high chlorophyll concentrations compared with the open oceans. First, the Autumn – Summer map is examined. The northwestern coastal area of Madagascar between ~12º S and ~45º E 16º S contains is dominated by positive change values in the range of 0.5 and 1.5. Moving southwards along the coast, from ~16º S to ~19º 30´S, the change pattern alternates. The coastal change values are here negative in the range 0.5 to 3. Further south, to about 24º S, there is an alternating pattern of high and low positive change values in the range of 0.1 to 1. At the southeastern part of the southern Mozambique a clear tongue of negative change values oriented in a southwestern direction is mapped. This tongue has its largest change values at ~47º E ~25º S, with a negative values ranging from about 0.5 to 1. The change negative change values gradually approaches zero in the southwestern direction. Along the eastern coast of Madagascar, the change pattern is alternating between positive and negative change values. From ~15º 30´S to 17º S there is a positive change area with measured change values up to 4.

Next, the Winter – Autumn map is examined. The coastal area between ~12º S and ~45º E 16º S in the northwest has generally negative change values, but with some patches of positive values. Southward along the coast, from ~16º S to ~19º 30´S, the change values are positive (from ~0.5 to ~2). Further south, at 19º 35´S, there is a small area of clear negative change in the magnitude of ~0.4 to 0.6. The rest of the southwestern coastal waters contain relative small negative change values, except some patches of pixels with positive change values. The tongue of change is also here clearly visible south of Madagascar. But now the changes are positive. At ~47º E ~25º S, the area with the largest positive change values, the values lie in the range of ~0.5 to 1. Further in the southwestern direction of the tongue, the change values ranges from 0.2 to 0.3 in the core of the tongue. In the edges, the values lie between 0.1 and 0.2. Northwards along the east coast of Madagascar the change pattern is patchy, with an emphasis on the positive values and some pockets of negative change.

The Spring – Winger map shows that the coastal waters of Madagascar generally contains negative change values. As an exception, the northwestern coast line from ~12º S to ~45º E

16º S where some patchy areas contain positive values. Southwards, the coastal waters from ~16º S to ~20º S contains relative large negative change values from around 0.5 to 2. The tongue shape south of Madagascar can also in this map be seen clearly. The relative change values are small compared with surrounding areas. The changes values are negative (between 0.1 and 0.2). Moving to the Summer – Spring image one can observe that the majority of the coastal waters hold positive change values. However, two distinct coastal areas contain negative change values. These are the northwestern coastline (~16º S to ~19º S) and a part of the southeastern coastline at around ~47ºE 25ºS.

6.1.4 Summary

To summarize the findings of the seasonal climatological changes there are two distinct patterns that dominates. The largest relative changes are found in the coastal area, while the smallest changes are found in the open oceans. Both, along the east coast of Africa and the coastal waters of Madagascar experience alternating patterns of change on average though the seasons. Coastal waters near river mouths seem to experience higher chlorophyll values in the summer months than in the rest of the seasons.

The monsoon cycle is influencing the precipitation pattern, and the summer rainy season leads to increased river runoff. River runoff data from selected rivers in Mozambique are presented in section 6.3, which show a clear seasonal pattern. The supplying of nutrients from the rivers leads to increased phytoplankton production. The influence of CDOM may lead to an overestimation of the chlorophyll measurements in the river runoff influenced coastal areas.

In the open oceans in the southern part of the study area, there seems to be a seasonal chlorophyll peak in the winter months. Obviously, the effect is not related to the sun illumination. The most reasonable answer is that the slight phytoplankton growth is due to an increased level of nutrients in the area. Increased wind mixing by winter storms is a likely explanation to the observed average effect.

The upwelling zone south of Madagascar and the effect of the southern east Madagascar current is clearly mapped by the change detection of the seasonal climatologies. There is a clear winter maximum found in the area. The findings are also found in Ho *et al.* (2004). However, no clear suggestion on why there is a seasonal effect on the upwelling has been given. The use of simple change detection technique such as the pairwise comparison of the

seasonal climatologies only reveals any change that can be related to the average pattern. Interannual or long term trends are not revealed. However, the method was efficient for highlighting spatial patterns in both the coastal zone and the open oceans. It is expected that some of these change patterns reappear when the Standardized Principle Component Analysis is performed on monthly and weekly averages form the SeaWiFS and MODIS Aqua sensors.

6.2 SPCA of the 9km monthly averaged SeaWiFS data set

A Standardized Principle Component Analysis was performed on SeaWiFS monthly averaged chlorophyll data. The dates range from September 1997 to September 2005. The output of this analysis comes in the form of component images and component loadings in the form of graphs. The loadings illustrate the degree of correlation between each of the monthly images and the component that has been mapped. If a month shows strong positive correlation with a component image, this indicates that the month contains a spatial pattern that has strong similarities to the component image. A strong negative correlation indicates that the monthly image has a pattern that is the inverse of the component image. As noted by Eastman & Fulk (1993) the strength of a component is determined by both the magnitude of the variability it explains and the area over which that variability occurs. Further, Eastman & Fulk (1993) notes that change elements in time series analysis are area weighted. This means that small magnitude changes may come out in early components if they influence large areas. On the other hand large effects may come out later components if they occupy small areas.

Component 1

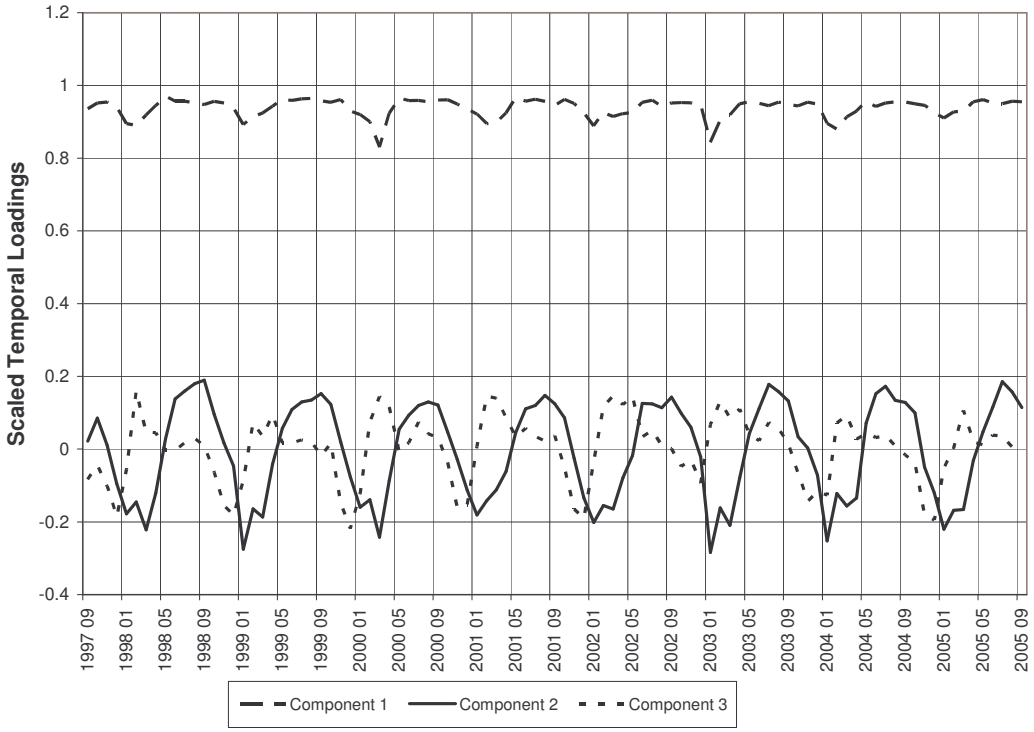

Figure 6-5. Loadings (Y-axis) of component 1, 2 and 3.

Figure 6-5 shows the loadings for the first three components. The first component image represents the characteristics chlorophyll values integrated through all the time series. To illustrate this is the 1st component image shown in Figure 6-6.

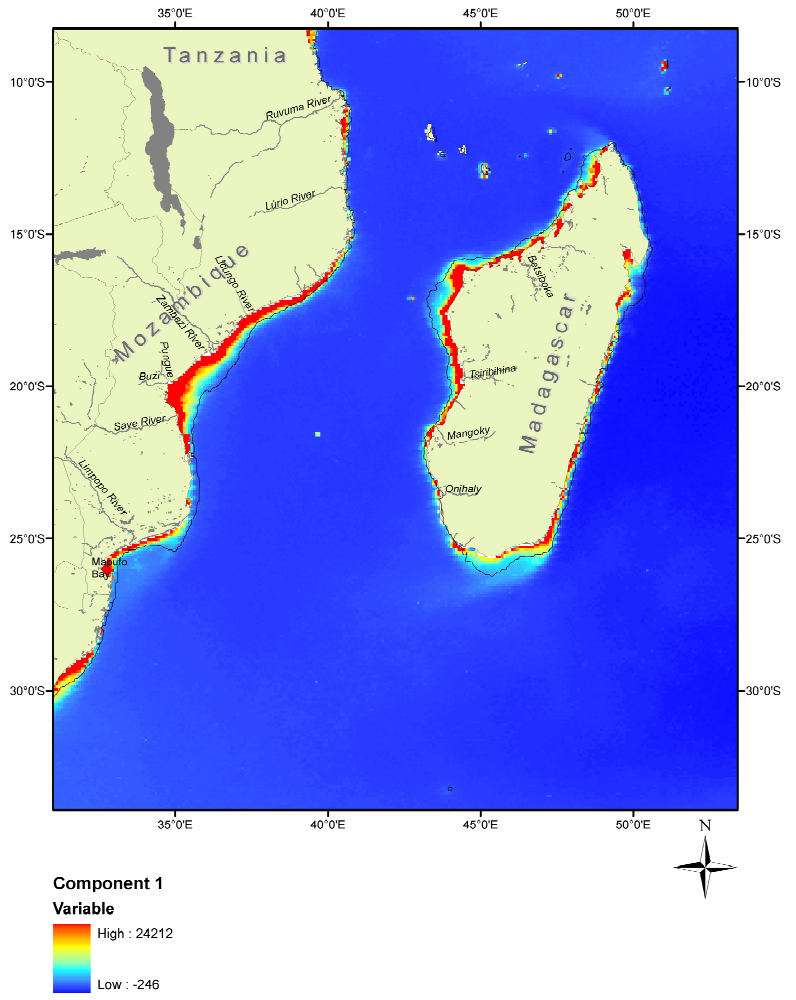

Figure 6-6. Component 1 image

The first component represent the characteristic chlorophyll levels integrated over all the months in the times series. The amount of variation is 88 %. The loadings for the first component show that there are some months which correlate less with the first component image than other months and that it is a clear temporal pattern. The loadings graph begins in September 1997, where the correlation is high. For each year, there are dips in March and flat periods between May and November.

What can be learned from the loadings from the first Component? First, the loadings show that there are seasonal variations throughout the time series. In the austral summer, the months of January, February and March are generally less consistent with the Component

image. In other words, there are some changes in the chlorophyll content that is differs from the average picture. This is the interannual variation Second, the through peaks of less correlation are not the same for each season. This is also true for the magnitude of the bottom peaks. The bottom peaks of March 2000 and January 2003 contain smaller correlation values then the other seasonal bottom peaks through the time series. The timing of the peaks are calculated also differs slightly from year to year. However, this may be an effect of the temporal binning in the SeaWiFS data set. The first component loadings show the interannual variation. Even if each year is similar to the other years there are some seasonal differences as indicated by the graph.

Component 2

2nd component image and the corresponding loadings are representations of the seasonal cycle of the chlorophyll content. Component 2 illustrates the first change component, which is the most prevalent element of variability in the chlorophyll content in the study area that is uncorrelated with the characteristics in Component 1. The second component accounts for 1.7 % of the variations. The pattern of the component loadings suggests that the major element of variation of chlorophyll is due to the influence of the seasons. The graph of the 2nd component loadings is given in more detail in Figure 6-7.

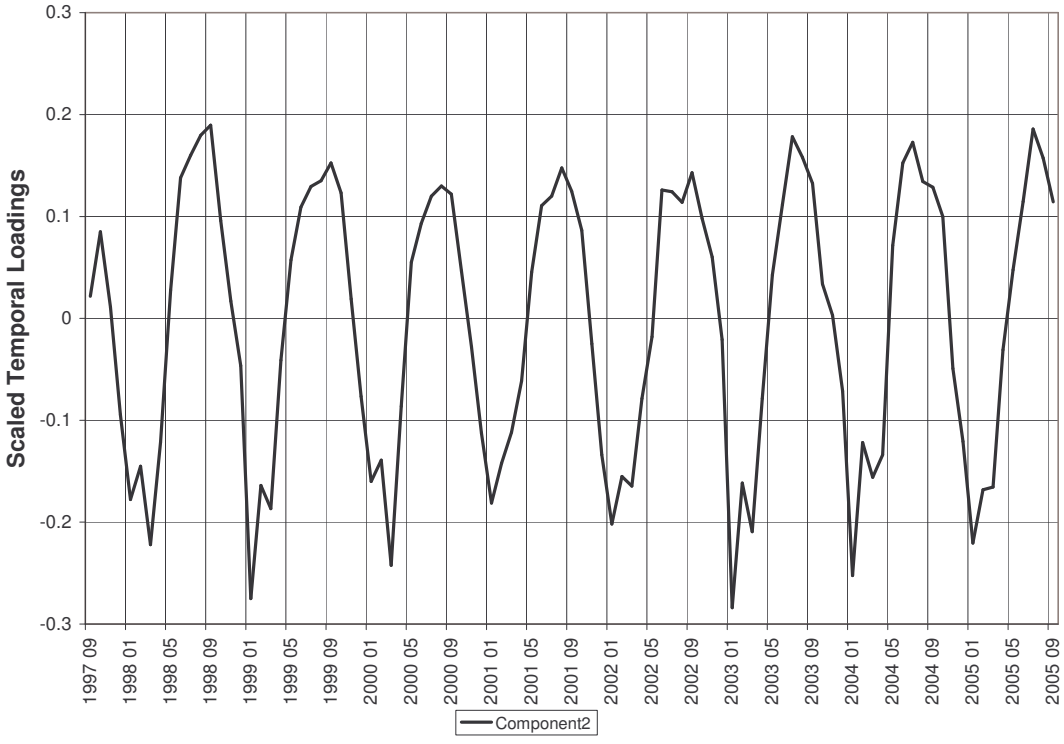

Figure 6-7. 2nd Component loadings

Positive correlation is found in the austral winter months and negative correlation is found in the austral summer months. There are some interesting patterns in the loadings of the component. First, the positive correlation peaks will be considered. The austral winter peaks are not present at the same time for each season, nor is the magnitude the same for each peak. In 1997 the peak is in October, followed by September 1998, September 1999, August 2000, August 2001, two peaks in June and September 2002, July 2003, July 2004 and finally in July 2005. A general trend is that the timing of the seasonal peak is arriving earlier in the year later as the time series develops. The magnitude of the 1997 October peak is much lower than the rest of the positive correlation peaks. The October 1998 high shows strong positive correlation with the component image. The 1999 and 2000 austral winter peaks show a successive fall in correlation. The peaks are more or less stable in 2001 and 2002 before the magnitude of the peaks is getting higher in 2003.

An interesting pattern is the double throughs. This occurs in each year except 2001 and, to a degree, in 2005 where only one peak is observed. The timing of the throughs occurs each year at the same months, namely in January and March. There is also a difference in which of the peaks has the greatest magnitude. In 1998, March has the lowest peak. In 1999 this shifts, when January has the greatest peak. In 2000, March shows the greatest magnitude.. An observed pattern is the oscillating trend of the negative correlation maximum. From 1998 to 1999 is the magnitude of the negative maximum increasing. From 2000 to 2001 the maximum peak is decreasing. In 2002 and 2003 the maximum is again increasing, before decreasing in 2004 and 2005. If we compare loadings of the first Component with the loadings of the 2nd Component (Figure 6-5) one can see that the months that correlates less with Component image 1 corresponds with the months of strong negative correlation in the loadings of Component 2.

The 2nd component image gives information on where the changes indicated by the component loadings take place (Figure 6-8). As was learned from the scrutinizing of the seasonal climatologies in section 6.1.2, the largest seasonal chlorophyll content differences were found in the coastal waters, while smaller differences were found in the open waters. What is expected is that the coastal waters correlate stronger with the component loadings than the open waters since the relative change values are of higher values in the coastal zone than in the open waters. In the second component image are the areas with high positive correlation with the component loadings colored with red. The areas with high negative

correlation with the component loadings are colored in blue. According to the colors seen in the Component 2 image is the coastal area those who correlates strongest, both positively and negatively, with the component loadings graph. The open ocean correlates less or has no correlation at all according to the image. However, it can be seen that the northern and

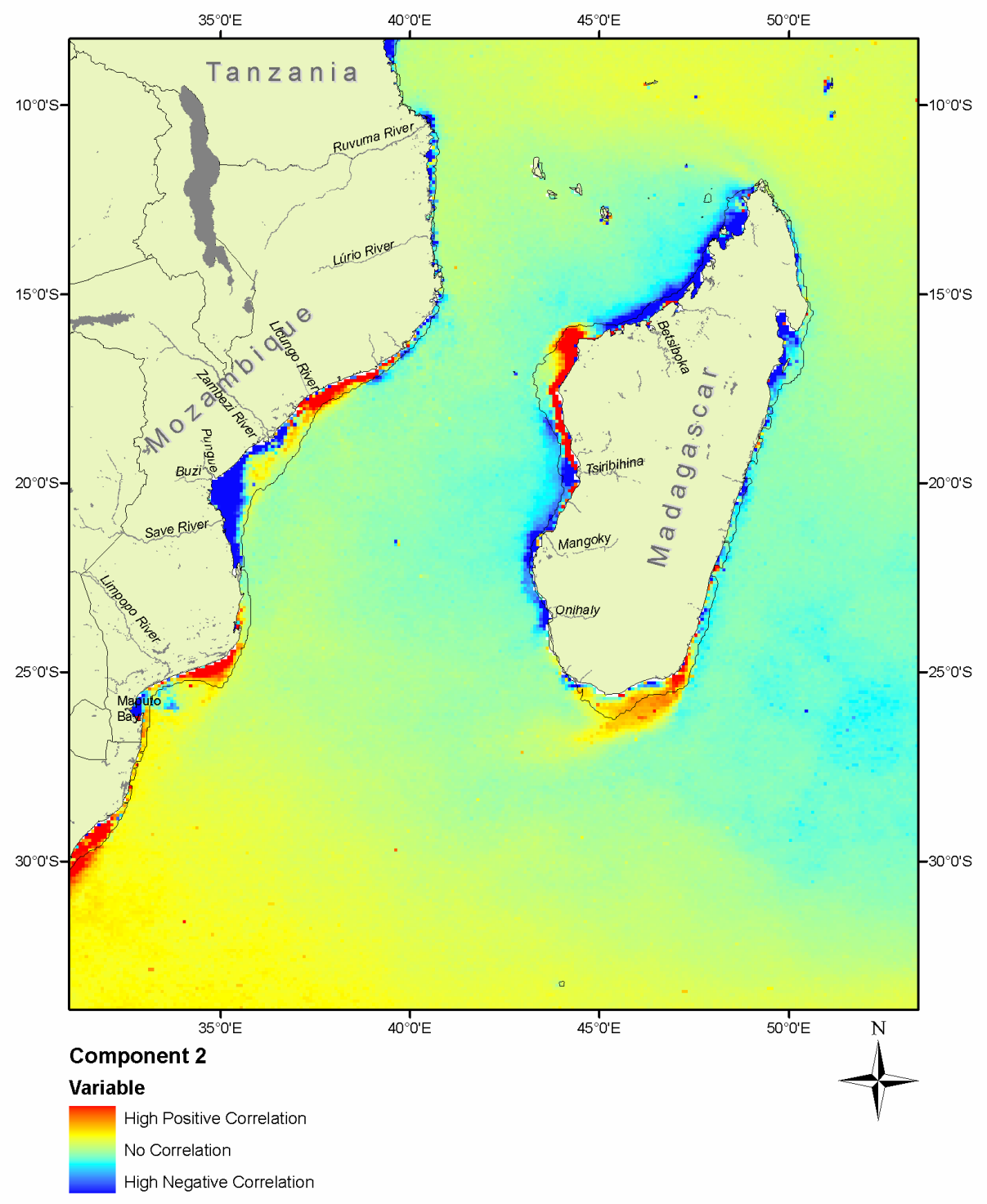

Figure 6-8. Standardized Principle Component Image 2 derived from monthly chlorophyll data, September 1997 to September 2005. 200m depth contour added.

southern open ocean of the study area contain positive correlation values, this is also confirmed by checking pixel values in the areas. Recalling from the inspection of the seasonal climatologies and climatological changes in section 6.1 and 6.1.1 it was found that the chlorophyll content was generally higher (between 0.2 and 0.3 mgChl-a/m³) in the austral winter than in the rest of the seasons. It was also clear that the austral summer months contained the least amount of chlorophyll in these areas (below 0.1 mg Chl-a/m³). The component loadings graph highlights the pattern of the changes in chlorophyll content. The late austral winter months and early spring months correlate positive with the high components in Figure 6-7 and correlates negative for the summer and early autumn. The reason why the Component 2 image shows that the correlation between the northern and southern part of the study area is small, is due the relative variation in the chlorophyll content through the seasons. The chlorophyll peaks or plankton blooms, indicated by the component loadings graph, shows that the timing of the bloom is not the same for each year and that the magnitude of the blooms also changes as described earlier in this section.

When it comes to examining the coastal waters, five distinct areas with high positive (colored in red) correlation can be distinguished in Figure 6-8. These are located at (1) the South African East coast at approximately 31º 30´E 30º S, (2) coastal waters east of the Limpopo River in Mozambique at ~35º E 25º S, (3) coastal waters close to the Zambezi River at approximately 38º E 17º 30´S, (4) waters along the north western Madagascar coast from ~16º S to ~19º 30´S and (5) the near coastal waters south of Madagascar from about 47ºE 25ºS to about 45º E 26º 30´S . These areas correlate strongly with the temporal loadings shown in Figure 6-7 and experiences higher levels of chlorophyll content in the winter and early spring. This confirms the findings in Figure 6-3 where the winter climatology clearly has a higher chlorophyll content in the same areas than the rest of the seasons. One can say that the above mentioned areas vary in phase with one another.

The areas with a high negative correlation (colored in blue) indicate a pattern that is inverse with the loadings graph. The most prominent areas include (1) the coastal waters in Maputo Bay in southern Mozambique, located approximately at ~33º E 26º S, (2) the coastal waters from ~37º E 18º 30´S which stretches from south of the Save River to east of the Zambezi river mouth, (3) some patchy coastal areas on the coast north of ~16º S, (4) the north western coastal area of Madagascar from the northern tip (~12º S) to ~16º S, (5) the coastal waters on the west coast of Madagascar from ~19º 30´S to 24º S, (note that the waters closest to the

southern Madagascar coast from ~44º E 25º S to 46º 30´E ~25º S correlate negatively), (6) the eastern coast of Madagascar that have some patchy regions of negative correlation. The high negative correlation means that the mentioned areas as seen in Figure 6-8 experience chlorophyll peaks in the austral summer. We now have a clearer impression on where the changes take place. There is, however, one consideration we have to make. The coastal waters that are influenced by river runoff can be classified as Case 2 waters. We know from chapter 4 that the chlorophyll values in these waters tend to be overestimated due to the influence of constituents in the waters which is not optically covarying with the chlorophyll. It is likely that that the results here are biased because of this effect

Component 3

Next, the third Component image and the corresponding loadings graph will be examined. The loadings are shown in Figure 6-9 and the component image is shown in Figure 6-10. The Component 3 image contains 0.8 % of the variance in the time series. There are some distinct seasonal patterns that can be seen in the loadings graph.

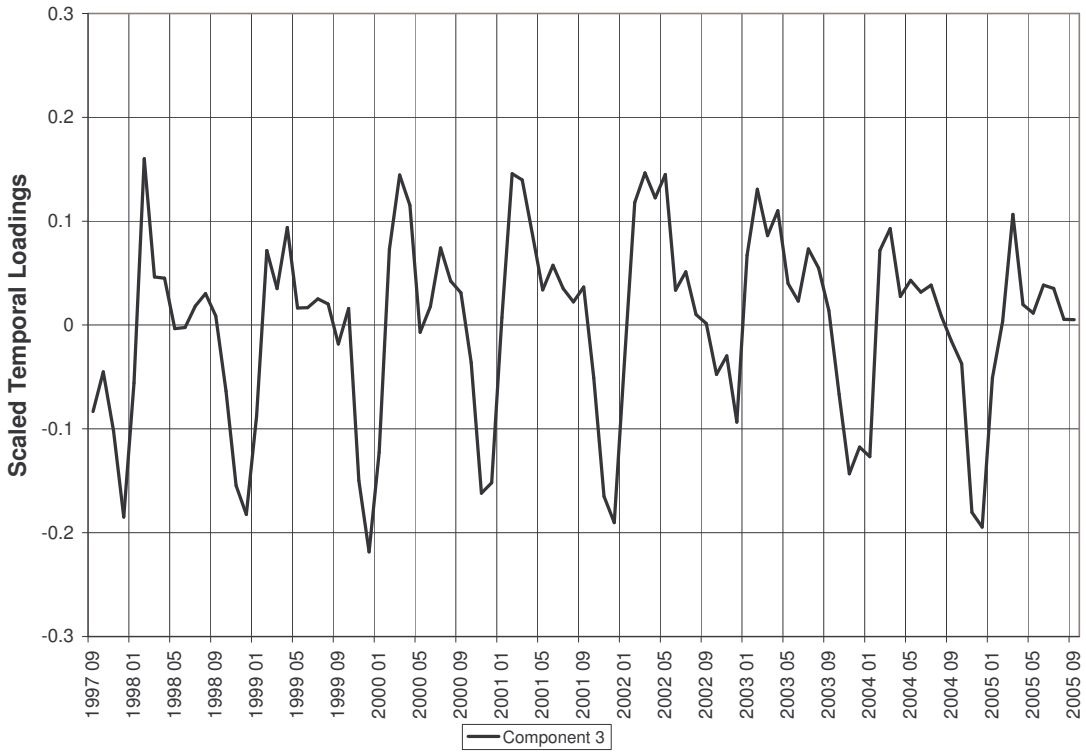

Figure 6-9. Loadings of Component 3.

First, a high positive loading high is found in the late summer and early autumn for each season. A negative through is found in December for all the seasons. What breaks the sinusoidal pattern is the presence of a distinct shoulder, in general from May to October. The

pattern suggest that the areas that are correlate positive with the temporal pattern in Figure 6-9 experience two chlorophyll blooms for each year in different magnitude. The loadings pattern shows that there are some clear differences in the magnitude of both the negative and the positive peaks. The timing of the positive peaks is not the same for each year. The 1998 positive peak is in February.. Moving to 1999 we see that there is a double peak in February and April. The peak in 2000 is in April, while the peak in 2001 is in both March and April. The magnitude of the peaks is not the same for each season either. This suggests interannual differences in the magnitude of the chlorophyll variations.

Moving to the shoulder seen in the austral Autumn and Winter months one can see that the shape, duration and magnitude of the shoulder changes from year to year. In 2002 the shoulder is not present at all. And is followed by a negative peak in December 2002, which is of less magnitude than the negative December peaks for the other years.

The corresponding component image (Figure 6-10) shows that the coastal waters of Madagascar contain values that are highly positive correlated with the temporal loadings. Open oceans show little or no correlation with the loadings. The chlorophyll variations proved to be small and are accounted for in the 1st component. The positive correlation patterns are found in the southern Mozambique from ~32º30´E 26ºS to ~34º30´E 25ºS and from ~35ºE 20ºS to ~40º30´E 16ºS. North of 16 ºS on the eastern coast of Africa, alternating coastal areas of both positive and negative correlation is seen. Significant areas of high negative correlation is restricted to (1) the coastal areas around ~32ºE 29ºS in the south western corner of the study area, (2) the coastal area in the southern Mozambique at about ~35ºE 24ºS (only minor negative correlation), (3) coastal areas south of the Save River at ~35º30´E 21º30´S and a limited area of the coast north of the Save River mouth at about 35ºE 20º30´E.

What can be concluded from these results? The patterns suggest that there might be two chlorophyll peaks per season in the coastal areas which is colored red in the 2nd component image. But again, we have to think of the possibility of a bias from the effect of CDOM. It is possible that the chlorophyll variations itself are not as clear as the component loadings suggest.

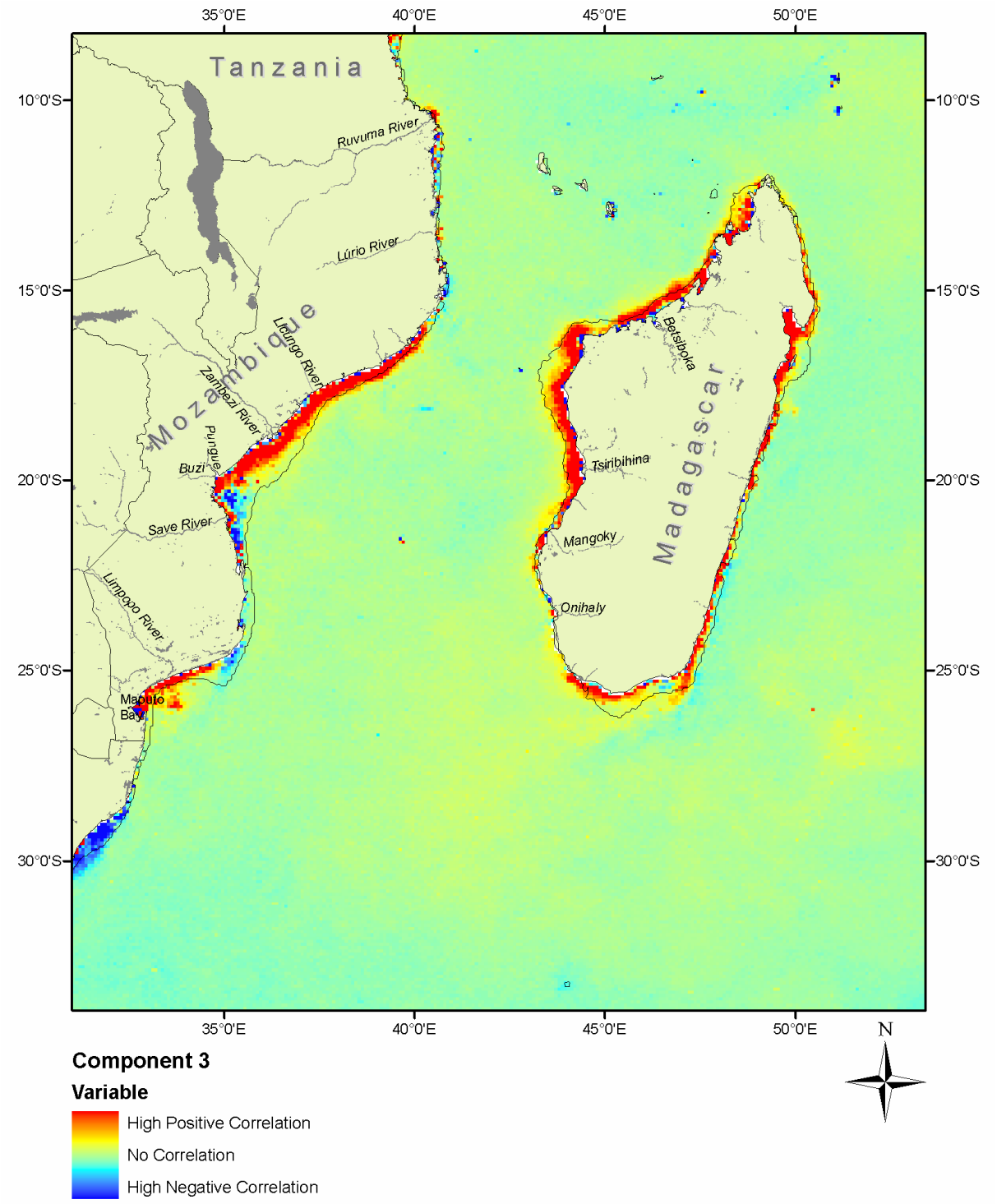

Figure 6-10. Component 3 image

Component 4

Next, the fourth component image (Figure 6-12), and the corresponding loadings (Figure 6-11) will be examined. The fourth component consists of 0.6 % of the total variation in the SeaWiFS data set. The component loadings show a pronounced and semi-annual sequence. The negative and positive peaks are all related to the same months. The positive peaks are

seen in March and October; the negative peaks are seen in January and June. The magnitude of the positive and negative peaks seems to have an alternating pattern. In 1998, 1999, 2000 and 2001 the highest positive peak is found in March and is increasing for each of the mentioned years. The positive peaks of the lowest magnitude are found in October for the mentioned years. These peaks are also increasing for the mentioned years. The March peak of 2002 is breaking the alternating pattern by having a very low positive magnitude. The following positive peaks are increasing from October 2002 and March 2003, before decreasing in October 2003 and March 2004. It is also seen that the magnitude of the negative peaks are changing through the time series.

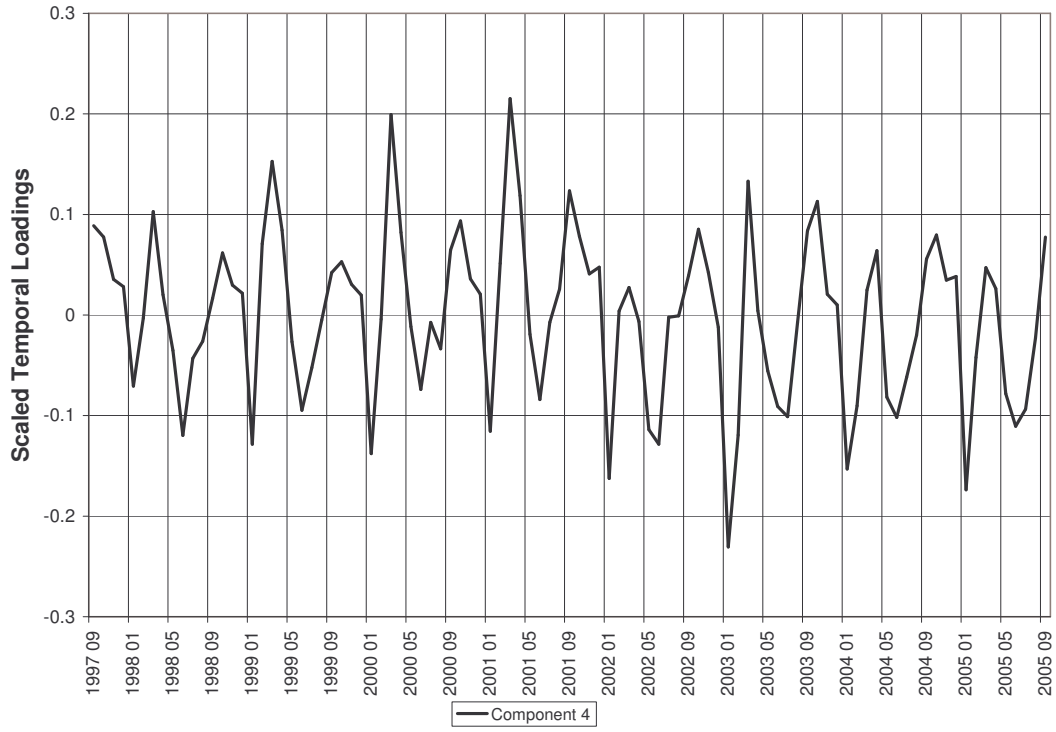

Figure 6-11. Loadings of Component 4.

The spatial patterns of the Component Image (Figure 6-12) shows that the open oceans are have none or little correlation with the component loadings. The positive correlated areas are mostly concentrated in the coastal waters of Madagascar, while the coastal areas of eastern Africa experience negative correlation with the component loadings. The most prominent of these areas are (1) the coastal waters in southern Mozambique from ~32º30´E 26ºS to ~35º30´E 24º30´S and (2) the coastal waters from ~35ºE 21ºS (near the Save River Mouth) to 39ºE 17ºS. The coastal African areas north of 17ºS do not a show a clear pattern. Why is this?

It is likely that the changes have been mapped earlier in the components. This removes the signal from the later components.

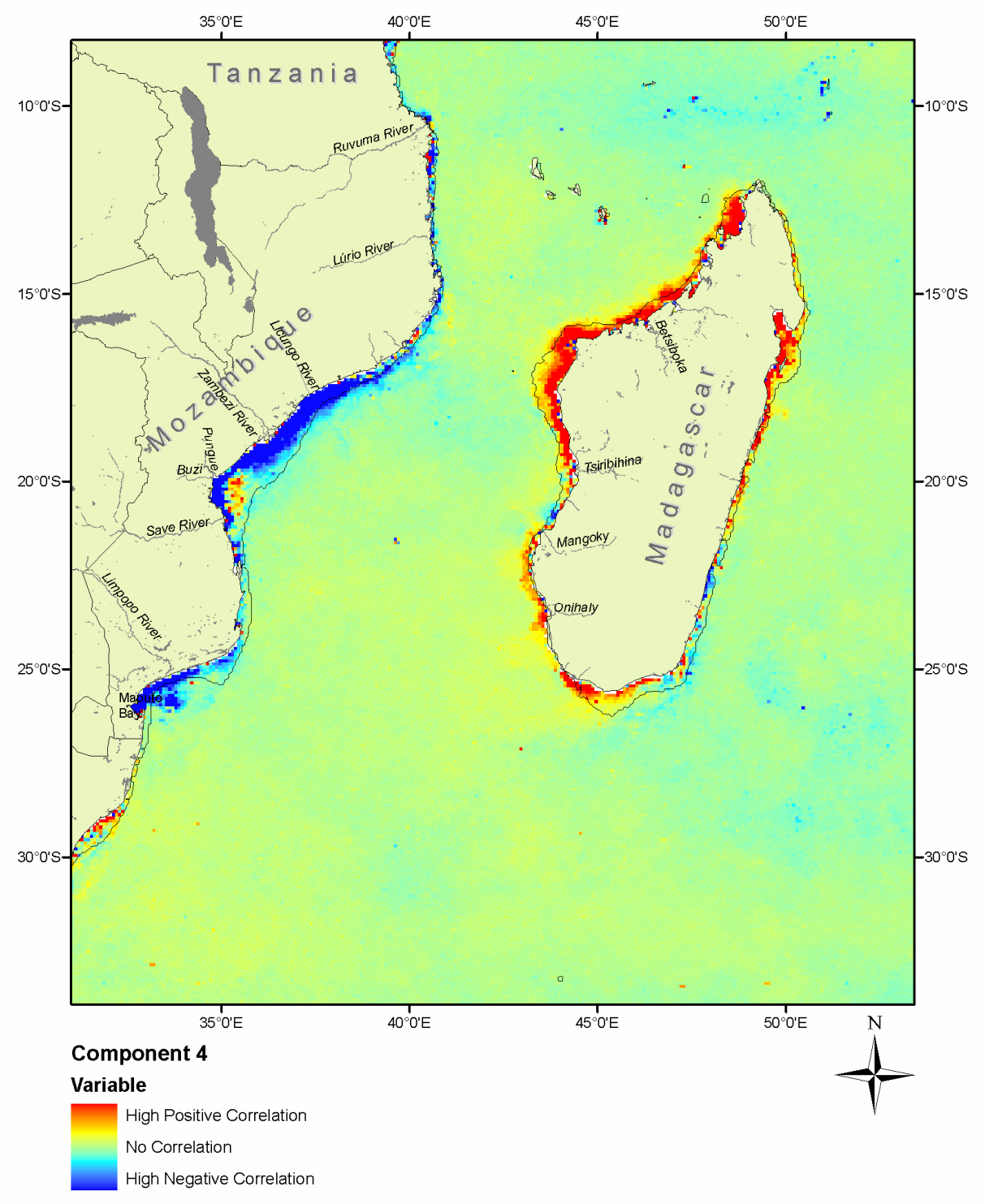

Figure 6-12. Component 4 image.

Component 8

The 8th component consists of 0.3 % of the total variation in the data set. When looking this deep into the data set, one might expect that the recorded effects occupy smaller areas over shorter periods of time as indicated by Eastman & Fulk (1993). This is exactly what might be the case for the data in the 8th component. Figure 6-13 shows a somewhat chaotic and irregular pattern, but contain to clear anomalies which stands out. In the months of February and March 2000, there is a strong positive anomaly present. In March 2001 there is a clear negative peak. Looking at the component map in Figure 6-14, one can see that there are some distinct regions which correlate highly positive with the component loadings. The strongest correlations are found (1) in the coastal areas of southern Mozambique from ~32º30´E 26ºS to 35ºE 23ºS, (2) the coastal near the Save River from ~35ºE 21º30´S to 35º30´E to 19º30´S, (3) and the coastal areas south and south east of Madagascar. An interpretation of the high component loading peak in February and March 2000 may be that there is an anomaly high and regional elevated chlorophyll peak in these months that is not a part of the seasonal variations. However, this has to be investigated further. The timing of the February/March peak is probably due to the extreme flooding in Mozambique in February 2000 caused by heavy rainfall (Dyson, 2000). CDOM, organic and inorganic matter may influence the signal as it enters the ocean. The nutrient supply may also trigger phytoplankton growth, and thus the chlorophyll signal is enhanced.

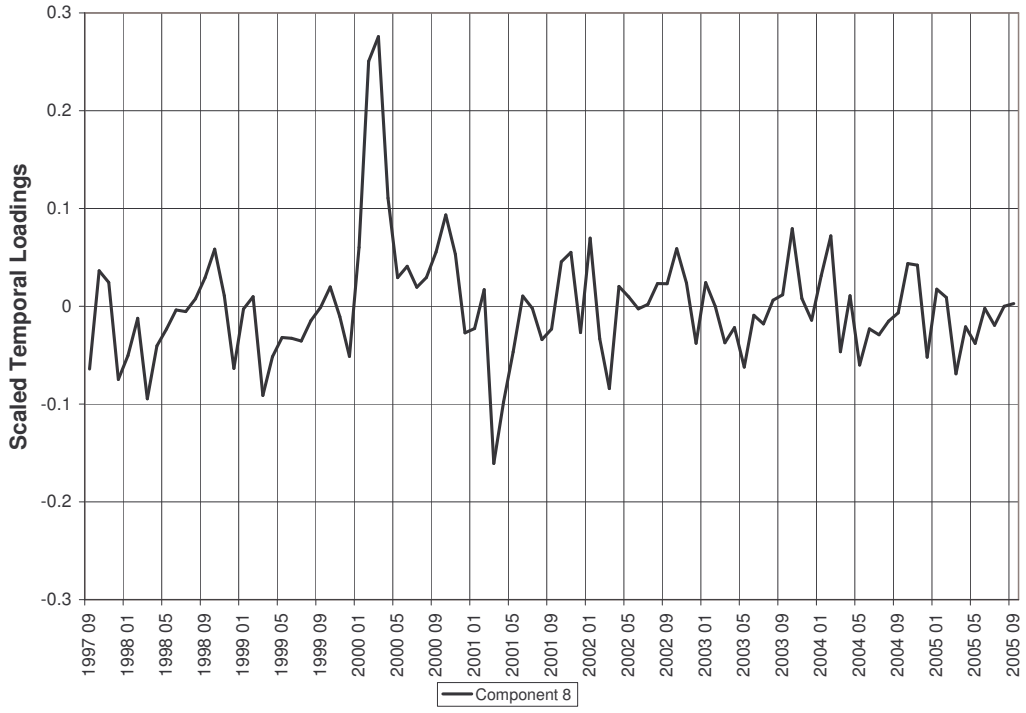

Figure 6-13. Loadings of Component 8

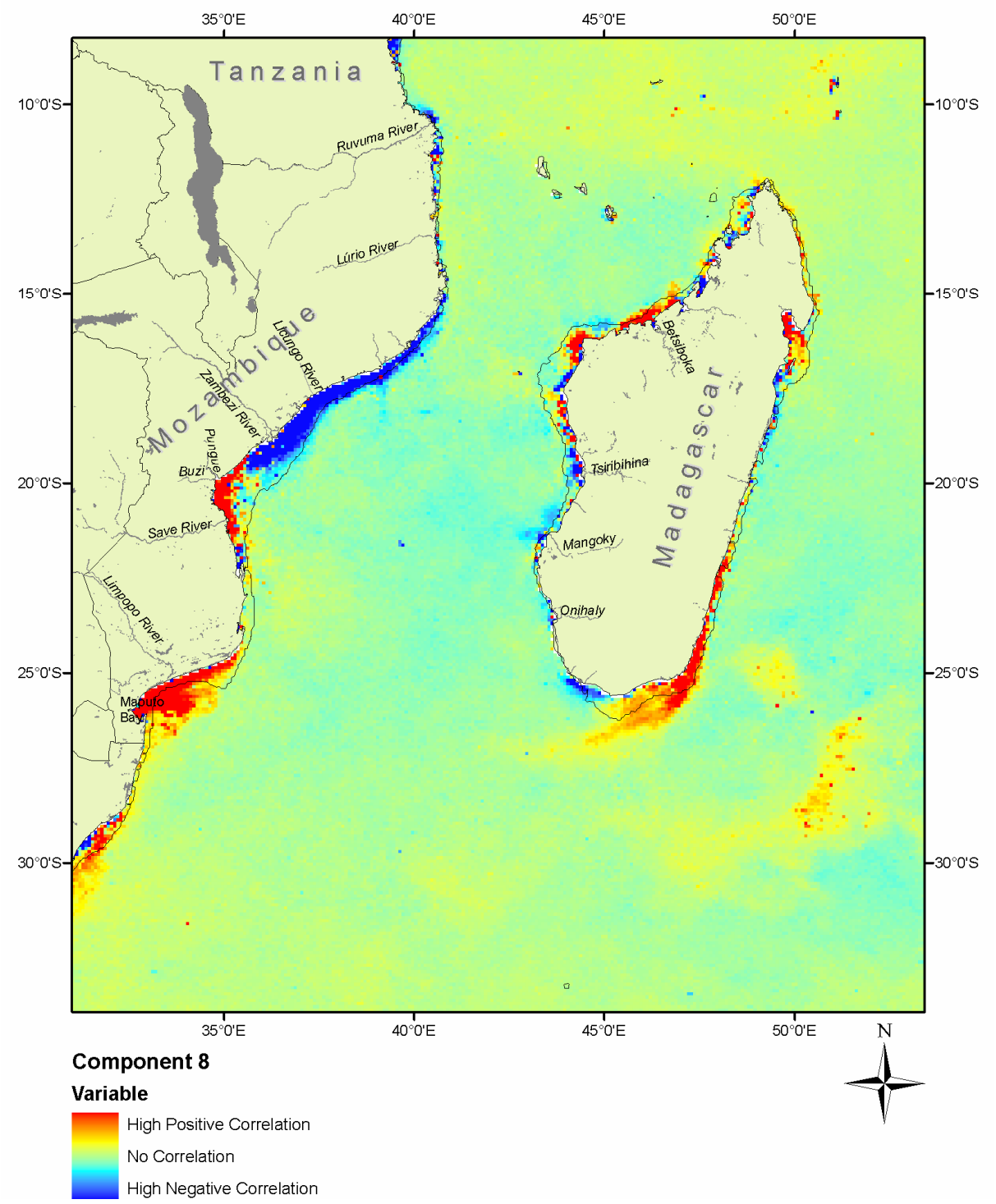

Figure 6-14. Component 8 image

Component 5, 6 and 7

These components did not show any significant results. The 5th component image and loadings can be seen in Appendix C. Component 6 and 7 are not shown.

6.2.1 Summary

Eight component images and the corresponding component loadings from the monthly SeaWiFS 9 km data set from September 1997 to September 2005 have been analyzed. The analysis revealed that it exist strong seasonal and interannual variation in the chlorophyll content. But how many components are necessary for describing the chlorophyll variations? The 8th component image and loading showed some patterns that reasonably could be connected to the flooding in Mozambique. Component 4, 5, 6 and 7 did not show any significant results.

As expected from the scrutinizing from the seasonal climatologies, the SPCA showed that the zones of high activity were located in the coastal zone. Minor, but significant change patterns are seen. The 2nd component loadings, which represents the main seasonal variations of chlorophyll in the study area showed a clear sinusoidal pattern, as expected. From the analysis of the seasonal climatologies it was expected that the southern open ocean in the study area should show a clear winter maximum. This came clearly out in the 2nd component. The timing of the peak is now more nuanced and the southern ocean maximum is located to the end winter/ beginning of the spring (August/September/October). This illustrates the problem of using seasonal climatologies as a source for interpreting change. The actual timing of the bloom is hidden in the calculation of the averages. The temporal location of a spring bloom, as indicated by the 2nd component loadings, leads to the notion that the increased illumination of light and increased temperature is a trigger to the phytoplankton bloom.

Coastal areas in eastern Africa and Madagascar which shows strong negative correlation with the 2nd component loadings are interpreted to experience a chlorophyll maximum in the summer/rainy season, induced by increased river runoff and favorable illumination conditions and temperature.

A study by Paula *et al.* (1998) of seasonal cycles of phytoplankton variations in the Maputo Bay (southern Mozambique), showed that there is a maximum chlorophyll peak in March. The chlorophyll values decreased in the following cooler months. A minor peak was found in September when the temperature begins to rise in the spring. It is noted that the main factor which is responsible for the chlorophyll maximum is accumulation of nutrients during the rain/summer season. It was also noted that much of the same pattern can be found along the

African coast, but it was mentioned that one must be precautious using this assumption without a more through studies.

The coastal areas of Madagascar and eastern Africa which are showing strong correlation with the 2nd component loadings can be interpreted to not be more influenced by spring/winter bloom than the rainy season bloom. The 3rd component illustrated this. Here, most of the coastal areas are positively correlated with the loadings. The highest maximum is found in the summer/rainy season and a minor peak is found in the late winter/early spring. These findings correlate well with the findings of Paula *et al.* (1998), even tough the study is only performed at one specific place.

6.3 Time Profiles

The scrutinizing of the SPCA analysis of the chlorophyll data identified geographic locations of regions of high and low activity. The component images contained information about the localization of the activity, while the component loadings indicated the timing and the magnitude of the variations. Next, time profiles of the chlorophyll content at selected areas (Figure 6-15) is produced in order to reveal the actual changes in chlorophyll content through the seasons with the use of the monthly SeaWiFS data set.

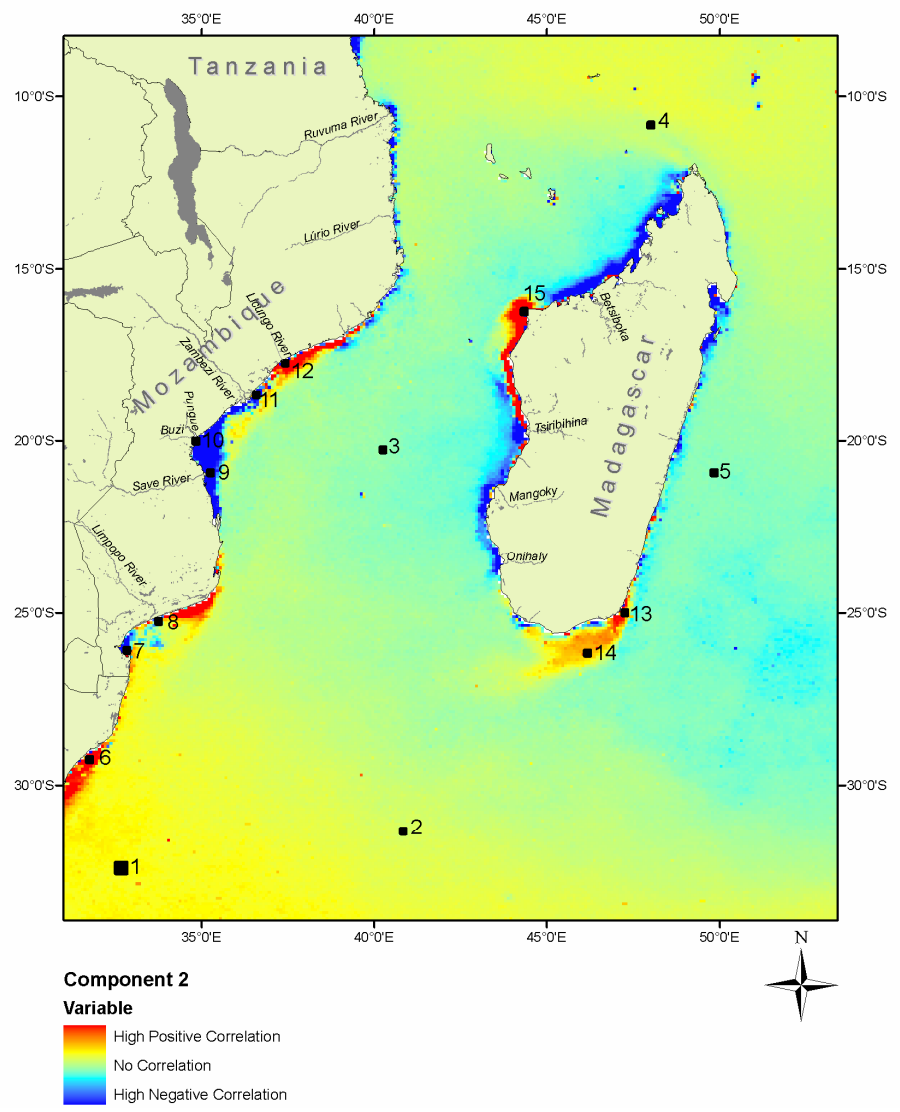

Figure 6-15. Map showing the sites used in the time profiles overlaid the 2nd component image from the SeaWiFS data set. Sites shown in black

The advantage of using time profiles is that the results (graph values) are shown in real values in contrast to the results of the SPCA analysis, which does not produce results that include physical variables. A direct interpretation of the changes in chlorophyll variations is then possible. Another goal is to verify the results of the SPCA analysis by comparing the time

profile graphs and the component loadings. The location of the time profile sites includes both open oceans and coastal water. Some of the locations were placed in the vicinity of selected river mouths. Available monthly river runoff data is used for comparison between the variations in the amount of river runoff and the chlorophyll variations. It is thought that the strong seasonal variations in the coastal areas are due to variations in river discharge. Some of the profile sites (9, 10, 11 and 12) are placed next to river mouths. Monthly river runoff data is compared with the graphs of the time profiles- The idea is to check if there is a correlation between river runoff and the variations in chlorophyll. Another point is to check if the 9 km spatial resolution is sufficient for detecting the effects of a plume. The river runoff data is provided as monthly averages. Therefore, the monthly averaged 9 km SeaWiFS data is used as the data set for creating the time profiles. Selected sites of 2*2 pixels from each monthly image in the SeaWiFS data set were extracted in order to produce the time profiles. The spatial extent of each site is approximately 18*18 km. The pixel values within each site are averaged and used in the time profile graphs. Site 1 in is an exception and is made up by 3*3 pixels from the SeaWiFS data.

Site 1 and 2

The spatial resolution is approximately 27*27 km. The figure below (Figure 6-16) shows the variations in chlorophyll content over time for site 1 and 2. The sites are located in the open oceans. In addition is the 2nd component loadings from the SPCA analysis added to the graph. Both sites are located at places which are positive correlated with the 2nd component image.

The seasonal variations of the chlorophyll content for site 1 and 2 are matching well with the variations of the loadings graph. The two sites are located in areas which are positive correlated with the loadings graph of Component 2. There is a clear seasonal cycle of relative high and low chlorophyll concentrations for both site 1 and site 2. There is a clear elevated amount of chlorophyll in the late winter and early spring months for the two sites. A corresponding low is found in the summer months.

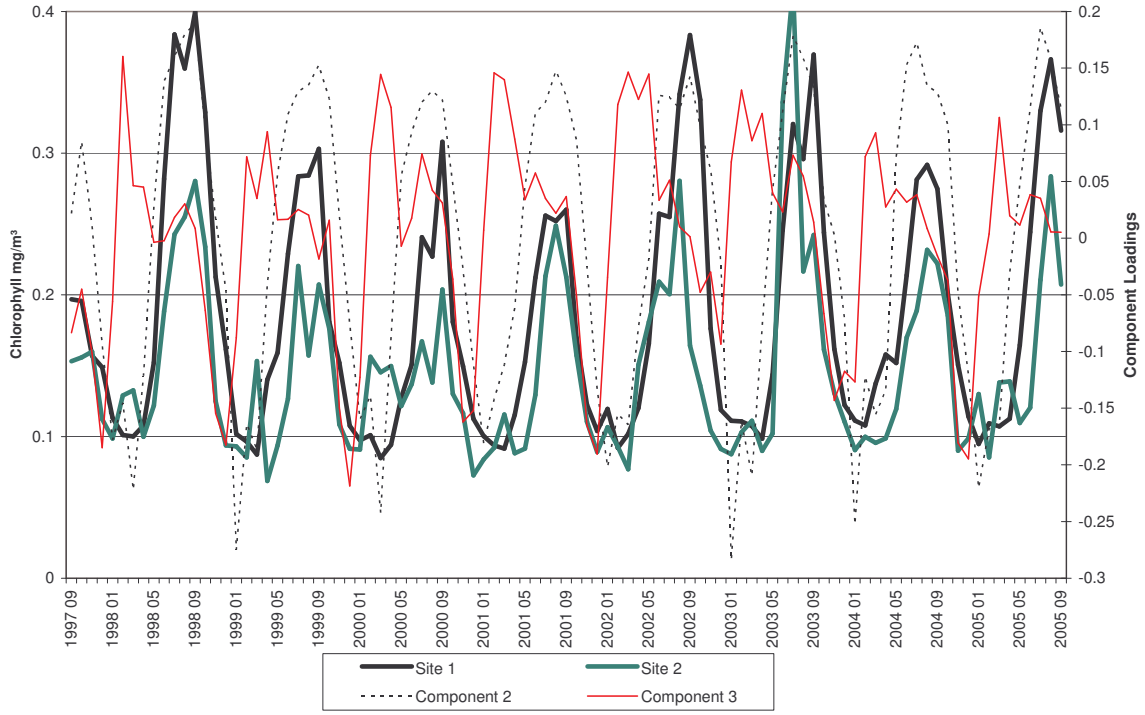

Figure 6-16. Time profile of site 1 and 2 showing chlorophyll content (left y-axis), and the corresponding 2nd and 3rd component loadings (right y-axis).

Site 3 and 4

The temporal profiles of site 3 and 4 are shown in Figure 6-17.

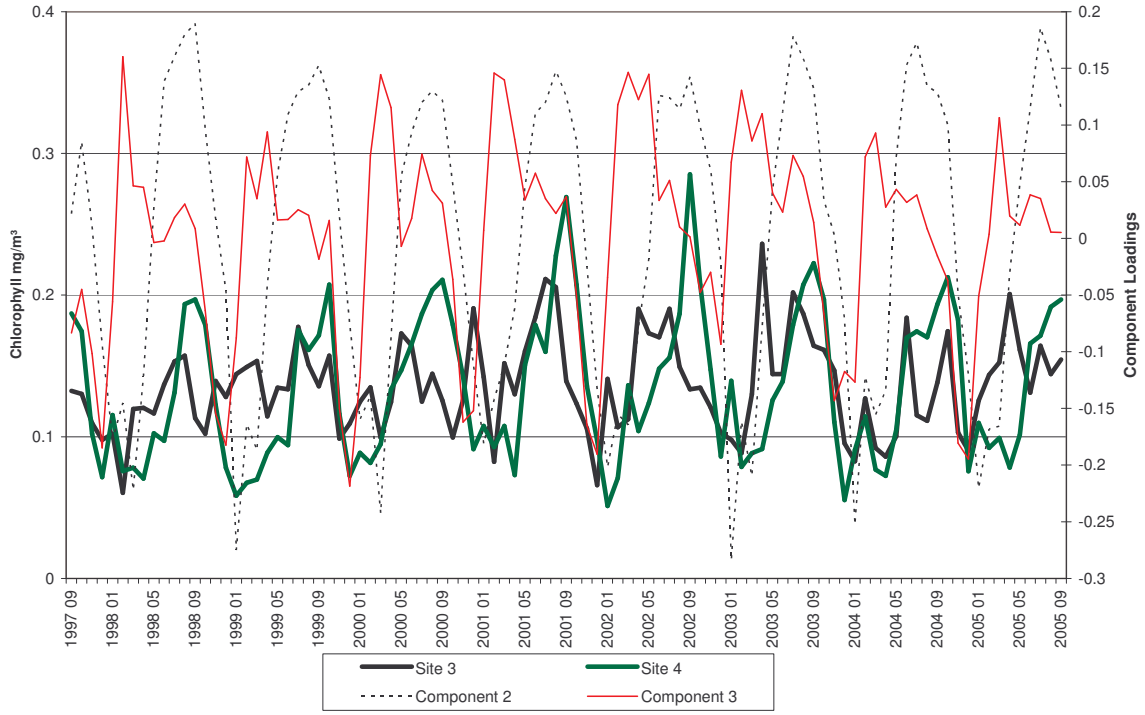

Figure 6-17. Time profile of site 3 and 4 showing chlorophyll content (left y-axis), and the corresponding 2nd and 3rd omponent loadings (right y-axis).

Site 3, which is located at an area with little correlation with the second component loadings is not showing a clear seasonal pattern compared with the 2nd component loadings graph. It is a possibility that the signal of site 3 is partly due to the passing of rotating eddies in the channel. Site 4 is located in the open ocean northwest of the northern tip of Madagascar. The site is located at an area which shows some correlation with the temporal loadings of the 2nd component, as seen in, and little correlation with the 3rd components. The chlorophyll content of site 4 shows seasonal variations that correlate well with the variations of Component 2. Site 5 shows a lesser degree of correlation with Component 2 which is expected since the site is located at an area with little seasonal variations of the chlorophyll content as indicated in the SPCA analysis. The temporal pattern of site 4 shows that the seasonal variations are very small and shows only at some events an agreement with the seasonal pattern indicated by the 2nd Component.

Site 5

Site 5 is located in the open oceans east of Madagascar which also shows some correlation with the temporal loadings of the 2nd Component. There is in some years a chlorophyll peak that corresponds with the 2nd component peaks. This explains the slight correlation with the 2nd component together with the very small variations. The profile of site 5 is shown in Figure 6-18

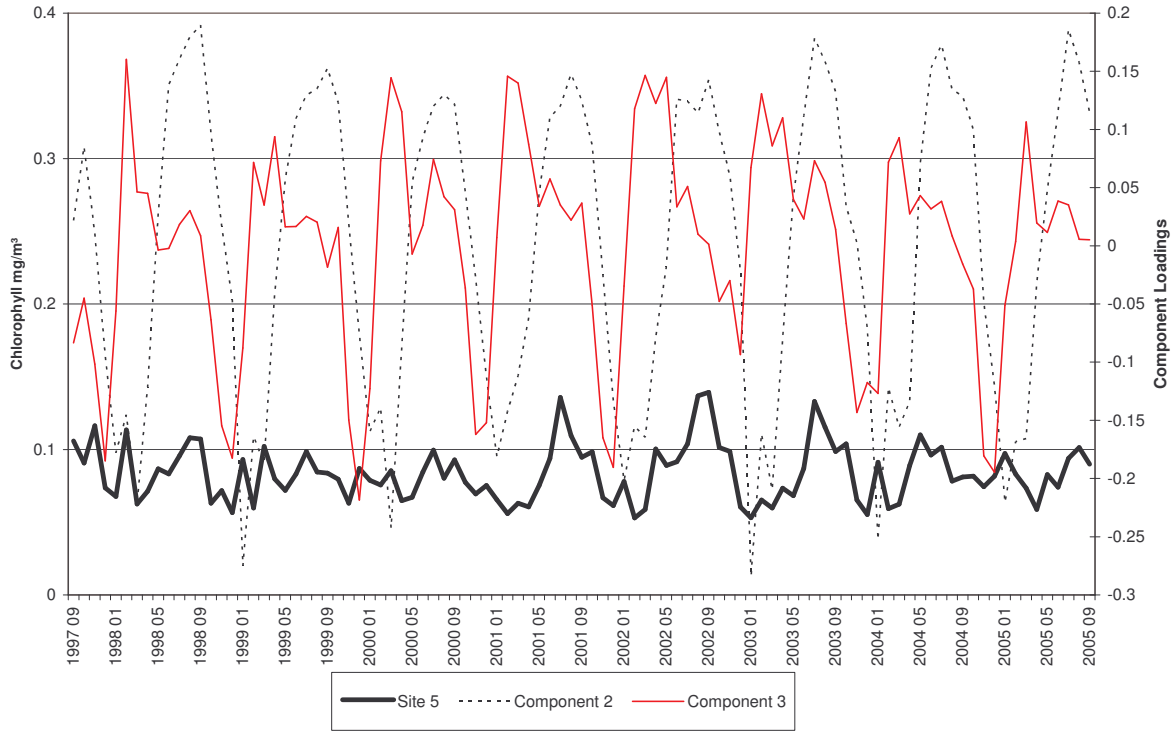

Figure 6-18. Time profile of site 5 showing chlorophyll content (left y-axis), and the corresponding 2nd and 3rd component loadings (right y-axis).

Site 6 and 7

Next, the temporal profiles for site 6 and 7 are shown in Figure 6-19. The sites are located in the vicinity of the east African coast. The center of site 6 is located at ~31° 45´E 29° 15´S, near the south African coast, which is an area that is dominated by a positive correlation with the 2nd Component loadings of the SPCA analysis as seen in. As is seen is the seasonal variations in the chlorophyll content for site 6 greater than those of the open oceans. The shape of the time profile follows, to a degree, the seasonal fluctuations as indicated by the second component graph. A main distortion is the lack of the regular sinusidonal shape as seen in the open waters sites and in the 2nd Component loadings. The elevated chlorophyll values are found in the late austral autumn and in the winter.

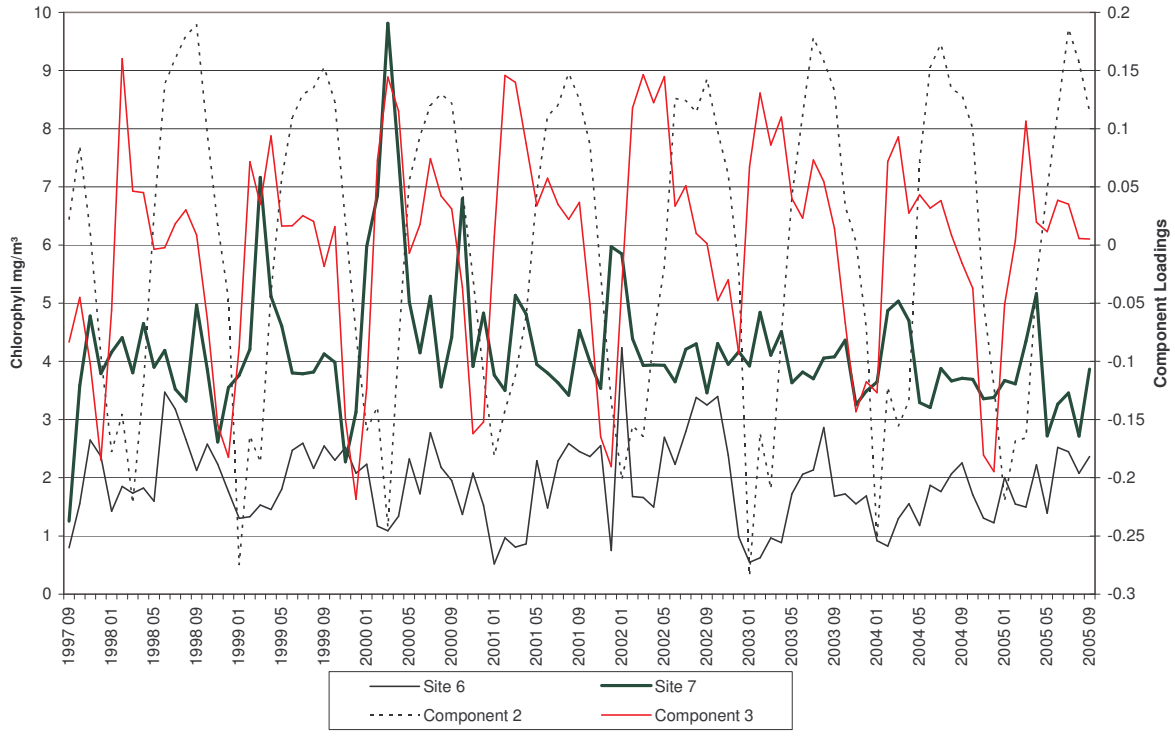

Figure 6-19. Time profile of site 6 & 7 showing chlorophyll content (left y-axis), and the corresponding 2nd component loadings (right y-axis).

A clear exception is the chlorophyll peak in January 2002. The 2nd Component experiences a negative peak at the same month. This illustrates that an area which correlates positive with a component loadings does not necessary follow the fluctuations. A reason why the area shows a strong positive in the SPCA analysis may be that the chlorophyll variations matches pretty well with the component loadings and that absolute values of those variations (in general between 1 and 3 mg/m³) are high compared with the variations in the open oceans.

The center of site 7 is located in the Maputo Bay at ~32º 50´E 26º 5´S as seen in. This site is located at an area which experiences a strong negative correlation with the 2nd Component loadings as seen in. This implies that the chlorophyll variations of the site follow a pattern that is inverse with the 2nd Component loadings graph. The reason why site 7 experiences a high negative correlation with the loadings graph can be seen in Figure 6-19: High chlorophyll peaks are located at months where the 2nd component loadings show maximum negative peaks. The most prominent months are clearly those of March 1999, March 2000 and January 2002. In the late summers and early autumns, the rest of the time series also experience visible elevated peaks of chlorophyll.

Site 8

Site 8 is placed in the vicinity of the Limpopo River mouth. The site is located at an area which has little correlation with the 2nd Component loadings. What can then be concluded is that the chlorophyll variations at this location do not follow a clear seasonal pattern. However, the site is located at an area which correlates very strong with the 8th Component, which is most likely brings out variations that occurs at a small spatial extension. As is seen in Figure 6-20 is site 8 having a large anomalous peak in February/March 2000 with a chlorophyll content of ~19 mg/m³.

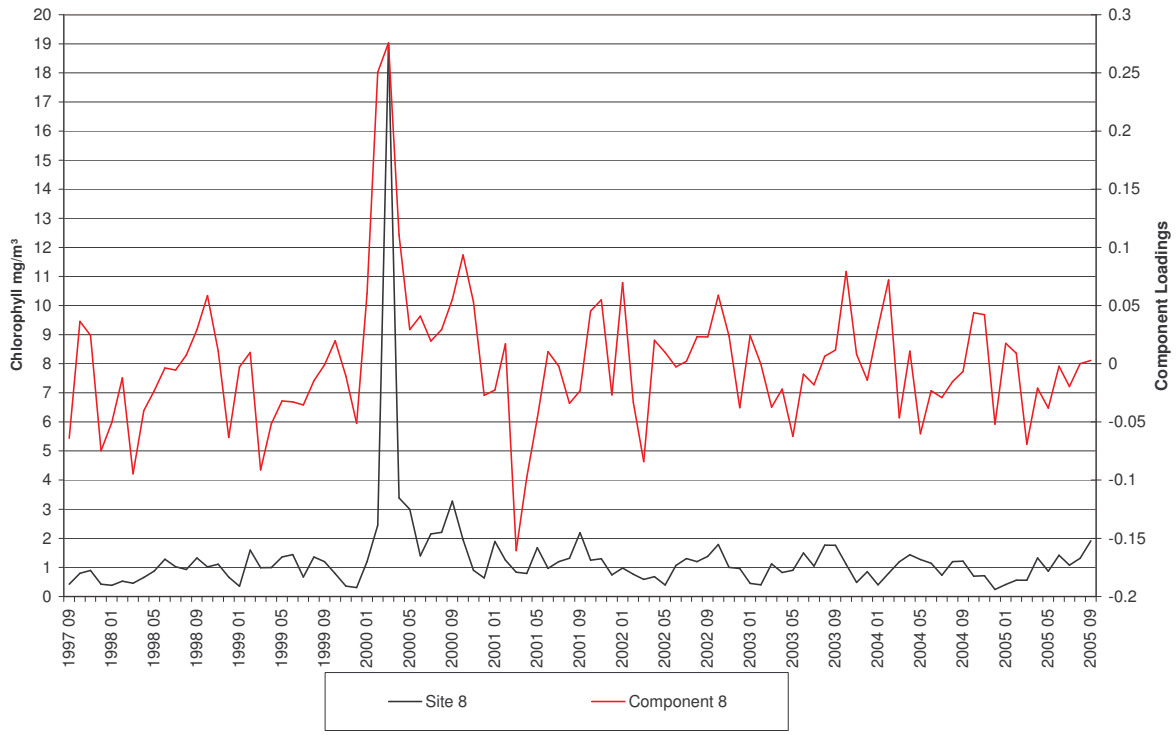

Figure 6-20. Time profile of site 8 showing chlorophyll content (left y-axis), and the corresponding 8th component loadings (right y-axis).

At the same month the component loadings also show a large peak. The timing of site 8 and the 8th component peaks correspond with the flooding of the Limpopo River in February 2000.

Site 9 and 10

Next, the focus is on site 9, which is placed in the vicinity of the Save River Mouth. Site 9 is place at a location which correlates highly negative with the fluctuations of the 2nd component loadings graph, as seen in Figure 6-21. There is a good agreement between the timing of the bottom peaks of the 2nd component and the chlorophyll peaks of site 9, which occur in January, February or March throughout the time series. In addition, there are also registered chlorophyll peaks in September 2000, 2001 and 2003 which can not be explained by the 2nd component loadings. Site 9 is also located at an area which has some correspondence with the 3rd Component. The loadings of the 3rd Component graph shows that in addition to the regular peak in January to March, there is also a back, or secondary peak that occurs at the same periods in late austral winter and early spring. These matches approximately the mentioned September peaks of site 9. The "missing" elevated chlorophyll peaks in September for Site 9, explains why the correlation of the site with the 3rd component loadings are not very high.

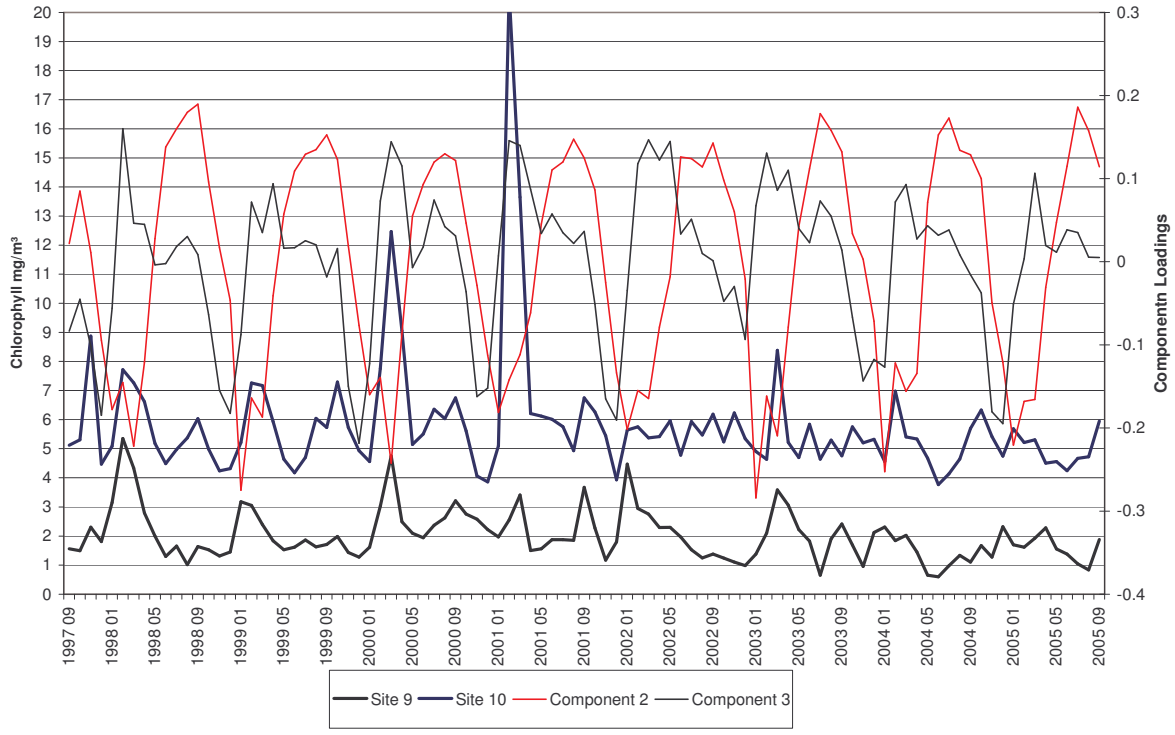

Figure 6-21. Time profile of site 9 and 10 showing chlorophyll content (left y-axis), and the corresponding 2nd and 3rd component loadings (right y-axis).

Tor Gammelsrød (Geophysical Institute, University of Bergen, Norway) made available some monthly river runoff data from the Save river, Buzi River, Licungo River and Zambezi River,

which originates from the National Directorate for Water in Mozambique. The amount of freshwater runoff in the coastal zone can influence phytoplankton abundance by providing variations in the nutrient supply, which is important for phytoplankton growth. Figure 6-22 shows the average monthly freshwater runoff in millions of cubic meters from the Save River. It must be noticed that the average is mostly based on data from the 1970 to 1982, with some sporadic measurements from 1983 to 2004. Assuming that the temporal pattern seen in Figure 6-22 is generally representative for the river runoff pattern in the SPCA time series, one can see that the runoff peak in February matches with the February chlorophyll peaks of site 9 (Figure 6-21). It is reasonably to assume that the runoff pattern from the Save River may have an influence on the chlorophyll concentration and, thus, phytoplankton concentration in the coastal waters near the Save River mouth. What the runoff pattern can not indicate is the sporadic chlorophyll peaks in September. No anomaly high measurements of water runoff are recorded in the austral winter and spring months in all of the available data.

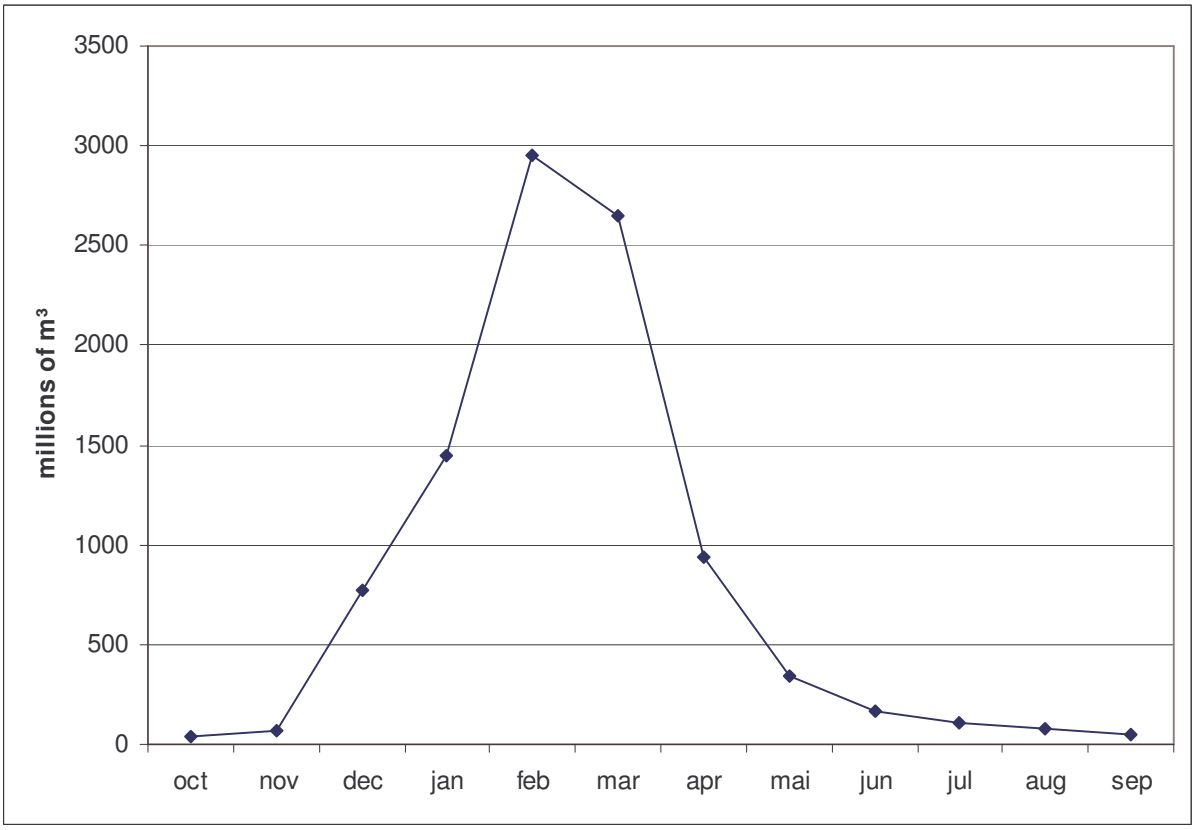

Figure 6-22. Average monthly river runoff from the Save river

Site 10 is placed in the coastal waters in the vicinity of the Pungue and Buzi River mouths. Clear seasonal variations in the chlorophyll content are seen during the time series (Figure 6-21). Site 10 is located in an area which highly correlates negatively with the 2nd component loadings and highly positive with the 3rd component loadings. Elevated chlorophyll values are

found in February/March (late summer and early autumn) for each year, with the exception of the year 2002 where no clear peak is standing out. The timing of the February/March chlorophyll peaks has a good correspondence with the bottom peaks of the 2nd component loadings as seen in Figure 6-21. Large interannual variations in the chlorophyll concentration's magnitude regarding the chlorophyll are measured. Most prominent are the anomalous chlorophyll peaks in March 2000 (12.5 mg/m³) and February 2001 (20.5 mg/m³). It is also observed a semi annual chlorophyll peak in the beginning and middle of the austral spring (September, October) for some of the seasons. Most clear are those of September 1998, October 1999, September 2000 and September 2001. In 2002 and 2003, there are no clear chlorophyll peaks in austral spring that stand out. If we disregard the years which do not contain any obvious elevated seasonal chlorophyll peaks, the chlorophyll variations of site 10 are fairly consistent with the loadings of the 3rd component.

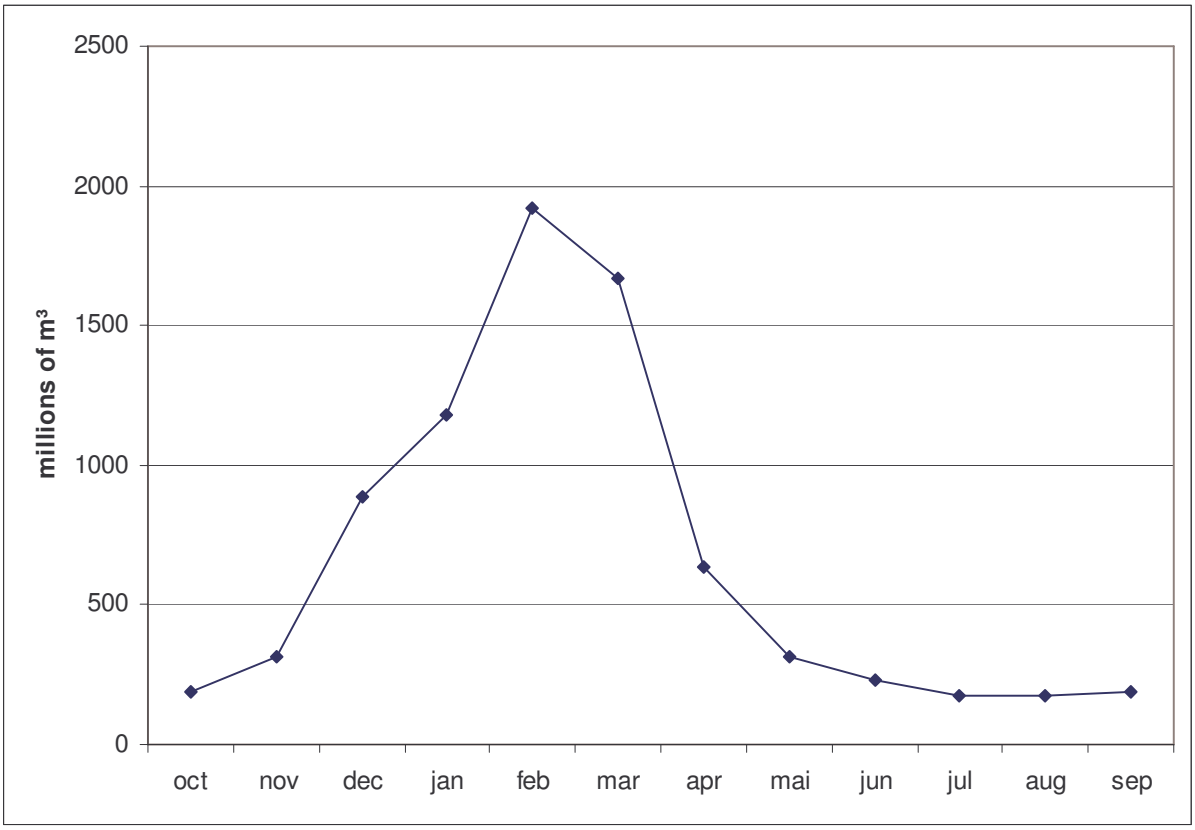

Figure 6-23. Average monthly river runoff from the Buzi River.

The average monthly river runoff data from the Buzi River is computed from monthly measurements from 1970 to 1990 in addition to runoff data from October 1994 to September 1996. This means that no measurements are available from the months the chlorophyll time profile cover for site 10. The runoff measurements can therefore not be directly related to the

chlorophyll values. But if one can assume that the average monthly data is representative for the general river runoff pattern, the data can still be useful. Figure 6-23 shows a clear seasonal variation in the amount of river runoff. The graph shows that the amount of runoff is starting to increase in November and is hitting a peak in February. March is also a having a relative high amount of freshwater runoff on average. The graph decreases sharply in April, before it flattens out in May, June and July. However, there is large interannual variability in the data set. For example, the month of February has a minimum and maximum amount of 158.8 and 3800.2 millions of m^3. If one compares the runoff data from the Buzi River in Figure 6-23 and site 10's chlorophyll time profile in Figure 6-21, one sees clearly that the chlorophyll peaks of February matches the runoff peak of the same month. This is a strong indicator that the amount of freshwater runoff controls the phytoplankton bloom that is represented by site 10. No runoff peak matches the chlorophyll peaks in September/October and, hence, there exist no direct relationship between those. The lack of temporally matching runoff data gives no clues that can explain the large variations in the February/March chlorophyll peaks. Given the large interannual river runoff variations in the existing data set, one plausible explanation is that there exists variation in the river runoff within the time series that induces variations in the chlorophyll content.

The river runoff from the Pungue River may influence the chlorophyll variations at site 10, which is placed in the vicinity of the river mouth. The available runoff data that overlaps the chlorophyll time series run from September 1997 to September 2003. The runoff time series shown in Figure 6-24 shows clearly that there is a seasonal cycle in the amount of freshwater runoff and also that the variation changes from year to year. The river discharge has its highest transport in the end of the austral summer/beginning of the austral autumn. The levels peak in February 1998, January-March 1999, March 2000, March 2001, January 2002 and March-April 2003. The timing of the runoff peaks matches the summer/autumn chlorophyll peaks closely. In the austral summer of 2001 there is both an anomalous high chlorophyll concentration and a high amount of freshwater runoff. For the other years, there is no clear correlation. There is also no correlation between the chlorophyll's austral spring bloom and the river runoff. This indicates that the increased abundance of phytoplankton is caused by other factors. It is possible that the influence from the Buzi river runoff is modifying the chlorophyll concentration, thereby creating a situation where the major chlorophyll variations can not be explained entirely by the river runoff from the Licungo River.

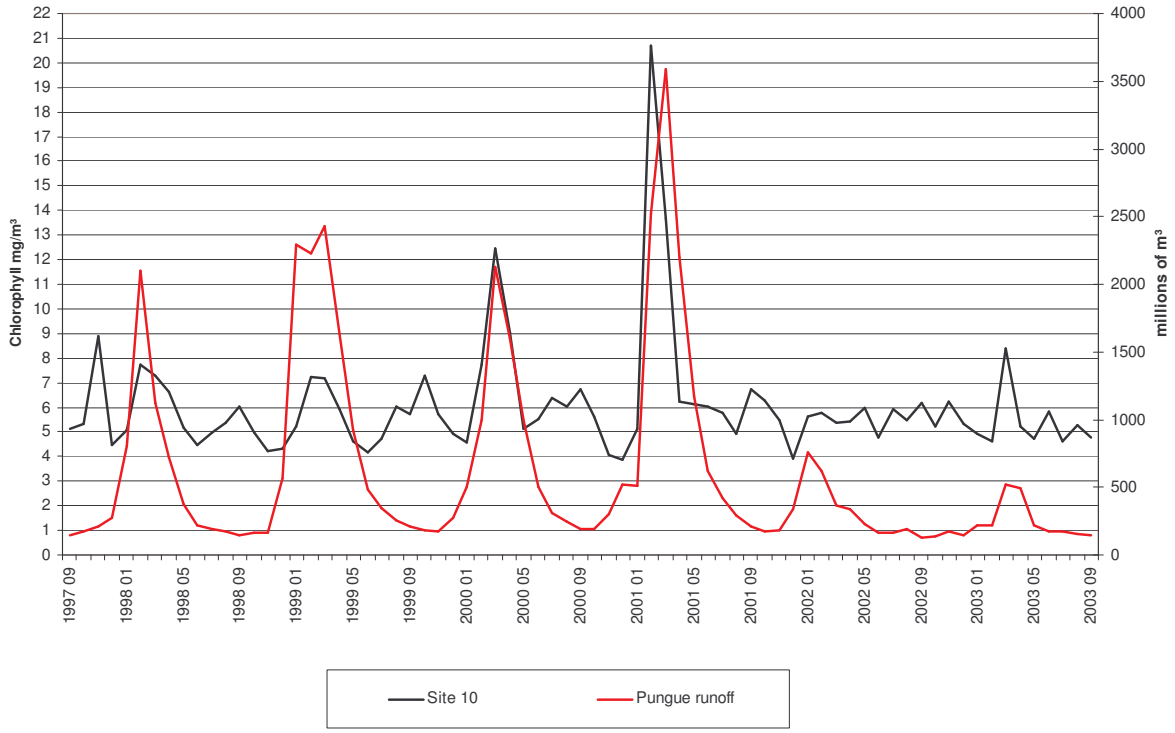

Figure 6-24. Time profile of site 10 showing chlorophyll content (left y-axis), and the corresponding river runoff (right y-axis).

Site 11

Site 11 is placed in the vicinity the Zambezi River mouth. The site is placed in an area that is highly negative correlated with the 2nd component loadings and positive correlated with the 3rd component loadings. The temporal profile of site 10 (shown in Figure 6-25) indicates that there are clear seasonal variations in the chlorophyll content. First, there are clear elevated chlorophyll values in the late austral summer/early autumn (February/March) throughout the time series. In addition, there are additional peaks/elevated values in the austral spring/winter for each year. These peaks are of a lower magnitude than the summer/autumn peaks. There is an interannual variation in the chlorophyll content from year to year. The timing of the chlorophyll peaks corresponds well with the timing of the negative peaks of the 2nd component loadings and gives an explanation why the area of site 10 correlates negatively with the 2nd component loadings. The timing of the positive peaks of the 3rd component graph and the chlorophyll peaks in the site 11 graph are fairly similar and explains why site 11 has a strong correlation with the 3rd component loadings.

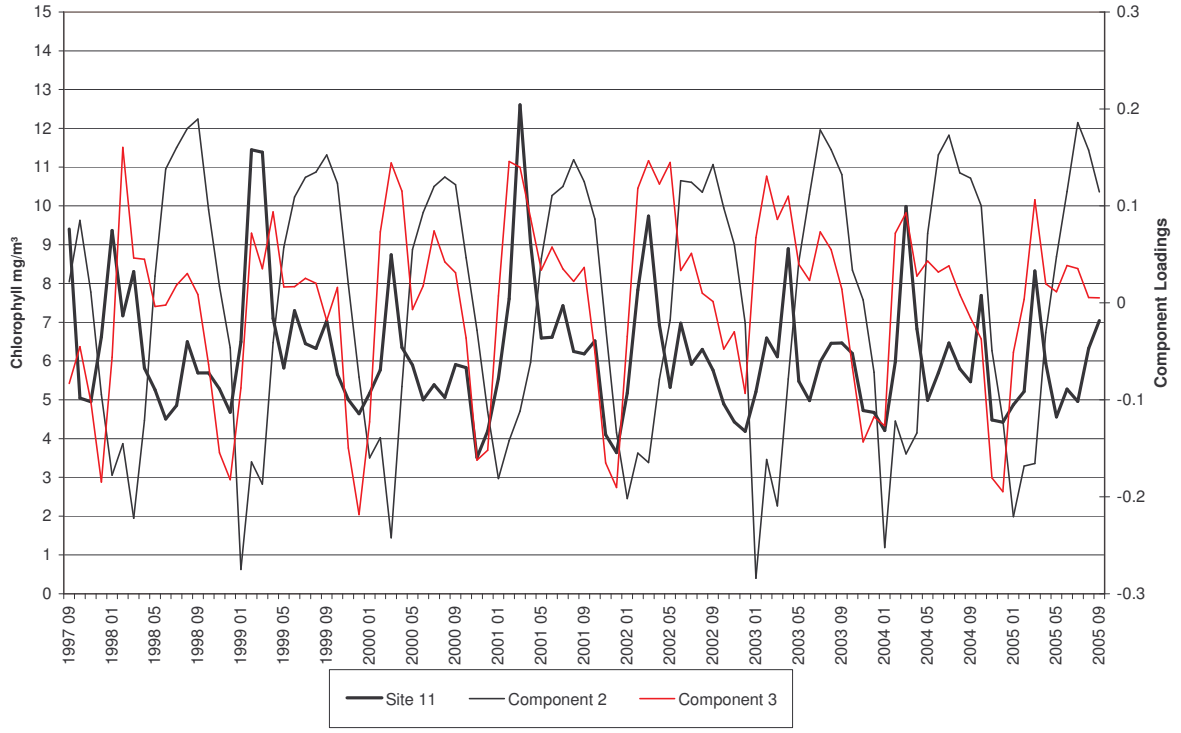

Figure 6-25. Time profile of site 11 showing chlorophyll content (left y-axis), and the corresponding 2nd and 3rd component loadings (right y-axis).

The available runoff data from the Zambezi River temporally overlaps the chlorophyll data series from September 1997 to August 2004. The discharge pattern is strongly seasonal, were a runoff peak is hit in the late austral summer/early autumn. However, there are strong interannual variations within the time series, where the highest summer/autumn discharge peak is measured in March 2001 (25118 million m³ of freshwater) and the lowest is measured in February/March 2002 (~3500 million m³). The graph shows that the timing of the summer/autumn chlorophyll peaks correspond well with the timing of the runoff peaks, thus strongly indicating that seasonal variations of the runoff peaks have an influence on the chlorophyll levels. The chlorophyll spring/winter peaks have no corresponding elevated discharges. Thus, it is likely that the river runoff is not the primary factor controlling the phytoplankton growth in this season.

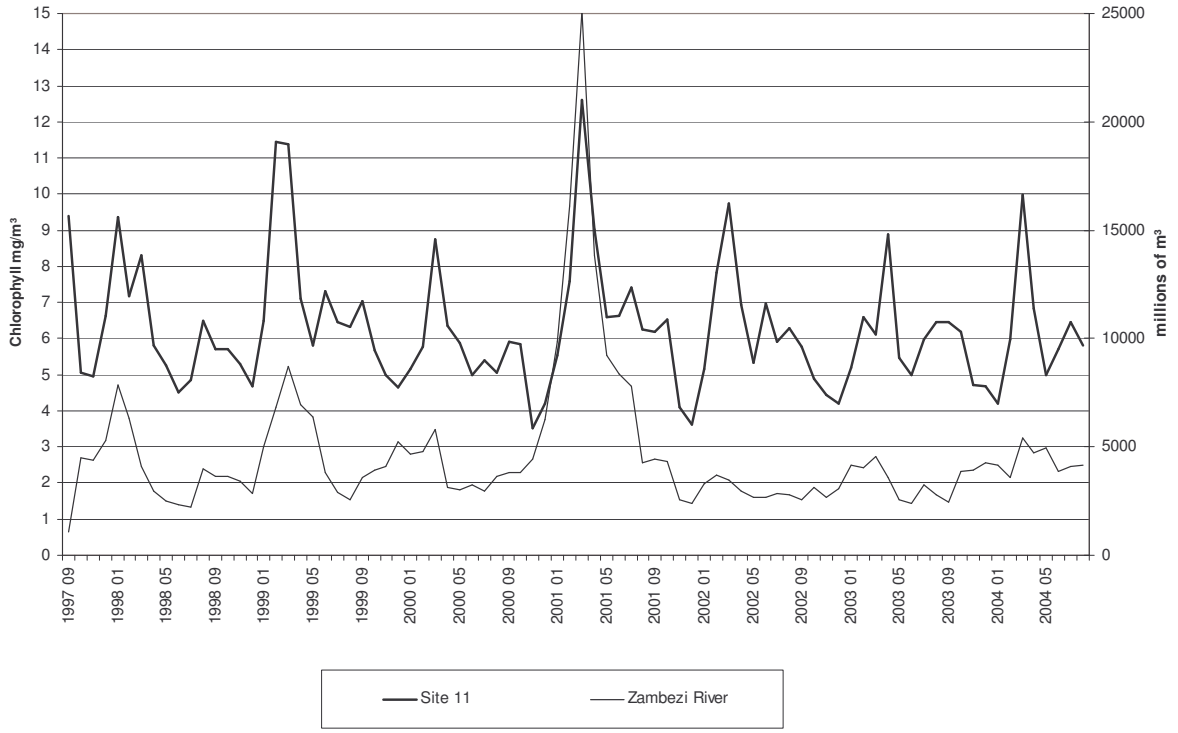

Figure 6-26. Time profile of site 11 showing chlorophyll content (left y-axis), and the corresponding 2nd component loadings (right y-axis).

Site 12

Site 12 is placed in the coastal waters next to the Licungo river mouth. Figure 6-27 show the chlorophyll variations of site 12 together with the 2nd and 3rd component loadings. The site is located at an area that has some positive correlation with the 2nd component loadings and a high positive correlation with the 3rd component loadings. The seasonal variations of the chlorophyll content exhibit two clear seasonal chlorophyll peaks per year through the time series. One peak is found in the end of the austral summer/beginning of autumn, and elevated values are found in the end of the winter/beginning of spring. Summer/autumn peaks are found in February 1998, April 1999, April 2004, March 2001, February 2002, March/April 2003, March 2003 and March 2005. The magnitude of the peaks lies between 4 and 7 mg/m³, with the exception of the anomalous peak in March 2001, which has a chlorophyll content of ~12 mg/m³. The elevated values in the late winter/early spring have in some of the years equal or higher chlorophyll content than those in the summer/autumn. This is true in 1999, 2000, 2002, 2003, 2004 and 2005 and explains why the site is positive correlated with the 2nd component loadings. The positive correlation between site 12 and the 3rd component is due to the coincident timing of the chlorophyll peaks and the positive peaks of the component loadings.

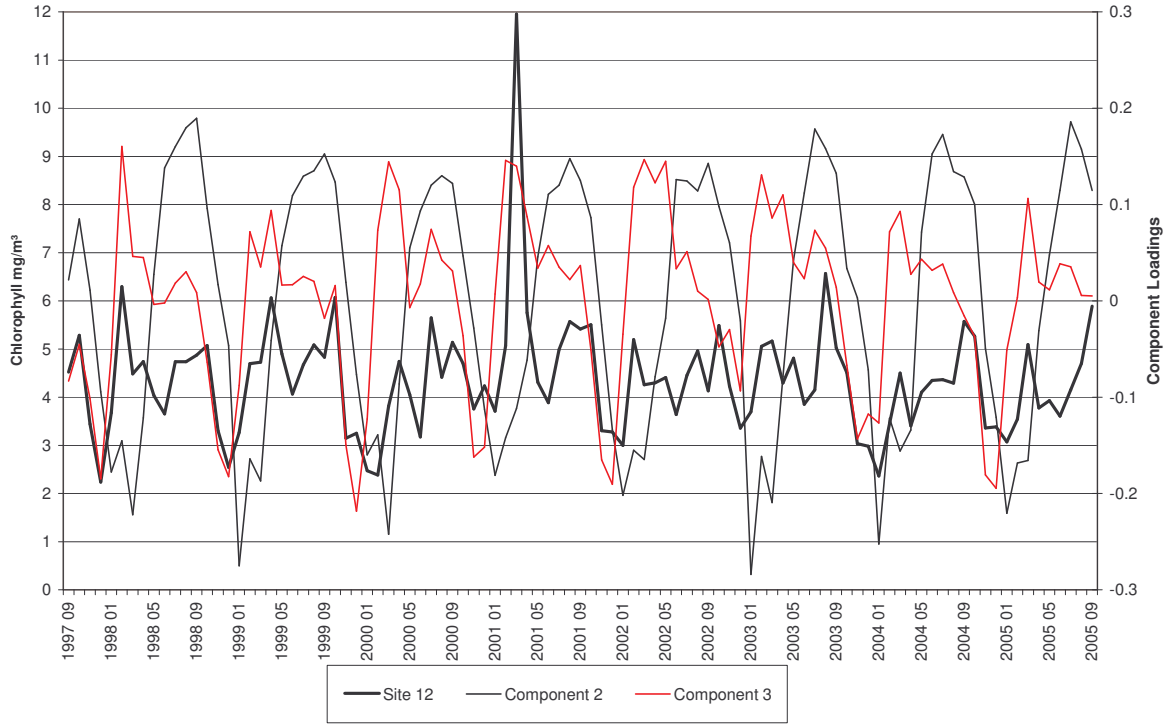

Figure 6-27. Time profile of site 12 showing chlorophyll content (left y-axis), and the corresponding 2nd and 3rd component loadings (right y-axis).

Figure 6-28 shows the chlorophyll values of site 12 and the corresponding discharge data from the Licungo River. Discharge data that covers the time series of site 12 reaches from September 1997 to June 2004. The runoff pattern from the Licungo River is clearly seasonal. The flow peaks in the late austral summer/early autumn. The graph peaks in January 1998, February-March, 1999, March/April 2000, February 2001, February 2002, January/February 2003 and March 2004. The seasonal discharge rate has large interannual variability. In the January 1998 peak, the water transport volume is measured to be 2382 million m³. In the February-March 1999 peaks, the amount of runoff is lesser than in 1998, with ~1400 million m³. Next year, in March/April 2000, the runoff is even less with 542 million m³. In February 2001 the runoff is sharply increased, 4234 million m³ of freshwater were measured. The runoff peak in the following year in February 2002 is distinctive lesser than in 2001 with 1217 million m³ measured. In January/February 2003, the runoff increases and reaches 2224 million m³, before the last peak in March 2004 lowers to a runoff of 371 million m³.

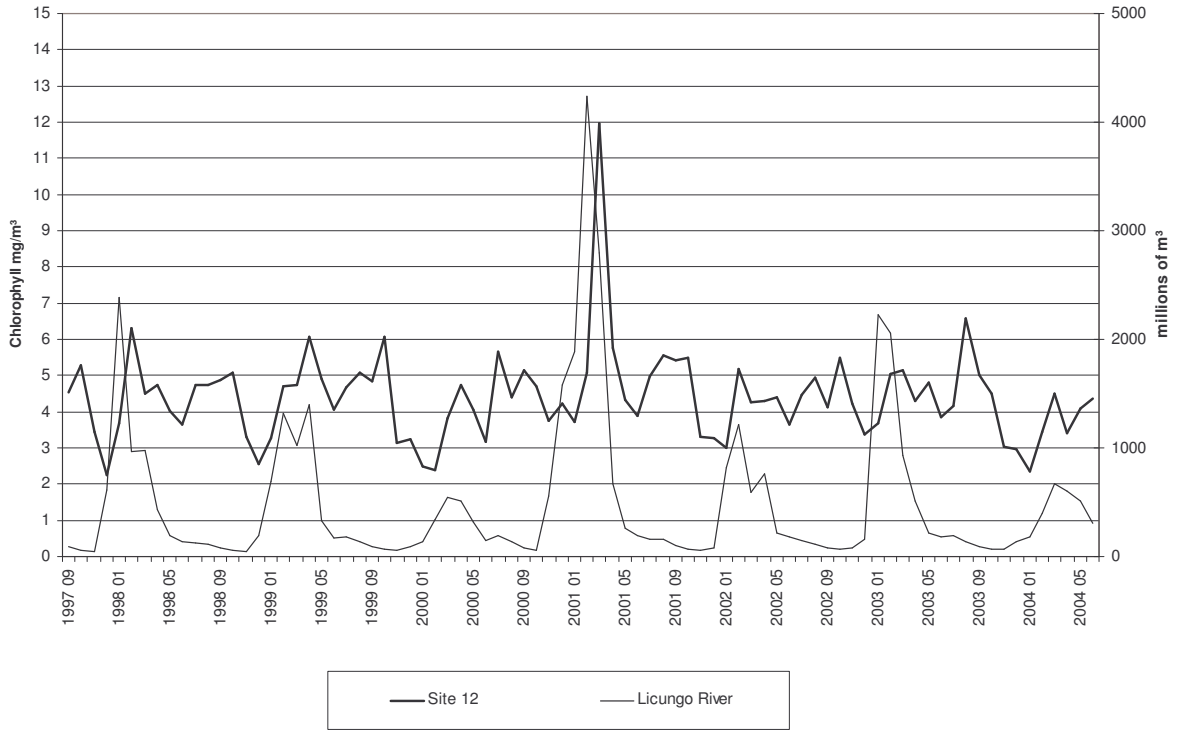

Figure 6-28. Time profile of site 12 showing chlorophyll content (left y-axis), and the corresponding river runoff from the Licungo River (right y-axis).

Comparing the runoff data with the chlorophyll data of site 12 in Figure 6-28, one can see that the timing of the late summer chlorophyll peaks generally coincide with the runoff peaks. The spring chlorophyll peaks in September/October have no match with the runoff data and, hence, one can assume that the spring peaks are induced by other factors, which will be discussed later in this chapter. In general, one might expect that there is a link between the amount of runoff and the phytoplankton abundance and, thus, the chlorophyll concentration. In the case of the February/March 2001 peaks, where both the chlorophyll concentration and the amount of runoff are anomalous high, one can assume that there is a direct relationship between increased runoff and increased chlorophyll concentration.

Site 13 is located at ~47º15´E 25ºS in the coastal waters of south eastern Madagascar. The east Madagascar current follows the continental shelf east of Madagascar from around 17ºS until it reaches the southern part of the island. Here, the current diverges and cause upwelling along the south coast of Madagascar (Ho *et al.*, 2004). Site 12 is placed at an area which has a high correspondence with the 2nd component loadings and a slightly correspondence with the 3rd component loadings. In an SPCA analysis performed by Ho *et al.*, (2004), on monthly Level 3 SeaWiFS chlorophyll images from September 1997 to November 2001. The results showed that “high chlorophyll concentration always exists along the south coast of

Madagascar." Further, it was revealed that chlorophyll peaks are found in the austral summer and in the austral winter. The winter peaks can be explained by current induced upwelling (Lutjeharms & Machu, 2000 in Ho *et al.*, 2004), while the summer peaks are most likely due to high wind stress (DiMarco *et al.*, 2000 in Ho *et al.*, 2004). It must be noticed that the area of site 13 is included in the area described above.

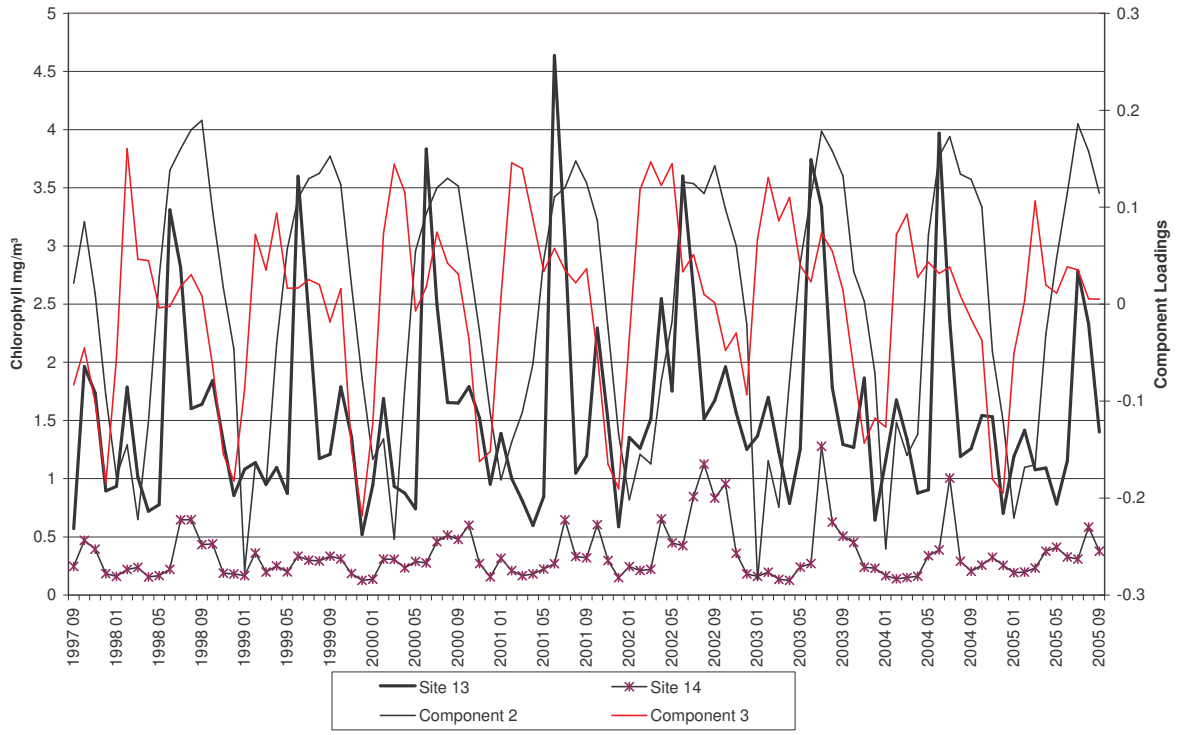

Figure 6-29. Time profile of site 13 and 14 showing chlorophyll content (left y-axis), and the corresponding 2nd and 3rd component loadings (right y-axis).

Figure 6-29 show the chlorophyll variations from site 13 together with the corresponding 2nd component loadings and the 3rd component loadings. High chlorophyll amplitudes occur in the beginning of the austral winter (June, July). This pattern is persistent throughout the time series. The timing of the chlorophyll peaks has a good agreement with the positive peaks of the 2nd component, and thus explaining the positive correlation between the chlorophyll content of site 13 and the 2nd component. The value of the chlorophyll peaks lies between 3 and 4 mg/m³, with the exception of June 2001 which has 4.6 mg/m³ and August 2005 which experience 2.7 mg/m³. The 3rd component graph show little correspondence with the chlorophyll variations of site 12, which was expected since the site was placed on an area with little correlation with the loadings. The regular summer chlorophyll peaks that was described by Ho *et al.* (2004) for the southern coast of does not have the same regularity at site 13.

The East Madagascar current hinders the chlorophyll rich coastal waters south of Madagascar to spread southward and eastward, and guides the waters in a south-westward direction, where the interaction between the East Madagascar current and the coastal upwelling causes meso-scale eddies, which propagate in the boundary area between the chlorophyll rich coastal waters and the east Madagascar current (Ho *et al.*, 2004). Site 14 is placed ~100 km off the southern Madagascar coast at about 46º9´E 26º10´S. The site has some correlation with the 2nd component, no correlation with the 3rd component and lies within the upwelling influenced waters. The average chlorophyll concentration over the time series is of a significant lower magnitude than that of site 13 (Figure 6-29). A reason for this may be that the meso-scale processes leads to horizontal mixing which again leads to relative lower chlorophyll concentration in upwelling area offshore. The chlorophyll concentration of site 14 shows a clear seasonal variation where the highest concentrations are found in the end of the austral winter/beginning of spring. An exception is the spring/winter in 1999, where no clear peak is seen. The timing of the elevated chlorophyll values are fairly consistent with the timing of the 2nd component peaks and, thus, give a reasonable description of the seasonal variations at the site. The chlorophyll concentration generally fluctuates between 0.2 mg/m³ in the summer/autumn months and 0.5 – 1 mg/m³ in the winter/spring months. In 2002, 2003 and 2004 are the chlorophyll peaks of a greater magnitude than the rest of the time series and showing that there is a degree of interannual variability.

Site 15 is placed in the coastal waters on the continental shelf in the north-western part of Madagascar at 47º20´E 16º15´S. The site is placed in an area which is strongly correlated with the 2nd component loadings and partly correlated with the 3rd component loadings. The chlorophyll concentration of site 15 (Figure 6-30) shows a clear seasonal alternating pattern through the time series, where the graph peaks in the late austral winter/early spring. In general, the chlorophyll peaks are containing chlorophyll values that lie between 8 and 11 mg/m³. The chlorophyll variations of site 15 are closely matched by the variations of the 2nd component loadings and thus, are describing the chlorophyll variations at the site in a precise manner.

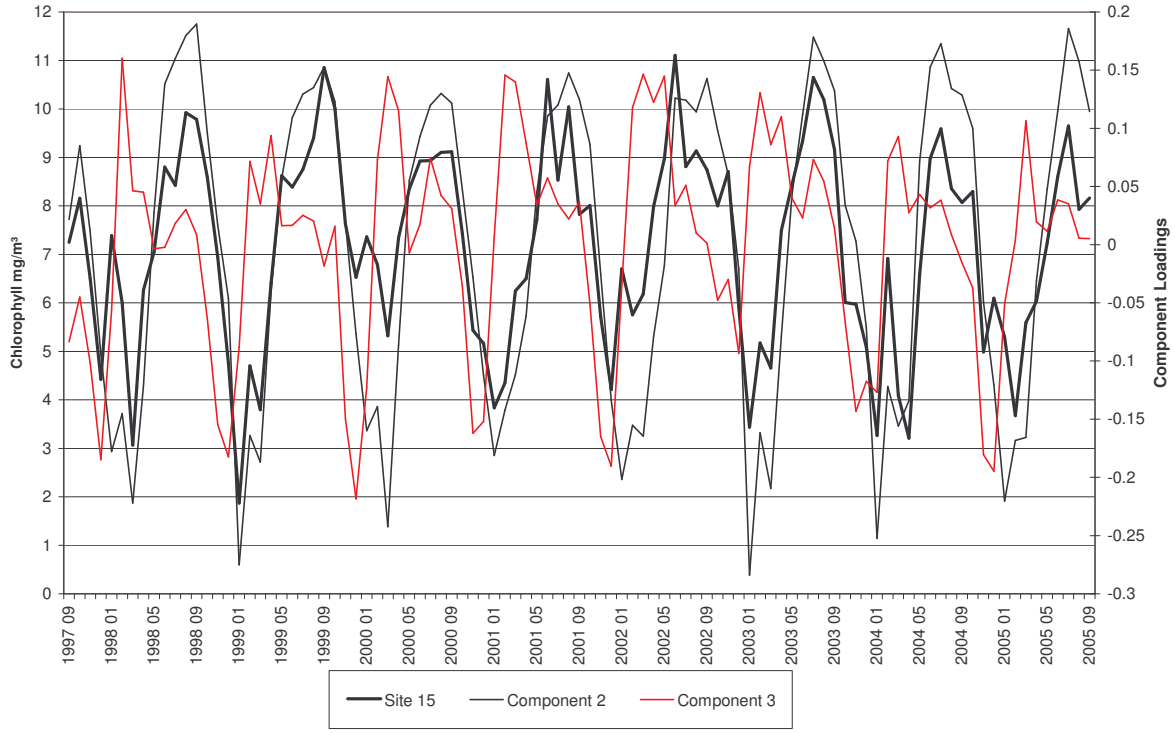

Figure 6-30. Time profile of site 15 showing chlorophyll content (left y-axis), and the corresponding 2nd component loadings (right y-axis).

6.3.1 Concluding remarks

Comparison between the time profiles and component loadings beyond the 3rd component did not lead to any significant results and are therefore not shown. The only exception is the site near Limpopo River, which showed a pattern similar to the 8th component. The study indicates that an SPCA output up to the 3rd component is sufficient for describing the seasonal variations in the study area.

6.4 Summary

Three different methods have been used that describes change through time: pairwise comparison, SPCA and time profiles. The different methods have their strength and weaknesses. By relying on various change detection and time series analysis techniques, different aspects of the SeaWiFS 9km monthly averaged data set are revealed.

The pairwise comparison of the seasonal climatologies using image differencing was useful in detecting the relative change between each season. However, the use of a 3 month long term mean for describing each season was problematic with respect to the temporal precision. For example, the southern open ocean showed a marked chlorophyll maximum in the winter months. The result from the SPCA indicated that the chlorophyll peak in fact was located in

the end of the winter/beginning of spring. The timing of the chlorophyll maximum is vital for the interpretation of the cause of bloom. A pure winter bloom in the southern ocean, as revealed by the seasonal climatologies, is possibly induced by enhanced mixing from winter storms. A late winter/early spring bloom is leading to the notion that increased temperature and intensified illumination from the sun are factors influencing the phytoplankton growth. The advantage of using seasonal climatologies is that the large amount of data is reduced to more easily interpretable images which can exemplify where and when the mean seasonal change takes place.

The SPCA analysis proved to be a useful method for describing the chlorophyll variations in the Mozambique Channel. Large amounts of data have been broken down into a few component images and corresponding component loadings. Both the variations in the coastal waters and the open oceans were described. The 2nd component is describing fairly consistent the chlorophyll variations in the study area as was revealed. To get a fuller picture the scrutinizing of the satellite data showed that is important to take the 3rd component into consideration because, because it is third component which reveals the existence of a spring bloom in the coastal waters that have a high correspondence with the 3rd component loadings. These areas include the major part of the coastal zone in the study area. The spring bloom is due to increased solar radiation. A summer/rainy season bloom is also mapped in the costal areas, most noticeably in the vicinity of river mouths. Most coastal areas will have higher nutrient content due to increased runoff. Certain areas, like south of Madagascar, are the increased chlorophyll values due to coastal upwelling. The upwelling zone is also showing seasonal variations. The reason for this is most likely due to variations in the wind stress in this region. This is concurrent with the findings of DiMarco *et al.* (2000) which noted a maximum upwelling in February/March 2000 from SST data. The timing matches the maximum values from the 2nd component loadings.

The results from SPCA analysis of the SeaWiFS data sets and the results from seasonal change analysis showed that the southwestern part of the study area experienced a marked seasonal oscillation. A temporal chlorophyll maximum is found in the winter while and a well marked minimum is found in the summer. The results are in agreement with the findings of Machu & Garcon (2001), which studied the seasonal phytoplankton variations in the Agulhas system with the help of ocean color data from the SeaWiFS sensor. Since the results in this thesis are based on similar data as those from Machu & Garcon (2001), the agreement is

expected. No signs of eddie activity have been noted in results of the SPCA. This is likely due to the use of monthly Level 3 data, which is not having a sufficient temporal resolution for mapping the eddies.

The temporal profiles proved useful for highlighting temporal change in absolute values at specific places. The time profiles of the sites near river plumes confirmed the results from the SPCA of a double bloom in the in the coastal zone. The time profiles of the open ocean, that showed a late winter/early spring bloom in the SPCA, showed a similar pattern. River runoff data from various rivers in Mozambique showed a temporal correlation with the runoff peaks in the rainy season and chlorophyll peaks from sites placed near river mouths.

7 SPCA of alternative data sets

The use of the SeaWiFS monthly averaged 9 km data set is in an SPCA analysis is only one of the available data set from the study area. Next, 8-day averaged 4km chlorophyll data from the MODIS sensor is analysis with the SPCA. The objective is to examine the similarities and differences between the two data sets. A SPCA is also been performed on the SeaWiFS data set. This time the original log scaling is kept prior to the analysis. The objectives are the same as for the first task in this chapter. The byte binary conversion of the original geophysical data changed the nature of the data and might influence the results. Therefore the idea of an analysis of the original data came up. The results from the SPCA of the log scaled data are compared with the results from the SPCA of the linearly scaled data.

7.1 SPCA of the 4km MODIS Aqua data set

The attention is now turned to the MODIS Aqua 4km resolution data set. The study area is the same as used in the SeaWiFS 9 km data set. A SPCA analysis is performed on the data set. The main differences between the SeaWiFS data set and the MODIS Aqua data set is that the latter one has a finer spatial and temporal resolution. The temporal average is here consisting of 8-day averages. In addition is the temporal length of the time series shorter compared to the SeaWiFS data set. The series starts on the 5th of July 2002 and ends on the 5th of September 2005. This means that the time series consist of 146 consecutive 8 day averaged images. The finer spatial resolution of the MODIS Aqua data set implies that finer features may be discriminated and that variation in the chlorophyll content for each month is accounted for in the time series. When it comes to near shore variations of the chlorophyll content, new spatial and temporal pattern may be discovered because of the better spatial resolution. In the open oceans will an improved resolution most likely not reveal any new information.

Component 1

The first component representing the characteristic chlorophyll level integrated over all the 8-day averages in the data set. According to the time series analysis is the first component consisting of 77.2 % of the total variation in the data set. Compared to the first component in the SeaWiFS data set, which consists of 88.1 %, it is clear that there are some differences that lead to different results. First, since the temporal resolution used is 8-day means, variations that are hidden in the monthly means are accounted for in the time series analysis. An example of this can be that if high chlorophyll concentrations exist in an area in the beginning

of a month, this can be clearly detected if 8-day averages are being used. If monthly means are used, the elevated levels of chlorophyll are hidden in the average. Thus, variations within a month will be detected by the 8-day average and accounted for in a time series analysis.

Since the temporal extent of the MODIS Aqua time series is almost 5 years shorter than the SeaWiFS time series the interannual and seasonal variability within the MODIS Aqua time series will have great influence on the result. The time series is starting on 5th of July 2002 and ending at the 5th of September 2005. The period from 5th of July to 5th of September is represented 4 times through the time series. The rest of the calendar year is represented three times. Since every image is weighted equal is the period from the beginning of July to the beginning of September having more influence on the average than the rest of the year.

Before looking at the loadings of the first component in Figure 7-1 we recall from the loadings of the first component from the SeaWiFS data set that the first months of the year (January, February, March) generally were the ones that had the lowest correlation with the 1st component image.

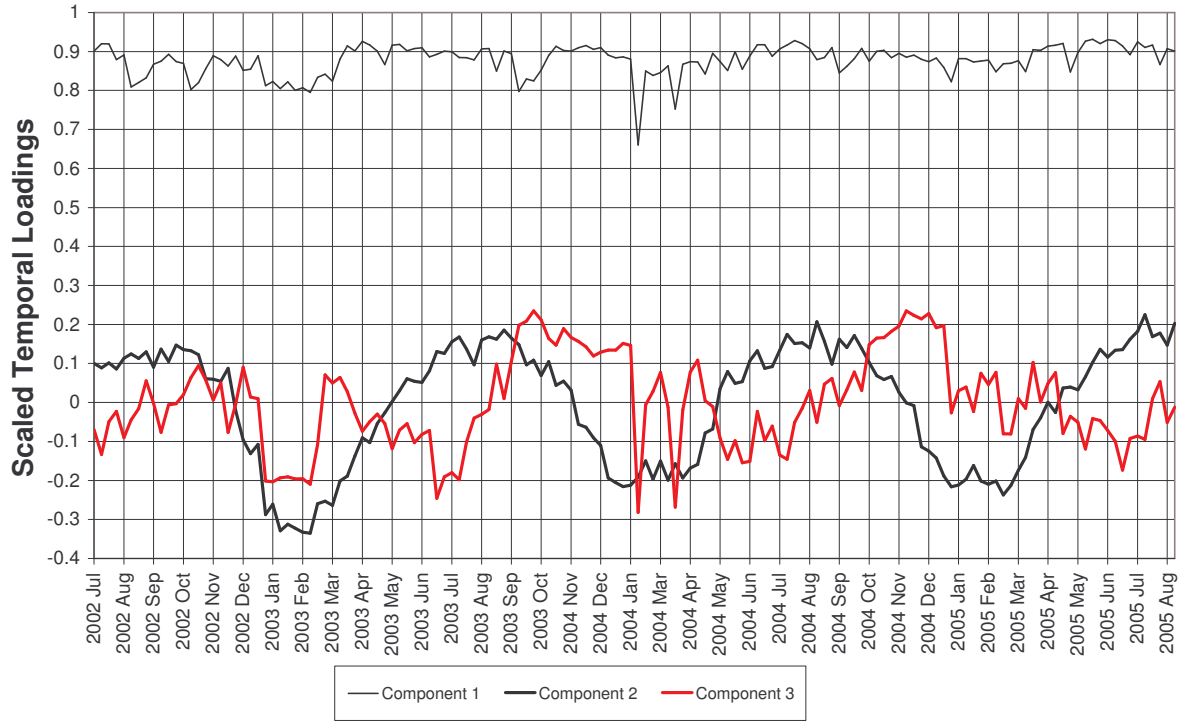

Figure 7-1. Loadings of Component 1, 2 and 3

Figure 7-1 shows that the 1st component of the MODIS Aqua data set does not have the same kind of pattern as the SeaWiFS 1st component. There is low correlation in the early months, but these are more localized in time (not stretching over longer time periods). In addition,

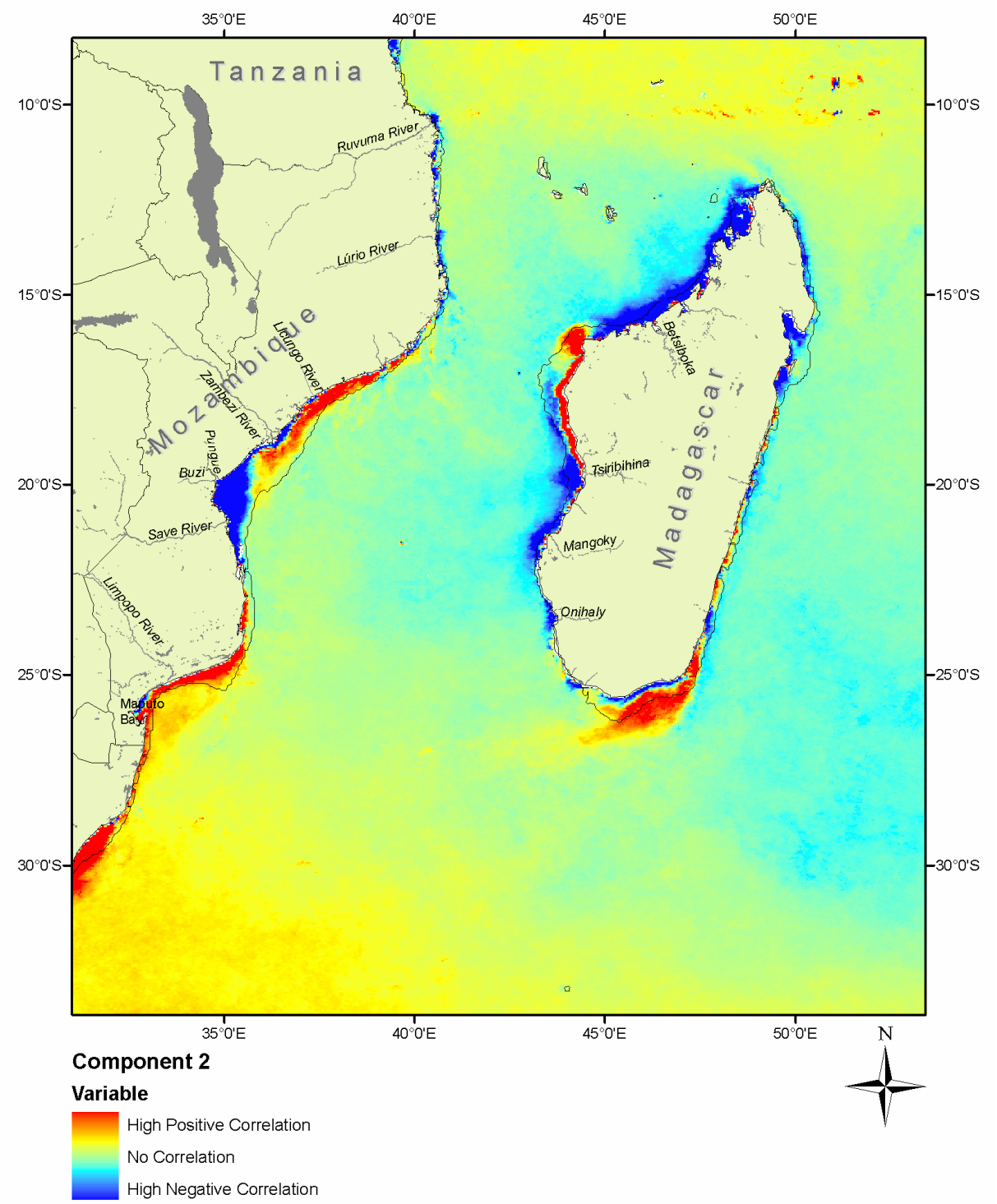

Figure 7-2. Component 2 image.

there are also other seasons that correlate low with the first component image. In the middle of August and October 2002, the loadings show that the there is little correlation with the component image. At these periods clear peaks are seen.

From the beginning of January 2003 to the middle of March there is also low correlation. The same is the case in the beginning and middle of October 2003. Two highly anomalous bottom peaks are seen in the beginning of February 2004 and in the middle of March 2004. In the first week of January 2005 a small negative peak is visible. The first component image (not shown) reveals a pattern that is similar to the SeaWiFS first component image. High chlorophyll concentrations are found in coastal areas, while low chlorophyll concentrations are found in the coastal areas.

Component 2

The second component consists of 2.2 % of the total variation in the data set. The shape of the component loadings graph is showing a clear sinusoidal cycle indicating that the second major element of variability of the chlorophyll content in the study area is that caused by the summer/winter dichotomy. The Austral summer and early autumn months correlate negative with the component while winter and early spring months correlate positive. The negative correlation indicates that the summer months tend to have an inverse pattern to the winter pattern shown. The SeaWiFS second component loadings also showed the same temporal pattern. The bottom peak in January and February 2003 is of greater magnitude than the bottom peaks in 2004 and 2005. The same pattern is observed in the 2nd component for the SeaWiFS data (Figure 6-8)

The corresponding component image, seen in Figure 7-2, shows largely the same spatial pattern as the SeaWiFS 2nd component image. There are, however, some small but significant differences. Along the southern Madagascar coastline, from ~45º E 25º 30´S to ~47º E 25º S, there is a clear belt of negative anomalies. This pattern is blurred in the SeaWiFS component image, which is most likely due to that the spatial averaging is hiding the major changes in chlorophyll content. Another area with a clear difference between the second component image of the SeaWiFS data set and the MODIS data set is the coastal waters of the Maputo Bay in the southern Mozambique. In the SeaWiFS 2nd component image, are the pixels in the bay negatively correlated with the component loadings. In the MODIS Aqua 2nd component image is the situation more nuanced. The north western part of the bay has clear high negative correlation, while the southern part of the bay has high positive correlation with the loadings graph. This positive area stretches further northeast along the southern Mozambican coast to about ~35º 30´E 23º S.

For the rest of the study area is the spatial pattern of the positive and negative and less correlated areas more or less the same for both the MODIS Aqua and SeaWiFS component 2 images, implying that the mapping of the major variations in the two data sets is not being influenced by the choice of spatial and temporal resolution.

Component 3

The third component is consisting of 1.3 % of the total variation in the MODIS data set. Recalling from the SeaWiFS component 3 loadings graph in Figure 6-9, we saw that there was a clear seasonal cycle with positive values in the late summer and early autumn. In addition there was a positive shoulder that interrupted the sinusoidal pattern which are generally found from May to September for each year (winter). A negative peak was found in November to December. This clear seasonal pattern is not seen in the Component 3 loadings in Figure 7-3 from the MODIS data set. At the first glance the loadings pattern seem chaotic. Some less distinct patterns can be seen although the magnitude of those differs greatly. First, the graph is alternating between highs and lows from the beginning July 2002 to the end of December 2002 when the graph drops to a bottom peak which lasts until the beginning of February 2003. Two anomalous lows are also seen in the beginning of February 2004 and in the middle of March 2004. A drop is also taking place in the end of the December 2004 but is stopping and alternates around 0 for the following months. What can be seen is that the loadings values drops in the end of December but that the interannual pattern is highly irregular. The same is true for positive values seen in the spring months of September, October and November. In 2002 are the loadings values for these months quite low, but in 2003 and 2004 are the component loadings clearly high.

The lack of clear and regular seasonal patterns in the loadings graph leads to the notion that it is local change that is described and not seasonal patterns. Another reason for the chaotic trends is that the 8-day averages may include changes within each month that is not accounted for in the monthly SeaWiFS data. The SeaWiFS component 3 loadings (Figure 6-9), showed that there was a clear variance from the regular pattern in the end of spring and beginning of summer. It is possible that the 8-day averages are nuancing this pattern by having a finer temporal resolution. Due to the lesser temporal extent used in the MODIS Aqua data set, may seasonal anomalies have greater influence on the total result and therefore shows a different pattern than the component 3 loadings from the SeaWiFS data set.

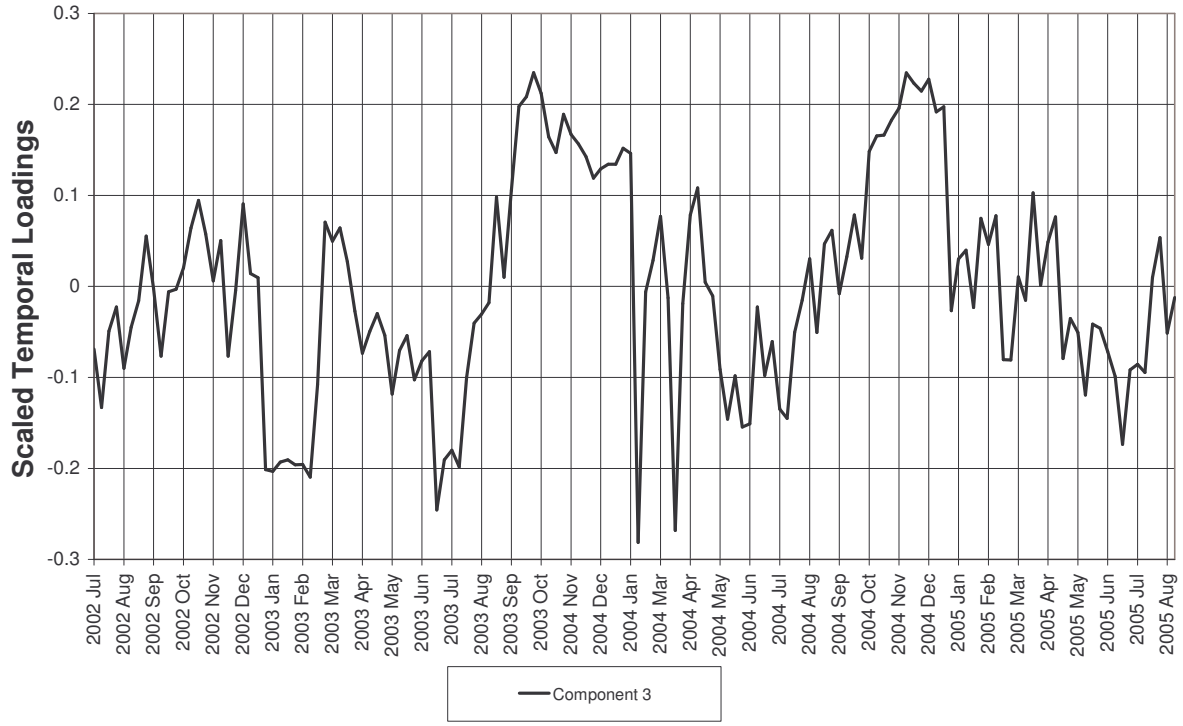

Figure 7-3. Loadings for component 3

The spatial patterns of the third component image in Figure 7-4 shows a distinct difference from the third component image from the SeaWiFS data set (Figure 6-10). The component 3 image from the SeaWiFS data set showed that the coastal waters of Mozambique and eastern Africa where highly positive correlated with the component loadings graph. It is difficult to directly compare the component images of the two data sets because they showed different patterns in the component loadings. The coastal waters of Mozambique are dominated by high negative correlation values. At various places near the coastline one can see small patches of positive correlated values. The open waters show little or no correlation with the component loadings. Interestingly, there are some small variances in the correlation values in the open oceans which may be contributed to the variations within each month that is detected by the 8-day averages and not by the monthly averages. The magnitude and pattern in the open ocean does not reveal any significant variations compared with the SeaWiFS 2nd component image (Figure 6-8). The coastal waters of eastern Africa show mostly areas with high positive correlation with the component loadings. An exception is the coastal waters from ~37ºE 18ºS to 40º30´E 15º30´S. Here, the waters are dominated by high negative correlation pixels. Closest to the coast in this area, single pixels with positive correlated values.

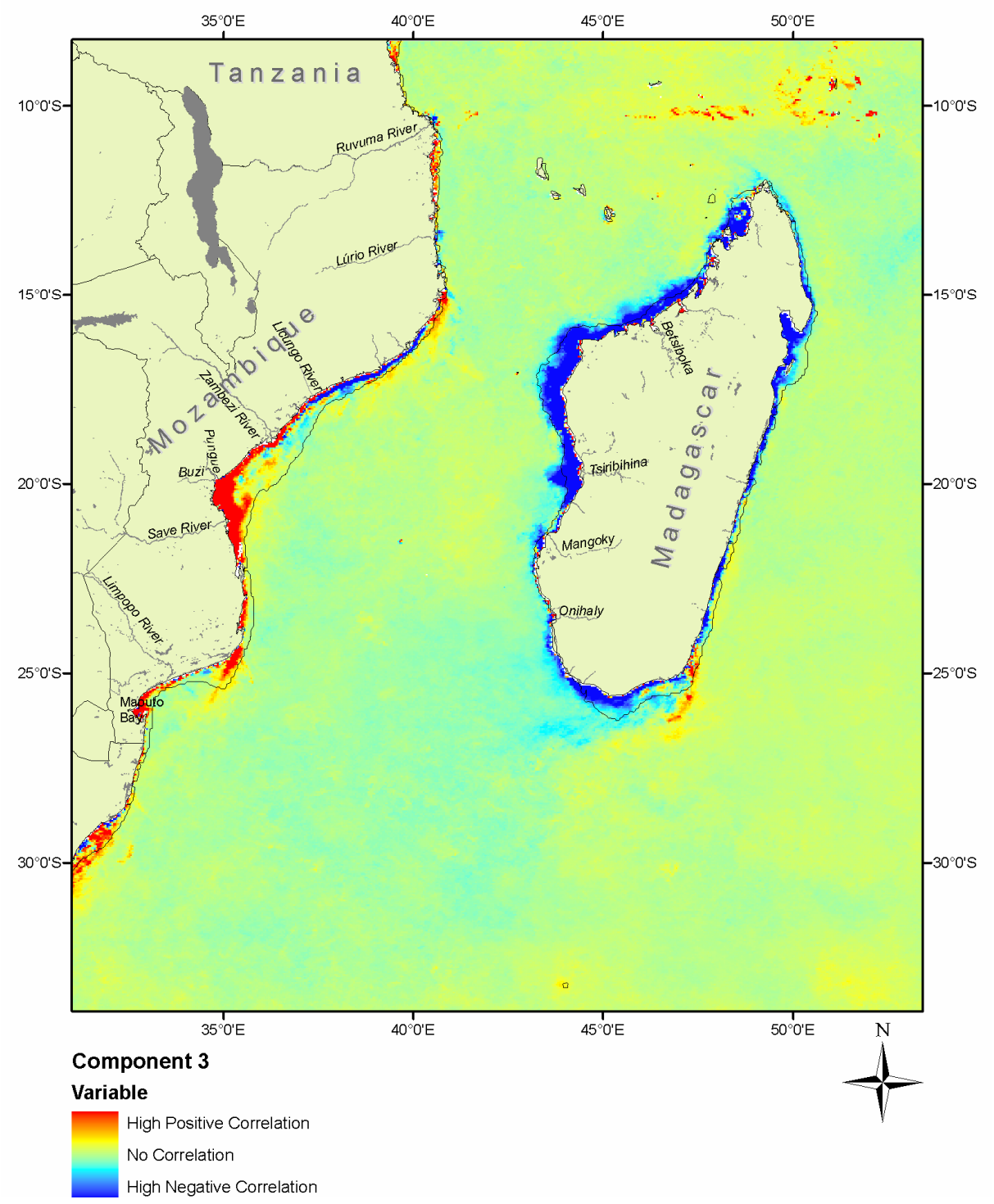

Figure 7-4. Component 3 image.

The clear high and low correlated areas in the coastal waters of the study area are due to the fact that the coastal areas are where the high magnitude variance is taking place because of terrestrial influence. Open oceans experience little absolute variance and is mostly accounted for in the second component. The somewhat chaotic pattern seen in the component loadings

graph gives the impression that there is a high degree of variance within each month that is accounted for in the 8-day time series. This might explain the differences between the SeaWiFS and MODIS Aqua Component 3 loadings graph. It must be noted that the areas that has a high positive and negative correlation with the component loadings graph is mostly located on the continental shelf, implying that it is change in the coastal regions that contributes to the different pattern detected by the 3rd component.

7.1.1 Concluding remarks

The 2nd component images and loadings for the MODIS and SeaWiFS data set showed similar patterns, thus indicating that the major seasonal variations are recorded in both data sets even if the spatial and temporal resolutions. The corresponding 2nd, 3rd 4th etc components did not show the same spatial pattern for the MODIS and SeaWiFS data sets respectively. Reasons for this can be:

- since the MODIS data set have a finer spatial resolution (~4 km) compared with the SeaWiFS data set (~9 km) features of a small spatial scale is recorded differently. This is especially the case in the coastal waters, were the 2nd components from the two data sets were clearly. The use of 9 km data seems to blur the pattern in the coastal zone.
- the temporal extent of the data sets were different. The SeaWiFS data sets have a longer record than the MODIS data set. The significantly shorter time series of the MODIS data leads to the notion that anomalies within the time period, which is recorded by the MODIS data set and not by the SeaWiFS data set, may influence the results.
- the difference in temporal resolution may lead to different results of the analysis. The 8-day averaged MODIS data can record short term variations in a more precise manner than the monthly averaged SeaWiFS data. The variations within each month have equal weight on the results and lead to different results

The 8day Level 3 data have a sufficient resolution for mapping the presence of eddies and gyres. However, the scrutinizing of the component images and loadings up to the 8th component did not show any patterns that could be contributed to such activity. It is possible that the SPCA is not a suitable method for discriminating and mapping of eddie activity. It is also possible that the linear classification of the data set have smoothed the appearance of eddies, thus hiding the presence of the eddies.

No clear guidelines have been found in the literature on the nature of which spatial and temporal resolutions should be chosen when performing a SPCA analysis. In this sense is the finding of the differences between the interesting from a GIS point of view. Both the data illustrates the same phenomenon, and the data is (chlorophyll content) collected by same method (remote sensing). The set up is, however, different with respect to the resolutions. When the same analysis is performed on the two data sets, the results turned out to be different. It is not the task of this thesis to put down a definitive recommendation on which kind of data that is most suitable, but the results indicates that there is a need for further investigation on the effect of the different data types have on the SPCA.

7.2 Linear versus log scaling

The doubt of the effect the different scalings would have on SPCA made it necessary to explore the two scalings in more detail. A SPCA analysis was performed on the monthly SeaWiFS data set with the log scaling. Some interesting differences between the two data sets came up. The first component of the log data set came up with 95.4% of the total variance, compared with 88.0% from the linear data set. As mentioned before is the 1st component representing the most of the variance, and thus the mean of the data set. The 1st component loadings from both the log and linear data sets are shown in Figure 7-5.

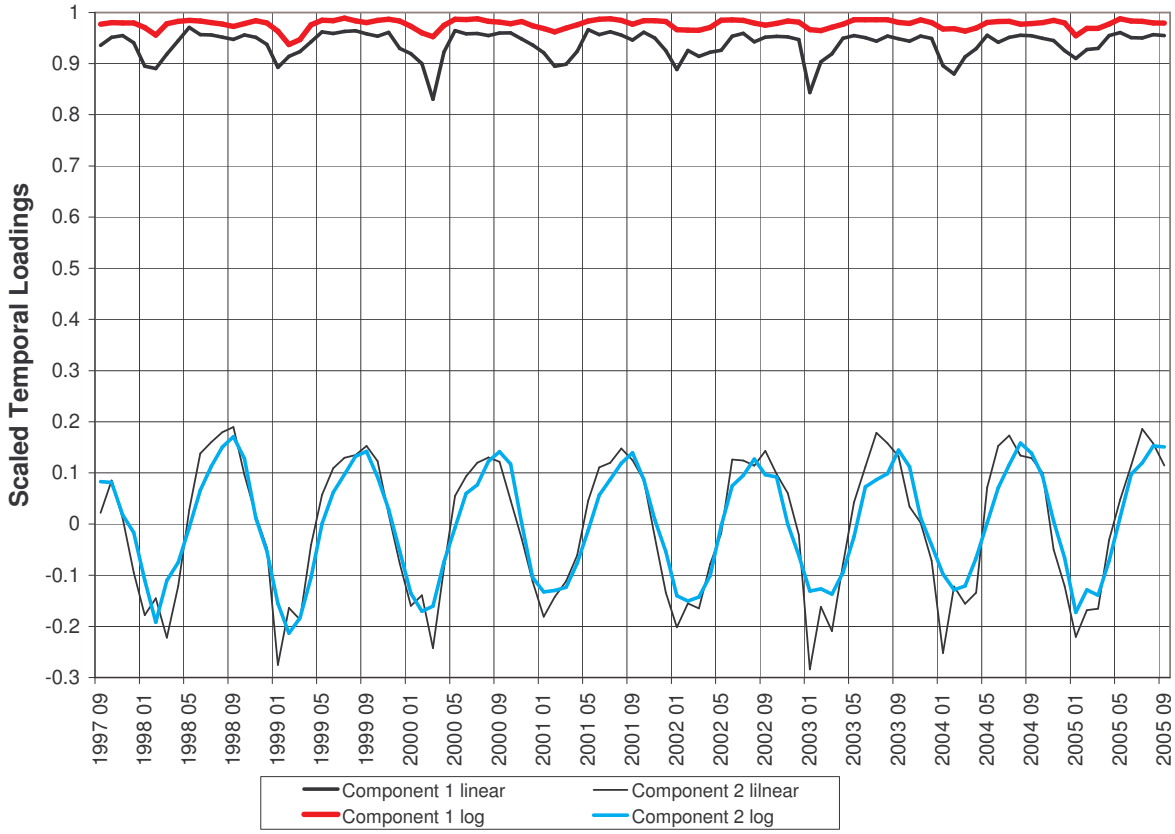

Figure 7-5. Linear and log scaled 1st and 2nd component loadings

The Component 1 log graph is, as expected, having eigenvalues that is close to 1 than the Component 1 linear graph. The seasonal variation in the log graph shows the same pattern, but the graph line is smoother. The 1st Component images from the log and the linear data set show similar patterns (not shown).

The 2nd component loadings show approximately the same pattern with only minor differences. The log graph is also somewhat smoother than the linear graph. This was expected since the 2nd component is showing the seasonal variations. The 2nd component is consisting of 1.1% of the total variance in the log data set, while the linear component consists of 1.7% of the variance in the linear data set. It is, however, some differences in the spatial distribution of positive and negative correlated areas in the 2nd Component image, as illustrated in Figure 7-6.

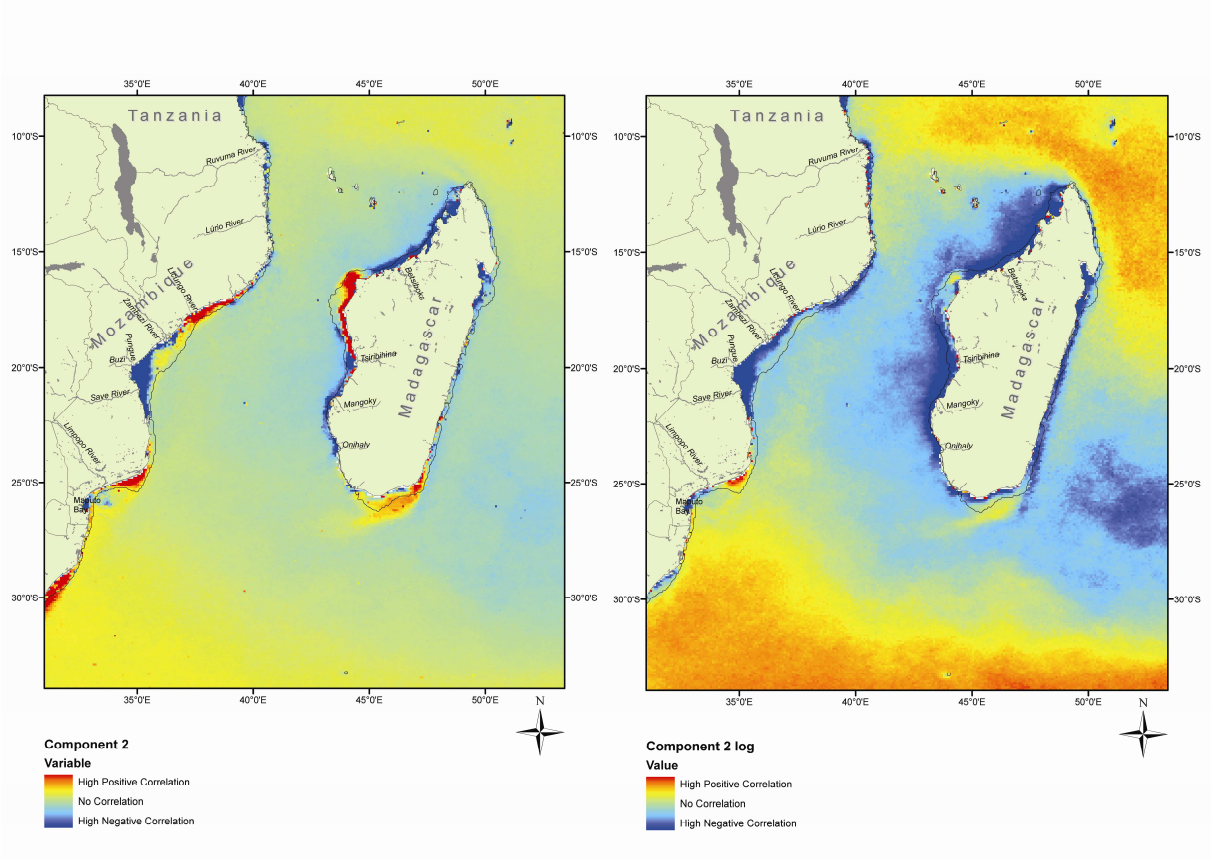

Figure 7-6. Linear data set Component 2 (left) and Log data set Component 2 (right).

The same color stretch has been applied on both the images. As is known is the log data set having more emphasize on the lower chlorophyll values than the linear data set. The effect this have on the analysis is quite clear. The open oceans, which contains low chlorophyll values and little but significant seasonal chlorophyll variations, comes out stronger in the 2nd component log data set because the log data provide more emphasize on the low chlorophyll values. The signal from the open ocean variations is also most likely overwhelming the some of the chlorophyll variations in the coastal zone. Clear differences are seen in some coastal areas of Madagascar and eastern Africa.

When it comes to the 3rd component loadings and images, the picture is totally changed. While the 2nd component images and loadings showed more or less the same pattern, with some minor differences in coastal areas, both the log and linear loadings and images are clearly different as seen in Figure 7-7 and Figure 7-8. The 3rd component loadings from the log data set are showing a somewhat chaotic pattern which is hard to interpret, opposed to the clear seasonal variations seen of the 2nd component linear graph, There is no clear seasonal variations seen.

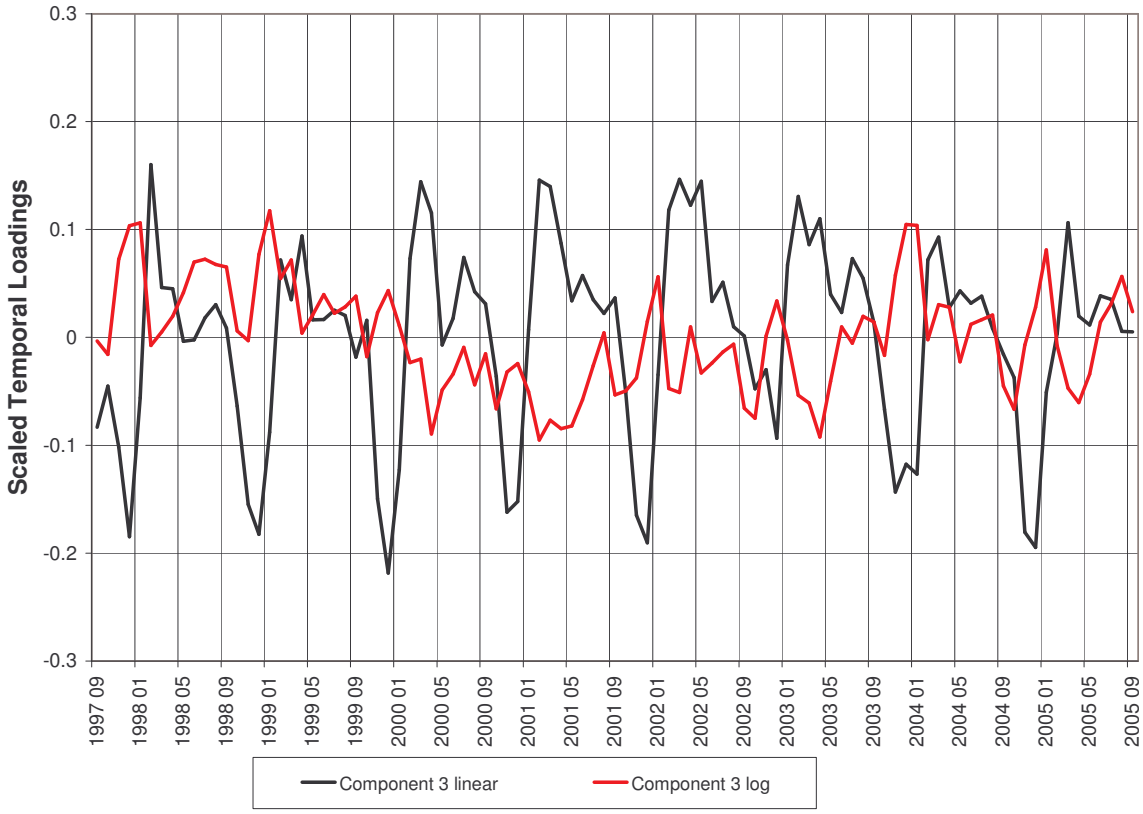

Figure 7-7. Linear and log scaled 3rd component loadings

The 3rd component images, Figure 7-8, are also showing different spatial patterns. Most interesting is the latitudinal variance in the log image, where the southern part of the study area is generally positively correlated with the component loadings and the northern part is negatively correlated with the component loadings. It is difficult to explain why this pattern occurs. It may be influenced by current movement and eddie activity but the chaotic spatial pattern makes an accurate interpretation difficult. The remaining components of the log scaled data did not show any significant patterns or trends in the component loadings or component images.

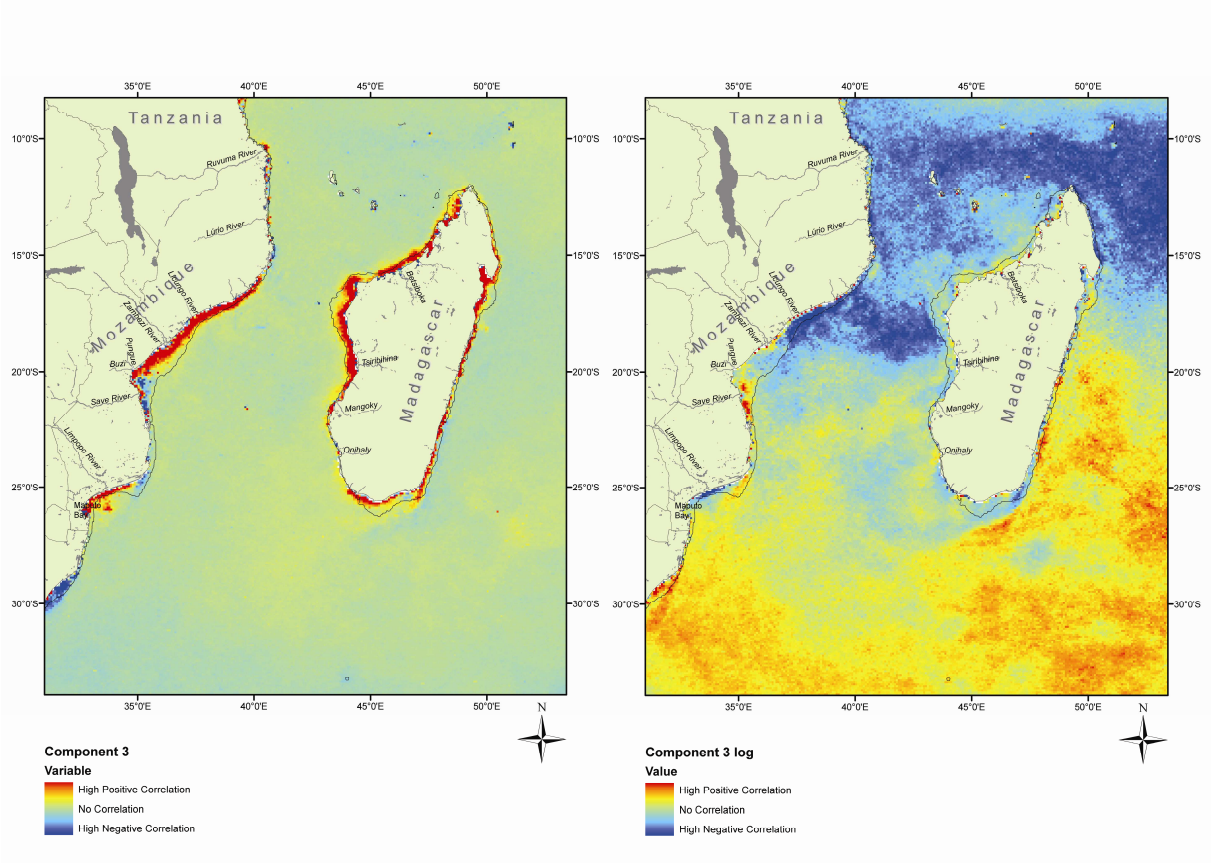

Figure 7-8. Linear data set Component 3 (left) and Log data set Component 3 (right)**.**

The important point is that the use of log scaled images instead of linearly scaled images do influence strongly on the results of an SPCA analysis. Further research need to be done in order to fully explore the effect of using the log versus linearly scaled data in a SPCA analysis. This short chapter has highlighted that there clearly is an effect on the results. The seasonal variations of low chlorophyll values are affecting the results stronger than in the linear data set. One can, however, not say that a log scaled data set is fit for use when it comes to analyzing open ocean conditions. The log data set is converging faster than the linear data

set which explains why fewer components are required to describe the chlorophyll variations properly.

7.3 Conclusion

The analysis in this chapter highlighted that the use of different data sets covering the same area and with the same parameters definitely showed different results when applied to the SPCA. The results from the MODIS 4km data set showed that a more detailed spatial resolution might lead to a better discrimination of coastal features. Some of the coastal areas that showed positive correlation with the 2nd component loadings in the SeaWiFS data set, now turned out to be negatively correlated. The negative correlation indicates a chlorophyll maximum in the rainy/summer season. It is reasonably to assume that the detailed resolution of the MODIS data is mapping effects of river discharge in areas with little, but significant, river discharge better than the 9 km SeaWiFS data. The near shore pixels will then have a relatively stronger signal. The coarser resolution of the 9 km SeaWiFS data will be likely to blur the coastal signal.

When it comes to the SPCA of the log scaled SeaWiFS data, the results from the 1st and 2nd components were as expected. The 3rd component showed a surprising spatial pattern which is difficult to interpret because of the rather chaotic temporal pattern. Why this pattern appears is not know, but it is likely that the low chlorophyll variations in the open oceans have an influence. The use of log scaled images is highlighting the pattern which is blurred with the use of the linear scaled images.

8 CONCLUSION

The initial intention in this study was to map the variability of phytoplankton abundance with the use of remotely sensed chlorophyll data over time in the Mozambique. The road to get there was not a trivial one. The search for the most suitable method for analyzing multiple images revealed that, at present, there are limited possibilities. Not many techniques are available in GIS software for the abstraction of change events. The problem is that the satellite images must be analyzed in both time and space. The solution was to use the SPCA analysis as implemented in the IDRISI software. First, the GIS implementation of the data is discussed. Second, the summary of the findings are discussed.

8.1 The GIS implementation

A concern was the restriction the IDRISI software provided when implementing the Level 3 data. The SPCA function can not handle values with decimals, but can only deal with data in a byte binary format. The solution was to reclassify the data into a linear byte binary format, which proved successful and made the data ready for the SPCA analysis. In order to keep the data sets linear, a reclassification was the only method of achieving the goal. A weakness of the method was that the geophysical data were changed, and that there was a change in data precision. It is not known how the change of the data is affecting the results of the SPCA as this must be tested before certain statements can be made. However, from the comparison between the log and linearly scaled SeaWiFS data set in chapter 7, the log scaled data had a stronger emphasize on the variations in the pixels with low pixel values compared with the linearly scaled data. We know that the open ocean case 1 waters contain low chlorophyll values and that the seasonal variations are also relative low. The reclassification can hide some of the chlorophyll variations in the low chlorophyll values and change may not be detected. How significant the effect may be is not known.

In the thesis I used SeaWiFS monthly data because the TSA function in IDRISI only up to 256 images could be analyzed. The use of weekly data would exceed the maximum number of images allowed. However, the investigation of the weekly SeaWiFS data would be the natural next step in the further investigation of the area with the use of chlorophyll data. Lucas & Budgell (2004) solved the problem of a limited number of images in IDRISI in their study of temporal variability of marine conditions in the North Sea by creating temporal subsets of the SST data they used. This method is a solution for an investigation of the SeaWiFS weekly data set.

It is clear that the software provided some restrictions on the performance of the analysis. The analysis could also be performed in the Matlab software as shown by Lucas & Budgell (2004). However, this thesis is more directed to the exploration of the possibilities in the IDRISI software, not the limitations. In this sense, the methods I used for solving the problems of the decimal data highly successful. The software laid no bond on the fulfillment of the objectives in this thesis.

8.2 Answers to the objectives

8.2.1 Objective 1

The first objective of this thesis was to provide a synoptic quantification of the spatial pattern, timing and relative magnitude of the large scale seasonal and interannual chlorophyll cycle in the Mozambique Channel using the SPCA analysis and pairwise comparison. The use of the SPCA proved to be a useful method for describing the seasonal and interannual variations in the study area. The use of the pairwise comparison was less successful, mainly because of the temporal averaging for each season did hide some important feature.

When it comes to comparing multiple images there are only two choices to make. Either, you can compare two images from two different time periods or you can analyze multiple images over time. In section 6.1.3. there was a pairwise comparison analysis performed on seasonal chlorophyll climatologies with the means of image differencing. A conceptual difficulty in using such an analysis is that it does not reveal true change from one season to another, but is a representation of the average seasonal change from a season to another integrated over the time period. Image differencing did prove useful information in that patterns were highlighted on where changes take place and the magnitude of those. Important findings includes: (1) that coastal waters in the vicinity of river mouths showed to have a higher chlorophyll content in the rainy season due to effects of river runoff, (2) there is a clear winter maximum in the southern part of the study area (subtropical gyre) due to increased wind mixing, (3) the upwelling area south of Madagascar seem to be at its strongest in the winter,(4) the Northern East Madagascar Current (NEMC) does not leave a specific signal detected by the thresholds given. The review of the seasonal climatologies in section 6.1.2 did reveal a mean seasonal signal in the NEMC through the seasons. This illustrates a classical problem of setting boundaries on natural phenomenon. The interpretation is easier, that is why we classify, but some data is lost. In this case it is the pattern of current. Why did I not use more precession,

i.e. more classes? The answer is that the use of more classes created a chaotic picture with respect to the coloring of the classes. It was then difficult to interpret the actual change values.

The use of seasonal climatologies to reveal the spatial pattern, timing and relative magnitude of the large scale seasonal and interannual chlorophyll cycle is only a first start, especially since the timing of the seasonal variations have already been set. This way of describing a phenomenon is a visualization of a cyclic view of time where the seasons follow each other continuously with no start or end. Naturally the data have been averaged, but the cartographic impression of the changes and differences is clearly cyclic. The interannual changes are not mapped, but the relative magnitude and change between those is mapped.

The SPCA of the monthly 9 km data set proved helpful in the search for the timing and magnitude of the chlorophyll variation in the Mozambique Channel. Important findings include :(1) the detection of a double bloom, one in the summer and one in the late winter/early spring, in coastal areas of eastern Africa and Madagascar, (2) the detection of the effect of the flooding in Mozambique in 2000, (3) the detection of clear seasonal chlorophyll variations in the open oceans, (4) the mapping of the upwelling south of Madagascar.

The gain of using the SPCA for analyzing the time series data was data reduction and isolation of temporal and spatial patterns. The 97 images was reduced into 4 interpretable components and corresponding loadings. The 1st component visualized the average chlorophyll content integrated over all of the time series. The 2nd and 3rd component mapped the seasonal cycles of the chlorophyll variations. The 8th component mapped an anomalous event, the flooding.

8.2.2 Objective 2

Another objective of this thesis was to verify the SPCA analysis with respect to the data itself. In other words how well is the description of the chlorophyll variability at specific sites compared with the output component loadings. A benefit from doing this is that one can see how the geophysical values of the chlorophyll variability changes in selected areas. Remembering that the loadings indicate the degree to which the components correlate with the component image, the method chosen to use time profiles. Chlorophyll time series from selected spatial sites in the study area were created from the SeaWiFS monthly data set. The degree of correlation each site had with the 2nd and 3rd component images was noted. For

example, a site which is located in an area which is positively correlated with the 2nd component loadings, it is excepted since the chlorophyll variations show a similar pattern as the loadings. The comparison showed that there was an acceptable agreement between most of the 2nd and 3rd component loadings and the time profile chlorophyll variations, with respect to the degree of correlation the sites have with the components. Sites on the Sofala Bank in Mozambique, which were positively correlated with the 3rd component loadings, showed temporal pattern that is consistent with the two chlorophyll blooms that was seen in the SPCA 3rd component. Available runoff data from selected rivers at the Sofala Bank in Mozambique were used for a comparison between chlorophyll values obtained from time profiles at the river mouths, and the amount of river runoff. The results showed a general agreement between the timing of the rainy season chlorophyll peaks in January-March and the seasonal runoff peaks in the same months indicating that there is a direct relationship between those.

How many components from the SPCA are necessary for a satisfying description of the chlorophyll variations in the study area? In general, the study showed that three components are enough for mapping the large scale seasonal variations. However, anomalous features which occur at a specific time period may come out later in the component sequence. This was the case of the 8th component of the SeaWiFS 9km monthly data set, which mapped high chlorophyll values in the coastal waters of Limpopo in February/March 2000 due effects of flooding. The SeaWiFS log data converged fast and no clear spatial and temporal trend is seen beyond the 3rd component. The MODIS data beyond the 3rd component showed some trends and variations, but where to noisy to be useful.

8.2.3 Objective 3

One useful feature of the SPCA analysis it the temporal series of remotely sensed images can be examined as a whole and change can be investigated in a progressive manner from most to least significant. The loadings of each of the images are then used to guide interpretation of when the change occurred. In this thesis different satellite measurements with different spatial and temporal resolutions were used. The motivation behind this was to study the effect of using different temporal and spatial resolutions in the SPCA analysis as mentioned in the objectives in chapter 1. In addition, there was a short study on the effect of using linearly scaled chlorophyll values versus log scaled values. These studies showed that there are clear differences in the output components from each of the data sets used, which includes 9 km

monthly SeaWiFS data, 4 km 8-day MODIS data and 9 km monthly log scaled SeaWiFS images.

Regarding the linearly scaled data, the MODIS and SeaWiFS data set is showing similar trends in the 1st component, which represents the characteristics of the chlorophyll content regardless of the season. The 2nd component, which is representing the most prevalent variability (seasonal variation) in the data set was similar, but showed some important differences related to the change pattern in the coastal zone of eastern Africa and Madagascar. The MODIS 2nd component showed a finer discrimination of the belt of negative correlated values in the component image, which suggested that there are high levels of chlorophyll in the these waters in January/February/March. This period corresponds to the rainy season. The area which is stands out most is the southern coastline of Madagascar. Here, no clear summer bloom is seen in the SeaWiFS data, but are clearly seen in the MODIS data. It is likely that the spatial averaging blurred the signal seasonal chlorophyll variations in the 9 km data compared with the 4 km. When it comes to the 3rd component there were large variations in both the spatial and temporal outputs between the two data sets. The SeaWiFS 3rd component suggested that there are two chlorophyll blooms per year in some clearly distinguishable coastal waters of Mozambique and Madagascar, most noticeably in the vicinity of river mouths. The strongest bloom signal was found in January/February/March while there is a weaker signal in general from August till October.

The MODIS data set showed a completely different situation, where the most of the coastal waters of Mozambique and Madagascar seemed to vary in opposite phase with each other. The corresponding loadings were somewhat seasonal but rather chaotic. The 8-day temporal resolution data may include variations that are hidden in the monthly SeaWiFS data. Since each image in a SPCA is given equal weight, the influence of variability in the 8-day data during each month may give different result than the monthly SeaWiFS data. The rest of the components for both the data set were also clearly different and rather noisy, which made them difficult to interpret.

The problems related to the reclassification of the geophysical data lead to the question of what temporal and spatial pattern that would come out if the original log scaled data would be used. The 9km SeaWiFS data was used for this purpose. The results showed that the 1st and 2nd components from the log scaled data had, in general, the same spatial and temporal pattern

as the linear scaled 9 km SeaWiFS data. The largest difference was a stronger spatial signal from the log 2nd component image in the open oceans. This effect was most likely due to that the log data is discriminating low chlorophyll values better than the linear data set. The low chlorophyll values in the log data set may therefore have greater influence on the open ocean variations than in the linearly scaled data set. But, it is difficult to argue that the log data is more suitable for mapping variations of low chlorophyll data in a SPCA than the linearly scaled data.

8.3 Summary

One of the insights gained in this study is that there are many concerns to take when performing a time series analysis such as SPCA based on satellite imagery. First, there is the question of the length of the time series. In order to reveal long time trends, the series should be as long as possible. In this sense, the obvious choice would be to use the SeaWiFS sensor because it provides the longest available time series. The Ocean Color Web, which distributes data from the SeaWiFS sensor, is only providing Level 3 data with a spatial resolution of 9 km. A finer resolution must be calculated by the user from available Level 2 data. A recommended task would be to calculate 8day Level 3 data with a spatial resolution of 4 km. The analysis of the 4 km MODIS data showed that there was a different temporal signal in some of the coastal areas. A long sequence SPCA using 4 km 8 day averaged SeaWiFS data would certainly be a data set to look closer into. Time consuming processing is then needed in order to achieve the results. The SPCA analysis proved useful for the analysis of trends and anomalies in long time series data. Especially effective were the isolation of the seasonal variations and the spatial location of the zones of high activity.

The search for a method that was suitable for a time and space analysis of ocean color data revealed that there was a limitation of options. In fact, the Standardized Principle Component Analysis as implemented in the IDIRSI was the only clear option that was available in the GIS software I scrutinized. The software had impact on the analysis by providing limitations on the amount of data and the structure of the data. Then two solutions could be made, either one can switch to another software or one can try to bypass the problems. I went for the last bit.

The results on exploring the differences of the effect of different spatial and temporal resolutions, and the effect of log versus linear scaling, in the SPCA analysis lead to some questions: Which data set is the most fit for use? Which data set would I use if I was doing the thesis all over again? The results have shown that the choice of data have an influence on the result because of the different spatial and temporal resolution, in addition to the length of the time series. What is demonstrated in this thesis is that all of the different data sets showed different temporal and spatial patterns in the SPCA. The differences came out strongly in the 3rd and following components, while the 1st and 2nd components where more similar for all the data sets that were analyzed in this thesis. This means that the seasonal signal is strong regardless of the scaling and the spatial and temporal resolution.

REFERENCES

Aiken, J., Moore, G.F., Trees, C.C., Hooker, S.B., & Clark, D.K. (1995) *The SeaWiFS CZCS-Type Pigment Algorithm.* SeaWiFS Technical Report Series, Vol 29. Hooker, S.B. & E.R. Firestone, E.R. (eds.). NASA Tech. Memo. 104566. Greenbelt, MD: NASA Goddard Space Flight Center

Aplin, P. (2006) On scales and dynamics in observing the environment. *International Journal of Remote Sensing* **27.** No. 11. 2123-2140

Arst, H. (2003) *Optical Properties and Remote Sensing of Multicomponental Water Bodies.* Springer -Verlag. Berlin, Heidelberg, New York.

Atkinson, P.M. & Foody, G.M. (2002) Uncertainty in Remote Sensing and GIS: Fundamentals. In: *Uncertainty in Remote Sensing and GIS*. Atkinson, P.M. & Foody, G.M., (eds.). Chichester, UK: Wiley

Barnes, W. L., Pagano, T.S. & Salomonson, V. V. (1998) Prelaunch Characteristics of the Moderate Resolution Imaging Spectroradiometer (MODIS) on EOS-AM1. *IEEE Transactions on Geoscience and Remote Sensing* **36.** No. 4, 1088-1100.

Bowers, D.G., Harker, G.E.L., Smith, P.S.D, & Tett, P. (2000) Optical Properties of a Region of Freshwater Influence (The Clyde Sea) *Estuarine, Coastal and Shelf Science* **50,** 717-726.

Bricaud, A., Morel, A. & Prieur, L. (1981) Absorption by dissolved organic matter of the sea (yellow substance) in the UV and visible domains. *Limnology and Oceanography* **26,** 43-53.

Campbell J.B. (2002) *Introduction to Remote Sensing.* Taylor & Francis. London & New York. 621p.

Carder, K.L., Chen, F.R., Lee, Z.P., Hawes, S.K. & Kamykowski, D. (1999) Semianalytic Moderate-Resolution Imaging Spectrometer algorithms for chlorophyll *a* and absorption with bio-optical domains based on nitrate-depletion temperatures. *Journal of geophysical research* **104**. No. C3, 5403-5421.

Carder, K.L., Chen, F.R., Cannizzaro, J.P., Campbell, J.W. & Mitchell, B.G. (2004) Performance of the MODIS semi-analytical ocean color algorithm for chlorophyll-*a*. *Advances in Space Research* **33**, 1152-1159.

Carder, K.L., Steward, R.G., Harvey, G.R. & Ortner, P.B. (1989) Marine humic and fulvic acids: Their effects on remote sensing of ocean chlorophyll. *Limnology & Oceanography* **34**, 68-81.

Claramunt, C. and Jiang, B., 2000, A representation of relationships in temporal spaces , in Innovations in GIS VII: GeoComputation, Ch. 4, P. Atkinson and D. Martin (eds.), Taylor and Francis, pp. 41-53.

Clark, D.K. Gordon, H.R., Voss, K.J., Broenkow, W. & Trees, C. (1997) Validation of atmospheric correction over the oceans. *Journal of geophysical research* **102,** No. D14, 17209-17217.

Cracknell, A.P. & Hayes, L.W.B. (1993) *Introduction to Remote Sensing.* Taylor & Francis. London, New York, Philadelphia. 279p.

Darecki, M., Weeks, A., Sagan, S., Kowalczuk, P., & Kaczmarek, S. (2003) Optical characteristics of two contrasting Case 2 waters and their influence on remote sensing algorithms. *Continental Shelf Research* **23**, 237-250.

Darecki, M. & Stramski, D. (2004) An evaluation of MODIS and SeaWiFS bio-optical algorithms in the Baltic Sea. *Remote Sensing of Environment* **89**, 326-350.

Dungan, J.L. (2002) Toward a Comprehensive view of Uncertainty in Remote Sensing Analysis. In: *Uncertainty in Remote Sensing and GIS.* Atkinson, P.M. & Foody, G.M., (eds.) Chichester, UK: Wiley

Dyson, L.L. (2000) *The Heavy Rainfall and Floods of February 2000: A Synoptic Overview. Southern Africa Floods of February 2000.* Department of Civil Eng., Univ. of Pretoria. Pretoria, RSA.

Eastman, J.R. & J.E. McKendry. (1991) *Change and time series analysis. Explorations in geographic information systems technology Vol. 1*.United Nations Institute for Training and Research, European Office, Palais des Nations CH-1211 Geneva 10, Switzerland

Eastman, J.R., & Fulk, M. (1993) Long Sequence Time Series Evaluation using Standardized Principal Components. *Photogrammetric Engineering and Remote Sensing* **59**: 1307-1312.

Emry, W.E. & Thomson, R.E. (1997) *Data Analysis Methods in Physical Oceanography*. Pergamon. Oxford, New York, Tokyo.

Esaias, W.E., Abbott, M.R., Barton, I., Brown, O.B., Campbell, J.W., Carder, K.L., Clark, D.K., Evans, R.H., Hoge, F.E., Gordon, H.R., Balch, W.M., Letelier, R. & Minnet, P.J., (1998) An overview of MODIS Capabilities for Ocean Science Observations. *IEEE Transactions on Geoscience and Remote Sensing* **36**, No. 4, 1250-1265.

Fisher, P. (1997) The pixel: a snare and a delusion. *International Journal of Remote Sensing* **18**. No. 3, 679-685.

Frank, A. (1998) Different Types of ”Time” in GIS. In: *Spatial and temporal reasoning in Geographic Information Systems*. Egenhofer, M.J. & Golledge R.G (eds.). Oxford University Press. New York, Oxford.

Gahegan, M. & Ehlers, M. (2000) *A framework for the modelling of uncertainty between remote sensing and geographical information systems.* ISPRS Journal of Photogrammetry & Remote Sensing **55**. 176-188

Galton, A. (2004) Fields and Objects in Space, Time and Space-time. *Spatial Cognition and Computation* **4.** No. 1, 1-29.

Garver, S.A. & Siegel, D.A. (1977) Inherent optical property inversion of ocean color spectra and its biochemical interpretation. 1. Time series from the Saragosso Sea. *Journal of geophysical research* **102,** No. C8, 18607-18625.

Grange, N., Whitfield, A.K., De Villiers, C.J. & Aøøamspm, B.R. (2000) The response of two South African east coast estuaries to altered river flow regimes. *Aquatic Conservation: Marine and freshwater ecosystems* **10**, 155-177.

Gordon, H.R. (1997) Atmospheric correction of ocean color imagery in the Earth Observing System era. *Journal of Geophysical research* **102**, No. D14, 17081-17106.

Gordon, H.R. (1998) In-Orbit Calibration Strategy for Ocean Color Sensors. *Remote Sensing of Environment* **63**, 265-278.

Gordon, H. R., & Wang, M. (1992) Surface roughness considerations for atmospheric correction of ocean color sensors. 2: Error in the retrieved water-leaving radiance. *Applied Optics* **31**, 4261-4267.

Hazelton, N.W.J. (1998) Some Operational Requirements for a Multi-Temporal 4-D GIS. In: Spatial and Temporal Reasoning in Geographic Information Systems. Egenhofer and Golledge (eds.). Oxford University Press.

Ho, C., Quanan, Z. & Kuo, N (2004) SeaWiFS observations of upwelling south of Madagascar: long-term variability and interaction with East Madagascar Current. *Deep Sea Research* II **51**. 59-67.

IDRISI Manual (2003). IDRISI Kilimanjaro Guide to GIS and Image Processing. (http://clarklabs.org)

Jensen, J.R. (2005) *Introductory Digital Image Processing. A Remote Sensing Perspective*. Prentice Hall.

Joint, I. & Groom, S.B. (2000) Estimation of phytoplankton production from space: current status and future potential of satellite remote sensing. *Journal of Experimental Marine Biology and Ecology* **205**. 253-255.

Keith, D.J., Yoder, J.A. & Freeman, S.A. (2002) Spatial and Temporal Distribution of Colored Dissolved Organic Matter (CDOM) in Narragansett Bay, Rhode Island: Implications for Phytoplankton in Coastal Waters. *Estuarine, Coastal and Shelf Science* **55**. 705-717.

Kiiveri, H. T. (1997) Assessing, representing and transmitting positional uncertainty in maps. *International Journal of Geographical Information Science* **11**. No. 1, 33-52.

Lucas, A.E. & Budgell, W.P. (2004) Characterising spatial and temporal variability of marine conditions in the North Sea, 1985-2000. In: GIS/Spatial Analyses in Fishery and Aquatic Sciences (Vol. 2) Fishery-Aquatic GIS Research Group, Nishida, T., Kaiola, P.J. & Hollingworth, C.E. Japan. 161-180.

Longely, P.A., Goodchild, M.F., Maguire, D.J. & Rhind, D.W. (2001) *Geographic Information Systems and Science,* Chichester, UK: Wiley

Lutjeharms, J.R.E., Bang, N.D. & Duncan, C.P. (1981) Characteristics of the currents east and south of Madagascar. *Deep. Sea Research* **35**. 879-899.

Lutjeharms, J.R.E. & Machu, E. (2000) An upwelling cell inshore of the East Madagascar Current. *Deep Sea Research* I **47**. 2405 - 2411.

Machu, E., Biastoch, A., Oschlies, A., Kawamiya, M, Lutjeharms, J.R.E. & Garcon, V. (2005) Phytoplankton distribution in the Agulhas system from a coupled physical-biological model. *Deep-Sea Research* I **52**. 1300 -1318.

Machu, E. & Garcon, V. (2001) Phytoplankton seasonal distribution from SeaWiFS data in the Agulhas system. *Journal of Marine Research* **59**. 795-812.

Manslow, J.F & Nixon, M.S. (2002) On the Ambiguity Induced by a Remore Sensor's PSF. In: *Uncertainty in Remote Sensing and GIS.* Atkinson, P.M. & Foody, G.M. (eds.). Chichester, UK: Wiley

Martin, S. (2004) *An Introduction to Ocean Remote Sensing.* Cambridge University Press. Cambridge.

Morel, A. (ed.) (1998) *Minimum Requirements for an Operational, Ocean-Color Sensor for the Open Ocean.* Reports of the International Ocean-Color Coordinating Group, No. 1, IOCCG, Darmouth, Canada

Morel, A. & Gentili, B. (1996) Diffuse reflectance of oceanic waters. III. Implication of bidirectionality for the remote-sensing problem. *Applied Optics* **35**. No. 24, 4850-4862.

Morel, A. & Prieur, L. (1977) Analysis of Variations in Ocean Color. *Limnology and Oceanography* **22**. 709-722.

Nadi, S. & Delavar, M.R. (2003) Spatio-Temporal Modeling of Dynamic Phenomena in GIS. In: ScanGIS'2003 - The 9th Scandinavian Research Conference on Geographical Information Science, Kirsi Virrantaus and Håvard Tveite (eds.). 4-6 June 2003, Espoo, Finland – Proceedings,

O'Reilly, J.E., Maritorena, S., O'Brien, M.C., Siegel, D.A., Toole, D., Menzies, D., Smith, R.C., Mueller, J.L., Mitchell, B.G., Kahru, M., Chavez, P., Strutton, P., Cotta, G.F., Hooker, S.B., McClain, C.R., Carder, K.L., Muller-Karger, F., Harding, L., Magnuson, A., Phinney, D., Moore, G.F., Aiken, J., Arrigo, K.R., Letelier, R. & Culver, M. (2000) SeaWiFS post-launch calibration and validation analysis, part 3. *NASA Technical Memorandum* – 2000 – 206892, Vol. 11, 49 pp.

Paula, J., Pinto, I., Guambe, I., Monterio, S., Gove, D. & Guerreiro, J. (1998) Seasonal cycle of plantonic communities at Inhaca Island, southern Mozambique. *Journal of Plankton Research* **20**. 2165-2178.

Pozdnyakov, P. & Grassl, H. (2003) *Colour of Inland and Coastal Waters.* Springer -Verlag. Berlin, Heidelberg, New York.

Prieur, L. & Sathyendranath, S. (1981) An optical classification of coastal and oceanic waters based on the specific spectral absorption curves of phytoplankton pigments, dissolved organic matter, and other particulate materials. *Limnology and Oceanography* **26**. 671-689.

Quartly, G.D. & Srokosz, M.A. (2004) Eddies in the Southern Mozambique Channel. *Deep Sea Research* II **51**. 69-83.

Ridderinkhof, H & De Ruijter, W.P.M. (2003) Moored Observations in the Mozambique Channel. *Deep-Sea Research* II **50**. 1933-1955.

Robinson, I.S. (2004) *Measuring the oceans from space.* Chichester, UK: Springer-Praxis

Rochelle-Newall, E.J. & Fisher, T.R. (2002) Production of chromophoric dissolved organic matter fluorescence in marine and estuarine environments: an investigation into the role of phytoplankton. *Marine Chemistry* **77**. No. 77, 7-21.

de Ruijter, W.P.M., Ridderinkhof, H., Lutjeharms, J.R.E., Schouten, M.W. & Vet, C. (2002) Observations of the flow in the Mozambique Channel. *Geophysical Research Letters* **29**. No. 10, 1052.

de Ruijter, W.P.M., van Aken, H.M., Beir, E.J., Lutjeharms, J.R.E., Matano, R.P. & Schouten, M.W. (2004) Eddies and dipoles around South Madagascar: formation, pathways and large-scale impact. *Deep-Sea Research* I **51**. 383 – 400.

Sathyendranath, S. (ed.) (2000) *Remote Sensing of Ocean Color in Coastal, and Other Optically-Complex, Waters.* Reports of the International Ocean-Color Coordinating Group, No. 3, IOCCG, Darmouth, Canada

Scott, F.A. & McCreary, J.P. (2002) The Monsoon circulation of the Indian Ocean. *Progress in Oceanography* **51**. 1 – 123.

Schouten, M.W., De Ruijter, W.P.M., van Leeuwen, P.J. & Ridderinkhof, H. (2003) Eddies and variability in the Mozambique Channel. *Deep Sea Research* II **50**, 1987-2003.

Schouten, M.W., de Ruijter, W.P.M. & Ridderinkhof, H. (2005) A seasonal intrusion of subtropical water in the Mozambique Channel. *Geophysical Research Letters* **32**, L18601, doi:10.1029/2005Gl023131

Segar, D.A. *Introduction to Ocean Sciences.* Wadsworth. Belmont, US. 498p

Siddorn, J.R., Bowers, D.G. & Hoguane, A.M. (2001) Detecting the Zambezi River Plume using Observed Optical Properties. *Marine Pollution Bulletin* **42**. 942-950.

Srokosz, M.A. (2000) Biological Oceanography by Remote Sensing *in Encyclopedia of Analytical Chemistry.* Meyers, R.A. (ed.) John Wiley & Sons Ltd Chichester pp8506-8533.

Sætre, R. (1985) Surface currents in the Mozambique Channel. *Deep-Sea Research* **31**. 485-508.

Sætre, R., & Jorge da Silva, A. (1984) The circulation of the Mozambique Channel. *Deep Sea Research* **31**. 485 – 508.

Tomczak, M. & Godfrey, J.S. (1994) *Regional Oceanography: An Introduction*. Pergamon, Oxford, 422pp.

Wachowicz, M (1999) *Object-oriented design for temporal GIS*. Taylor & Francis, London.

Wang, M. & Gordon, H.R. (2002) Calibration of ocean color scanners: how much error is acceptable in the near infrared? *Remote Sensing of Environment* **82.** 497-504.

Woodcock, C.E. (2002) Uncertainty in Remote Sensing. In, *Uncertainty in Remote Sensing and GIS,* Atkinson, P.M. & Foody, G.M., (eds.). Chichester, UK: Wiley

Worboys, M.F. (1998) A generic Model for Spatio-Bitemporal Geographic Information. In: *Spatial and Temporal Reasoning in Geographic Information Systems*, Egenhofer and Golledge (eds.). Oxford University Press.

Yoder, J.A., Schollaert, S.E. & O'Reilly, J.E. (2002) Climatological phytoplankton chlorophyll and sea surface temperature patterns in continental shelf and slope waters off the northeast U.S. coast. *Limnology and Oceanography* **47.** No.3, 672-682.

Yoder, J.A. (ed.) (1999) *Status and plans for Satellite Ocean-Color Missions: Considerations for Complementary Missions*. Reports of the International Ocean-Color Coordinating Group, No. 2, IOCCG, Darmouth, Canada.

Zubkov, M.V. & Quartly, G.D. (2003) Ultraplankton distribution in surface waters of the Mozambique Channel—flow cytometry and satellite imagery. *Aquatic Microbial Ecology* **33**, 155-161.

APPENDIX

A: Flowchart showing the processing of the Level 3 data

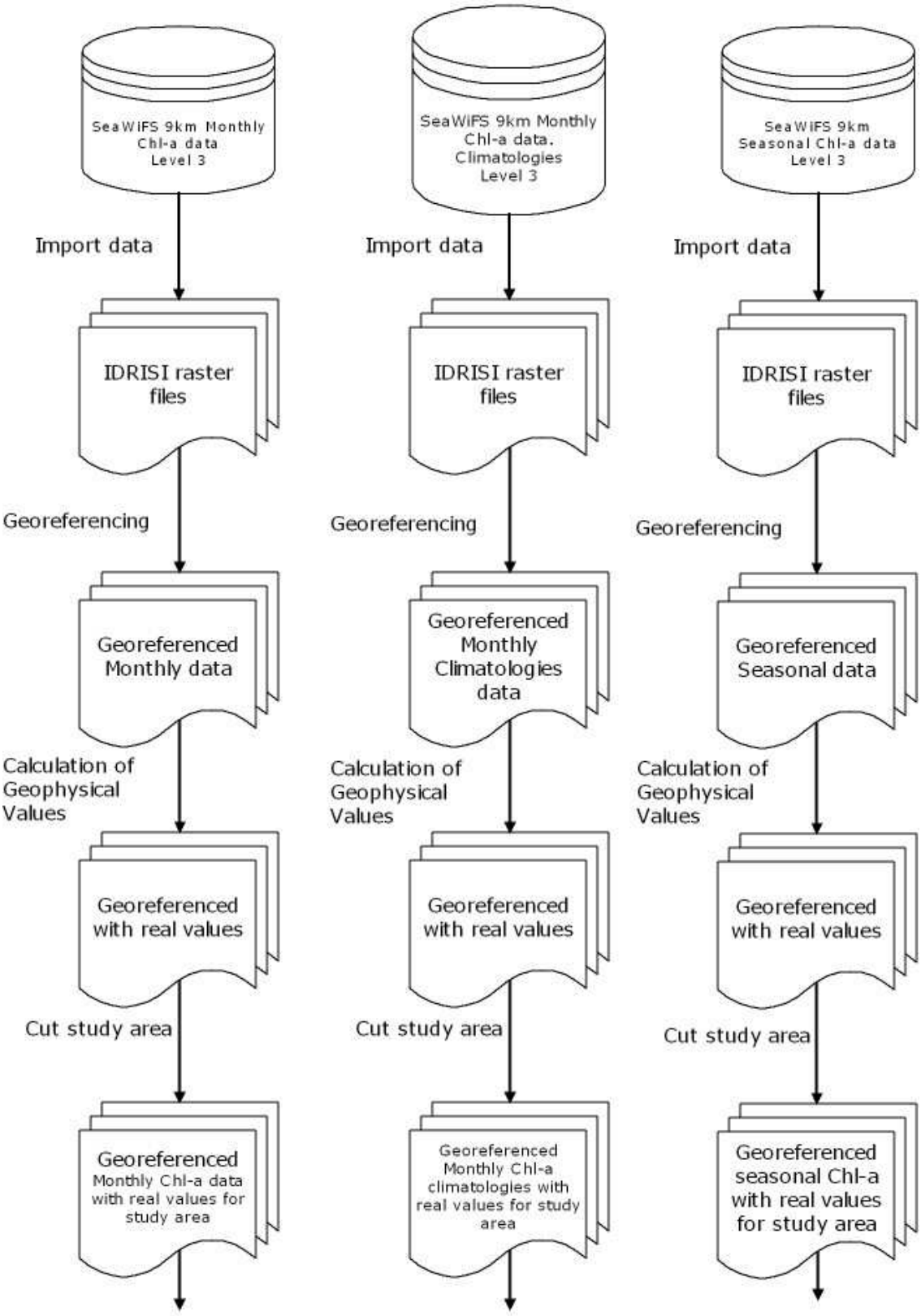

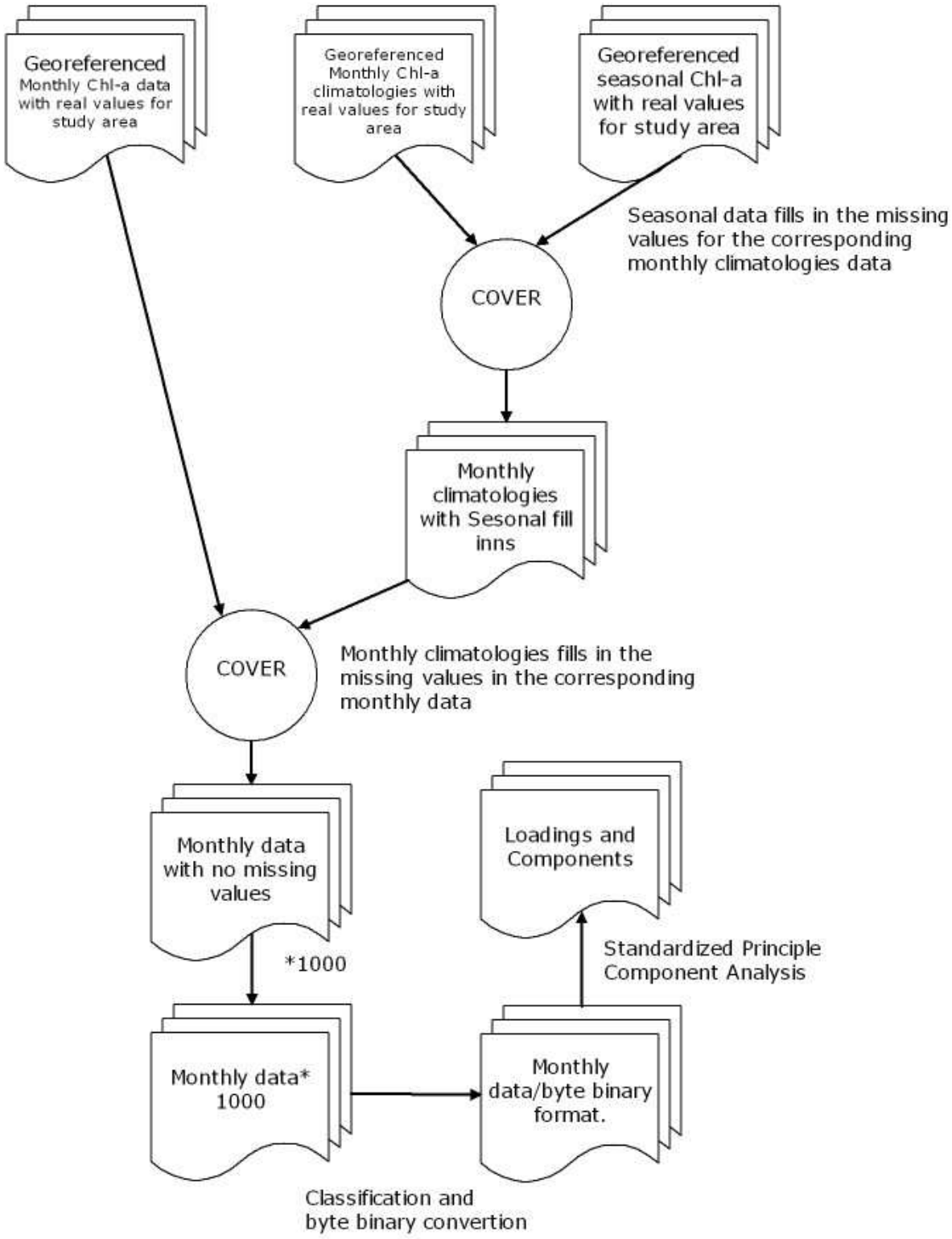

Flowchart showing the process flow from Level 3 raw data to the Time Series Analysis for the SeaWiFS data

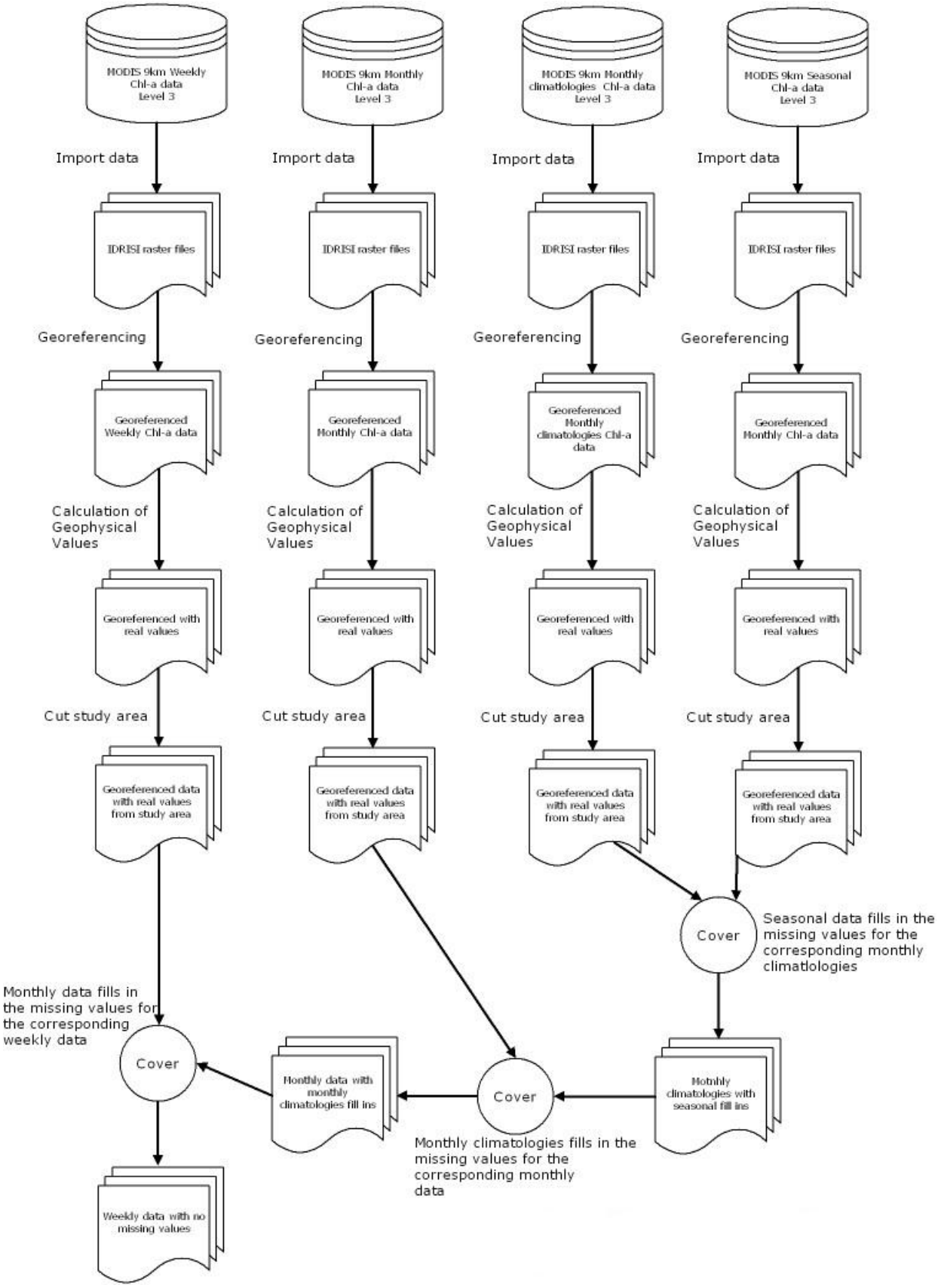

Continues on the next page…

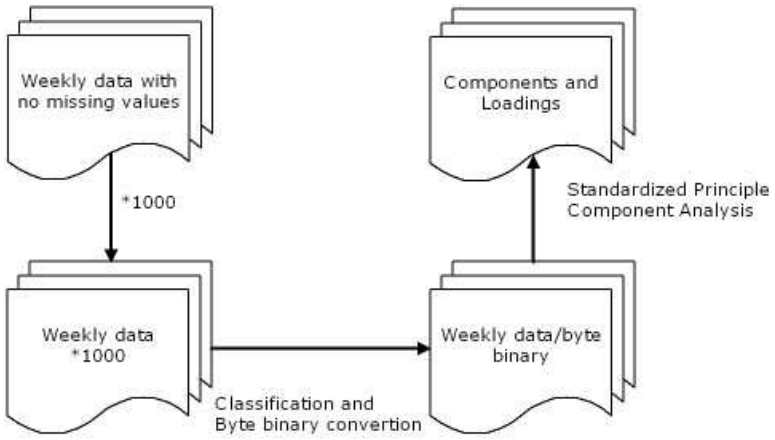

Flowchart showing the process flow from Level 3 raw data to the Time Series Analysis for the MODIS data

B: Formal description of the SPCA

The information as a whole is taken from Jensen (2005). To perform SPCA we apply a transformation to a correlated set of data. This means that the data must have a relationship between the time series data. In my study the data sets are classified chlorophyll-a measurements from sequential time periods. The application of the transformation to the correlated time series data will produce an uncorrelated dataset. This can be conceptualized by considering two remotely sensed images from two different time periods covering the same area containing chlorophyll values for each pixel distributed in two dimensions as shown in part a in Figure 1.

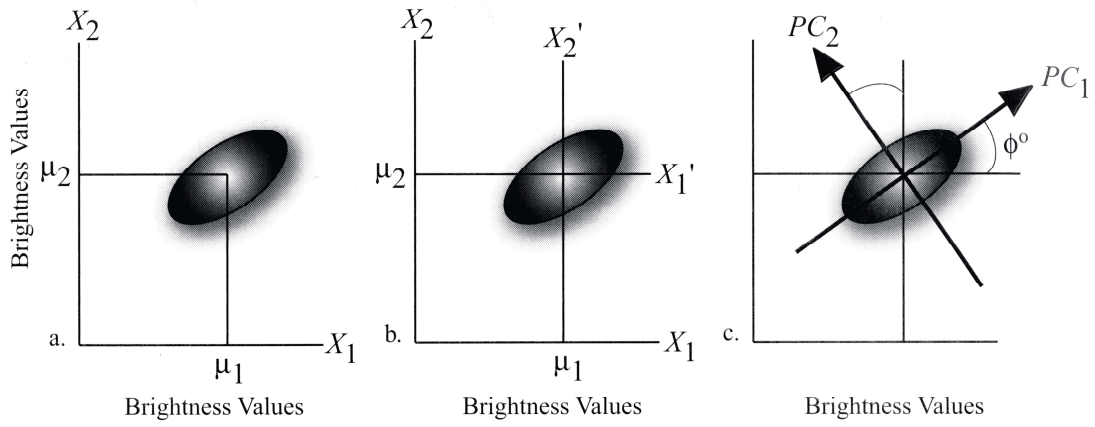

Figure 1 Modified from Jensen (2005)

The distribution of the pixel values in the two images are labeled X_1 and X_2. μ_1 and μ_2 represent the mean chlorophyll value for each image. Variance in the data is a measure of

the spread in the data and is indicating the correlation between the images or bands. The next step is to rotate the original axes in a way that the original values from X_1 and X_2 are reprojected onto a new set of axes, X_1' and X_2'. An example (as shown in Figure 1 b.) of a rotation can be a subtraction of the mean from the original data sets: $X_1' = X_1 - \mu_1$ and $X_2' = X_2 - \mu_2$. The result is that the origo of the new coordinate systems lies at the location of both means. The new coordinate system can now be rotated around its new origo in such a way that the first axis X_1' corresponds to the maximum variance of the scatter points. This new axis is called the first principle component ($PC_1 = \lambda_1$). The second principle component ($PC_2 = \lambda_2$) is placed in a direction orthogonal to PC_1. In order to reproject the original data from the X_1 and X_2 axes to the PC_1 and PC_2, the reprojection coefficients must be linearly applied to the original pixel values from the original images. To create the PC axis, it is necessary to calculate the length of the PC axes and their directions. These are computed by determining the eigenvalues (length) and eigenvectors (direction) from the covariance matrix.

Before moving on I will describe more closely the correlation matrix and the covariance matrix. The covariance matrix is a matrix which describes how dimensions vary from the mean with respect to each other. For an *n* dimensional data set, you can calculate $\frac{n!}{(n-2)!\times 2}$ different covariance values. Covariance is measured between two dimensions. If we have a 3-dimensional data set (*x,y,z*), then you could measure the *x* and *y* dimensions, and the *x* and *z* dimensions. The equation for covariance between two data sets (*X;Y*) is given by

$$\operatorname{cov}(X,Y) = \frac{\sum_{i=1}^{n}(X_i - \bar{X})(Y_i - \bar{Y})}{(n-1)}$$

where $\bar{X}$ and $\bar{Y}$ is the mean of the data sets. If we have multidimensional data sets it is useful to set up all the different covariance data in a covariance matrix. A definition of such a matrix for a data set of *n* dimensions is given by

$$C^{n\times n} = (c_{i,j}, c_{i,j} = \operatorname{cov}(Dim_i Dim_j))$$

where $C^{n\times n}$ is a matrix with *n* rows and *n* columns, and Dim_x is the *x*th dimension. The matrix is square and each entry in the matrix is the result of calculating covariance between two separate dimensions. For the calculation of a correlation matrix, each entry is subtracted by the mean and divided by the standard deviation. The result is a matrix of standard scores with numbers between 0 and 1. The number given is indicating the degree of similarity between all the possible combinations of data, in this case, how similar each image is to one another. The correlation matrix is later on used in a Standardized Principle Component Analysis.

The SPCA analysis

Next, there will be a step by step presentation of the procedure of a SPCA as presented by Jensen (2005). SPCA is making sure that each image has equal weight when computing new component images by using the $n\times n$ Correlation Matrix as the basis for the transformation of the original data set. This is to make sure that the seasonal effects and outliers are not influencing the final result, which is important when dealing with single variable time series data. The eigenvalues, $E = [\lambda_{1,1}, \lambda_{2.2}, ..., \lambda_{n,n}]$, and eigenvectors, $EV = [a_{kp} ...$ for $k = 1$ to n images, and $p = 1$ to n components], of the correlation matrix are computed such that:

$$EV \cdot Cor \cdot EV^T = \overset{E}{\begin{bmatrix} \lambda_{1,1} & 0 & 0 & 0 \\ 0 & \lambda_{2,2} & 0 & 0 \\ 0 & 0 & ... & 0 \\ 0 & 0 & 0 & \lambda_{n.n} \end{bmatrix}}$$

where EV^T is the transpose of the eigenvector matrix EV, and E is a diagonal matrix whose eigenvalues corresponds to the principle components, where $p = 1$ to *n* describe which component is shown. The eigenvectors with the highest eigenvalues is the principle component PC_1. From the eigenvalues it is possible to determine the amount of variance which each principle component contributes:

$$\%_p = \frac{\lambda_p \cdot 100}{\sum_{p=1}^{n} \lambda_p}$$

where λ_p is the *p*th eigenvalues from a possible *n*. It is now possible to determine how each image, *k,* is associated with the principle components, *p*, in the following way.

$$R_{kp} = \frac{a_{kp} \cdot \sqrt{\lambda_p}}{\sqrt{Var_k}}$$

where a_{kp} is the eigenvector for image k and component *p,* λ_p is the *p*th eigenvalue and Var_k is the variance of image *k* in the covariance matrix. The results of these computations, often called loadings, are a new matrix of loadings where each component is associated with each image in a time series. In the IDRISI TSA these loadings are given in a spreadsheet and contain valuable information about how each image is correlated with the different components. Thus, it is possible to describe the spatial variations of a variable over time.

Each image in the time series data contributes to calculate the new component images. The new pixel values for the new component images are computed in the following way

$$newValue_{i,j,p} = \sum_{k=1}^{n} a_{kp} \times oldValue_{i,j,k}$$

where a_{kp} is the eigenvectors, $oldvalue_{i,j,k}$ is the pixel value in image *k* for the pixel at row *i*, column *j* and *n* is the number of images. The new pixel values are no longer containing information about geophysical values.

C: SeaWiFS Components

Component 5

The fifth component is consisting of 0.5 % of the total variation of the data set. The loadings graph in Figure 2 shows chaotic pattern in the first glance, but reveals some seasonal trends. First, there is a clear negative peak in January for each year, but the magnitude of the peaks varies greatly. The peak of greatest magnitude is in January 1998, which suggests a anomaly month. January 1999 also stands clearly out. The other January peaks are of lesser magnitude. Second, in each December and each February there are clear positive peaks, although the pattern and the magnitude of those seem are varying greatly from year to year.

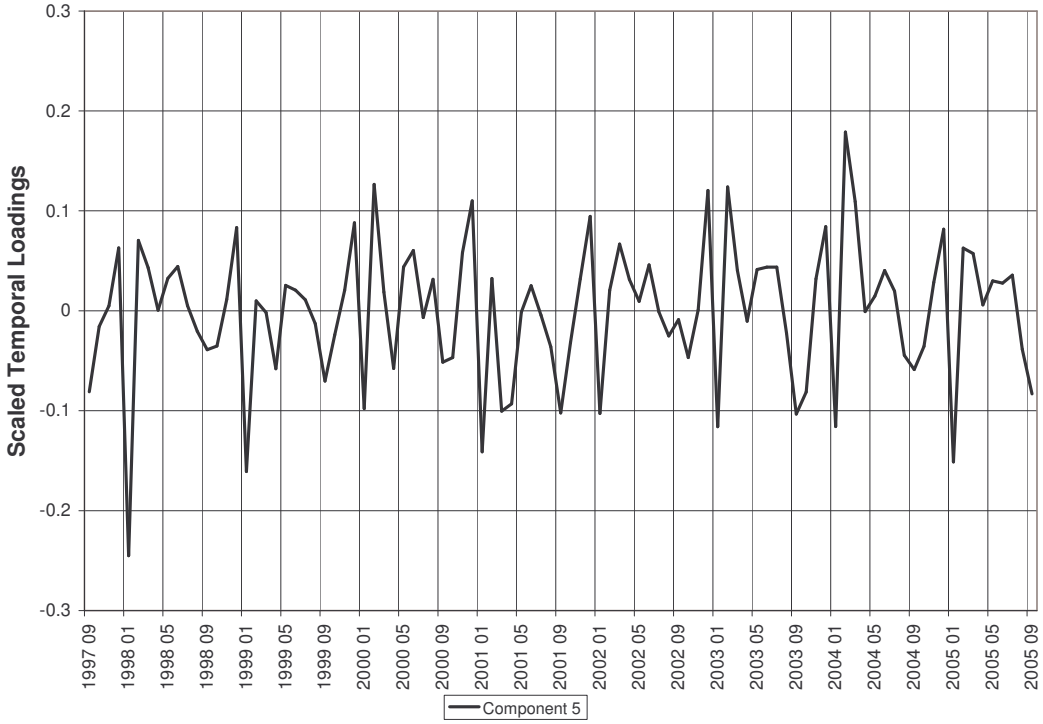

Figure 2. Loadings of Component 5

Figure 3, the fifth component map, shows that areas with high negative and positive correlation have a clear spatial pattern. Most of the coastal and near coastal waters of Madagascar are dominated by pixels of high negative correlation with the loadings graph. Some small patchy areas along the west coast and east coast contain positive correlation values. These areas include the coastal waters of western Madagascar from south of the Onihaly river.

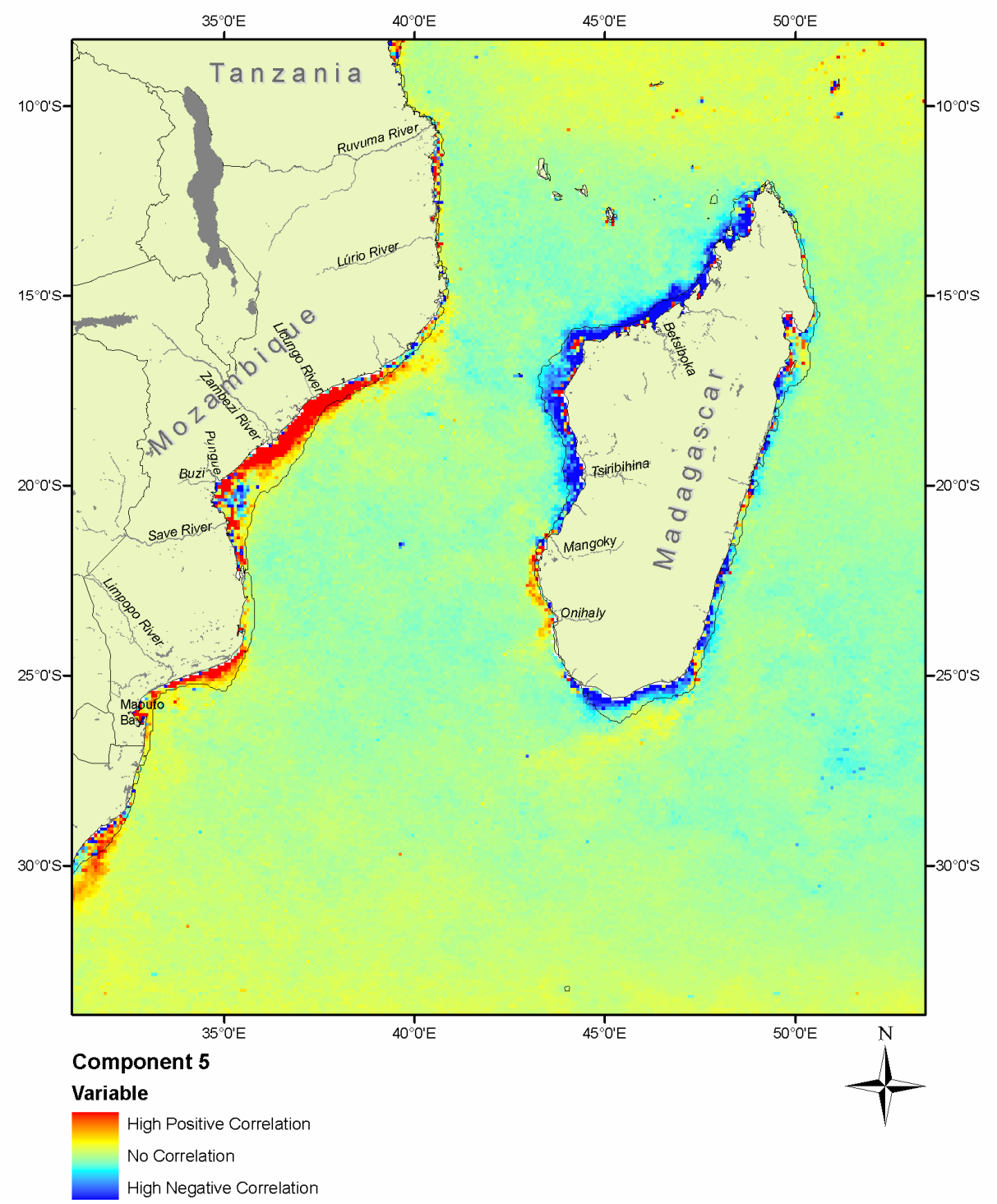

Figure 3. Component 5 image.

Component 6 and 7

Component 6 and 7 showed chaotic patterns in both the loadings and images. The results are most likely due to noise and the components are therefore not shown.

D:MODIS Components

Component 4

The fourth component consists of 1 % of the total variations in the MODIS Aqua data set. Figure 4 shows the component 4 loadings. In the beginning of July 2002 the graph starts of with loadings values just beneath zero. From the beginning of August 2002 to February 2003 there are clear positive loadings values that is not seen in the rest of the time series. From March 2003 to the beginning of September 2005 the loadings values are mostly negative and is not showing a clear seasonal pattern or anomalous loadings values. This leads to the notion that there may be elevated levels of chlorophyll in the time period between August 2002 and February 2003 in those areas that correlate positive with the loadings graph.
One the other hand may the areas which correlate negatively with the loadings graph experience anomalous low chlorophyll values compared with the rest of the time series.

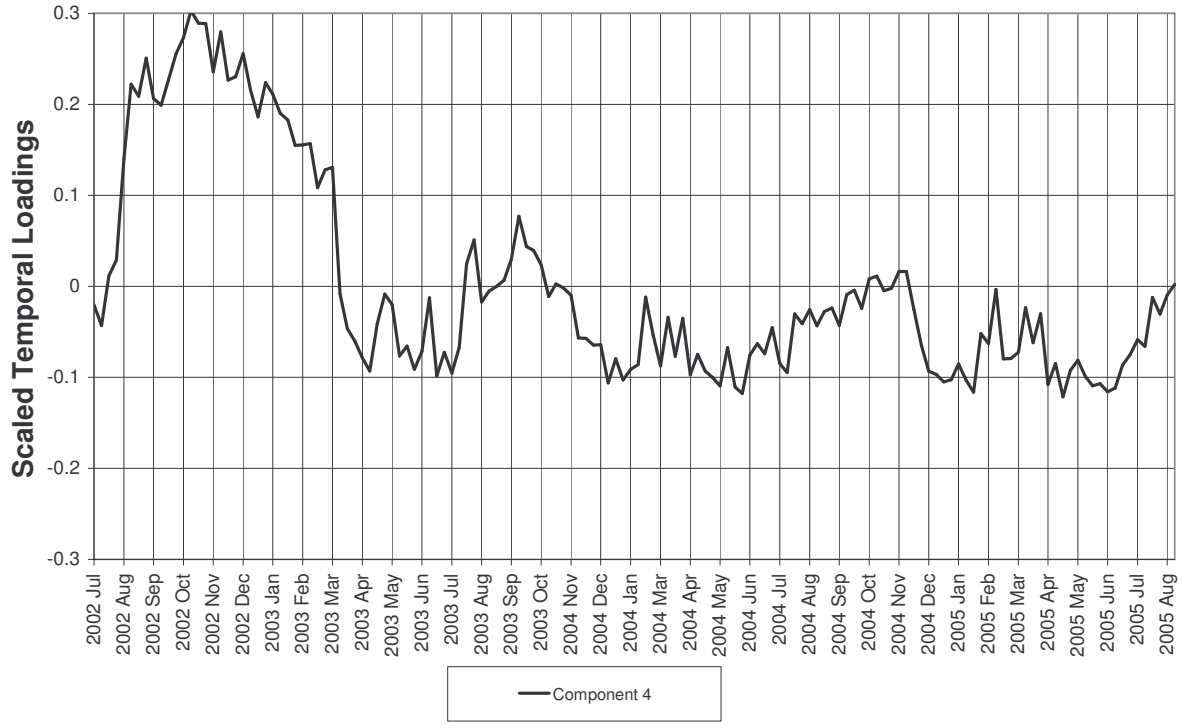

Figure 4. Loadings for Component 4.

Figure 5 shows the component 4 image. The waters south and south east of Madagascar particularly stand out as the most highlighted area which correlates highly with the temporal loadings. Near the coast of northern Madagascar (~48º30´E 13ºS) the waters are containing highly positive correlated values. This is also the case for most of the near shore waters of the African coast. Negative correlated areas are found in the vicinity of the western Madagascar coastline, coastal waters south of the Save River and coastal waters near the Zambezi river

mouth. The signature south of Madagascar may be due to enhanced coastal upwelling in this period.

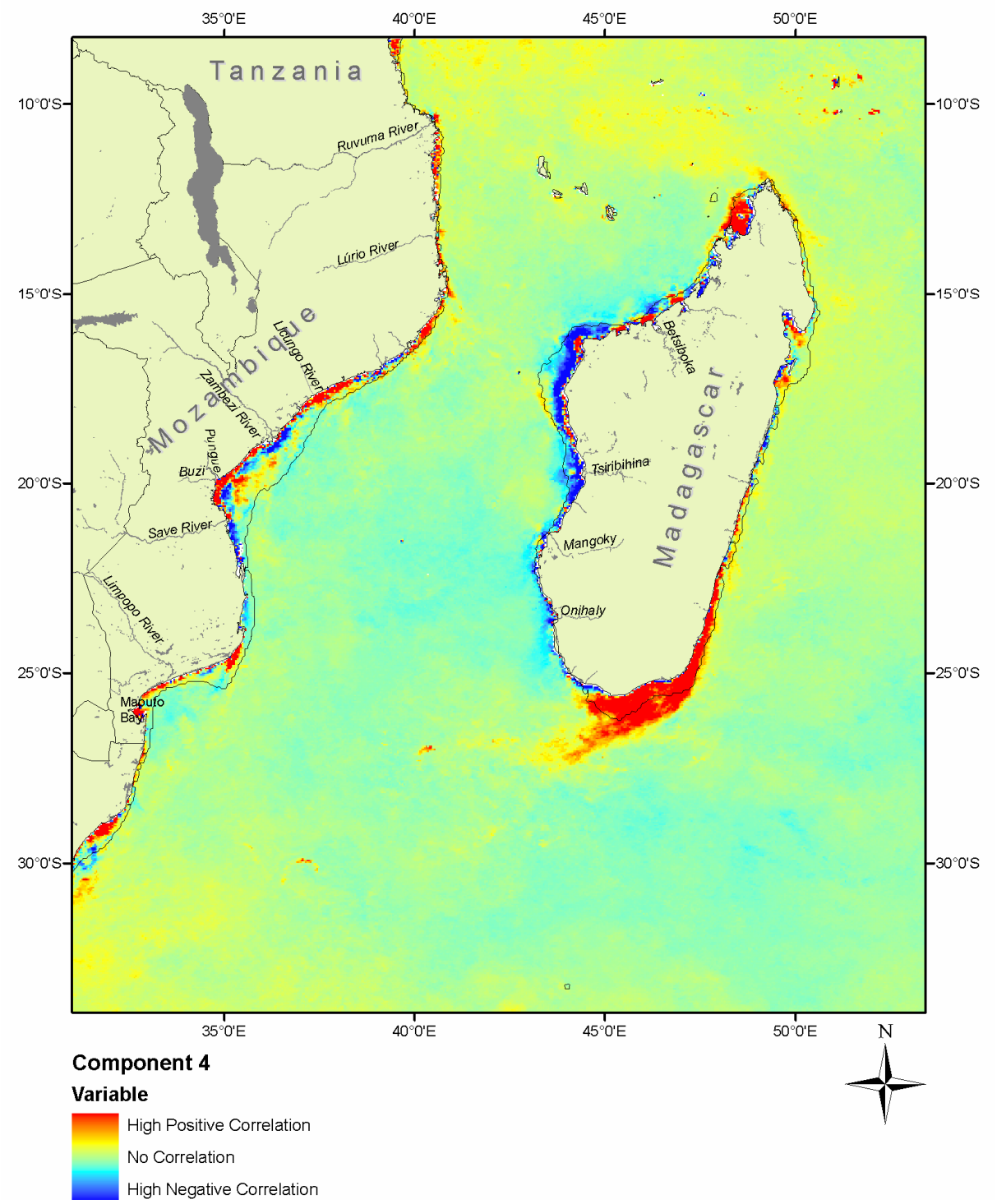

Figure 5. Component 4 image

Component 5

The fifth component consists of 0.9 % of the total variation in the data set. As can be seen in Figure 6, are the temporal loadings showing a negative progressive trend from the beginning of July 2002 to the beginning of January 2004 where a bottom peak is reached. The loadings values rises in the following weeks and reaches a local high in the beginning of May 2004. The following months shows an alternating positive pattern with no clear seasonal pattern.

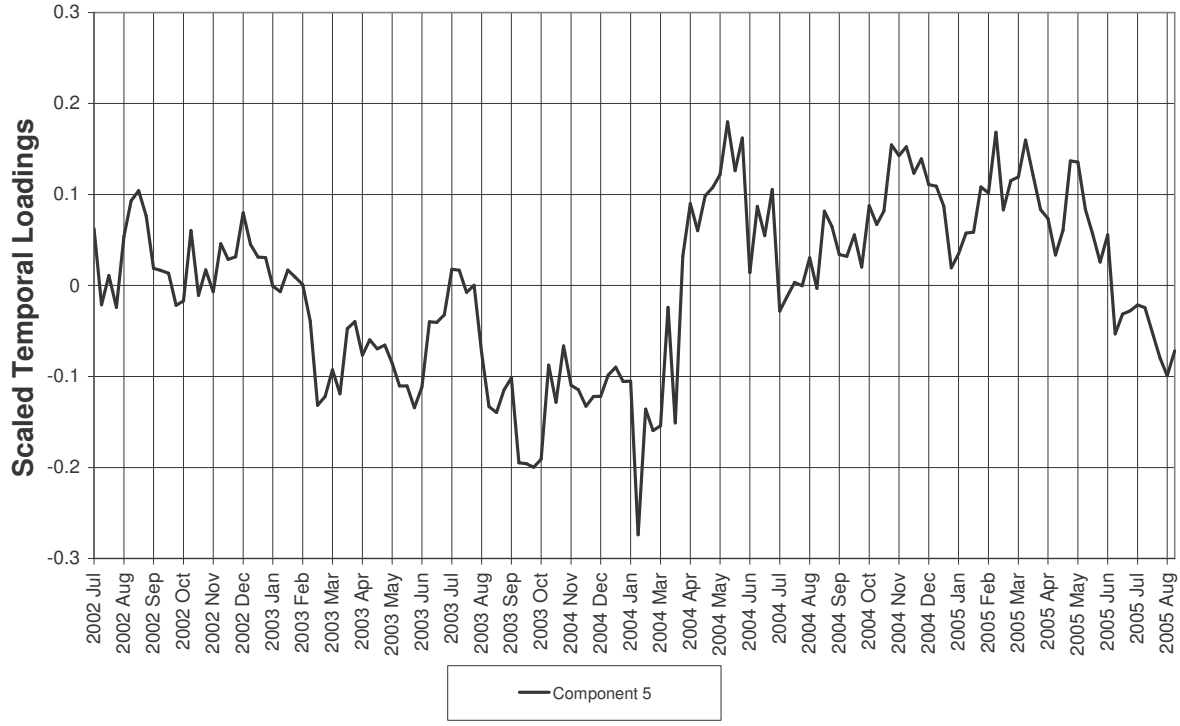

Figure 6. Loadings of Component 5.

The component 5 image map shows a clear pattern regarding the spatial distribution of the areas with high positive and negative correlation. As with the component 2, 3 and 4, are the areas of high activity localized in the coastal areas of Madagascar and the east Africa. Positive correlated regions are found (1) south of Madagascar, (2) in the north eastern coastal waters from 12ºS to 20ºS, (3) in the small belt nearest the west coast of Madagascar, (4) in the southwestern part of the study area at ~31º30´E 30ºS and some small patchy coastal areas along the east coast of Africa. Negative correlated areas are found next to the positive correlated areas of the western coast of Madagascar and along the coast of Mozambique.

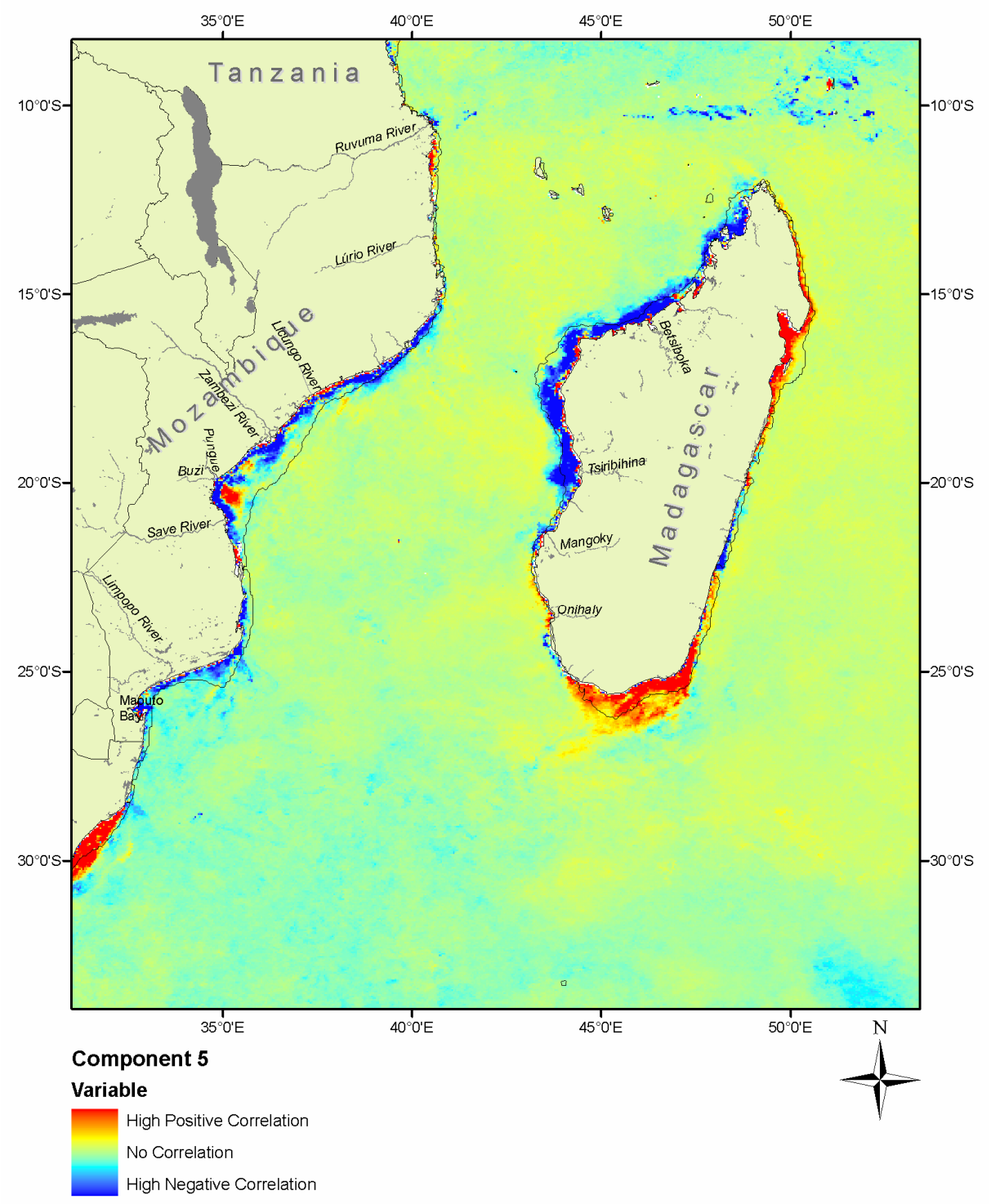

Figure 7. Component 5 image